IGNITION BEHAVIOR AND AIR DELIVERY REQUIREMENTS OBSERVED DURING THE CARBONIZATION OF PRESSURIZED PACKED BEDS OF BIOMASS

A THESIS SUBMITTED TO THE GRADUATE DIVISION OF THE UNIVERSITY OF HAWAI'I IN PARTIAL FULFILLMENT OF THE REQUIREMENTS FOR THE DEGREE OF

MASTER OF SCIENCE

IN

MECHANICAL ENGINEERING

December 2005

By
Samuel R. Wade

Thesis Committee:

Michael J. Antal, Jr., Chairperson
Carlos F. M. Coimbra
Beei-Huan Chao

We certify that we have read this thesis and that, in our opinion, it is satisfactory in scope and quality as a dissertation for the degree of Master of Science in Mechanical Engineering.

THESIS COMMITTEE

Chairperson

To my family, for teaching me the strength to focus on this type of project.
To Georgia, for permitting me to drag her to paradise.

Acknowledgements

I would like to gratefully acknowledge the mentorship offered to me by Dr. Michael J. Antal, Jr. whose support and guidance made this work possible. I would also like to thank Dr. Carlos Coimbra and Dr. Beei-Huan Chao for serving on my thesis committee, and for being positive and helpful instructors. Michael Lurvey has my appreciation for his business tips and financial support of my work. Further thanks are due to all of the members of the R^3 laboratory who created a constantly evolving, intellectually stimulating, environment for me to share in. Specifically, I thank Dr. Teppei Nunoura for his enthusiastic ability to make the complex comprehensible, Dr. Lloyd Paredes for his mechanical and anthropological insights, and Jared Bourke for his moral support and lightning teamwork.

Abstract

Flash Carbonization™ (FC) is a novel procedure by which biomass is converted to bio-carbon (i.e. charcoal) quickly and efficiently. To begin this process, a canister containing a packed bed of feedstock is placed within a pressure vessel, compressed air is used to charge the system to an initial pressure of ~1-2 MPa, and a flash fire is ignited at the bottom of the bed. After approximately two minutes, air is delivered to the top of the bed and the biomass is converted to a high-yield bio-carbon. This technology has progressed to the point that a commercial-scale demonstration reactor is currently being assembled on the campus of the University of Hawaii, Manoa. The adaptation of the technology from the lab-scale reactor to the larger pilot plant is the underlying theme of this thesis. Specifically, the subjects of ignition behavior and air delivery are explored in detail.

In lab-scale tests of the FC process, some fuels have been observed to ignite violently, resulting in a sudden drastic pressure rise ($\Delta P \sim 1$ MPa within 2-3 seconds). Because this event could be potentially hazardous, a study of this phenomenon was undertaken in preparation for the scale-up of the FC process. The influence of initial pressure, feed moisture content, and ignition heater power were examined following a 2^3 full factorial experimental design approach. It was determined that the violence of the ignition is related to the moisture content of the feedstock and the operating pressure of the process. The information gained from this study was used to size the emergency venting components of the pilot plant. Additionally, this work details the impact of compressibility effects on previously published air-to-biomass ratios (ABRs)—a value used to indicate the optimum level of air delivery for an individual biomass feedstock. As a result of this study, the accuracy of the ABR values were improved for all feedstock types.

Table of Contents

List of Tables

List of Figures

Nomenclature

$(dP/dt)_{max}$ Maximum Slope of a Pressure vs. Time Curve

ΔN Change in Moles

ΔP_{max} Maximum Change in Pressure

η_{char} Energy Conversion Efficiency

$\dot{m}$ Mass Flow Rate

$\dot{v}$ Volumetric Flow Rate

A Cross-Sectional Area

a_0, a_1, a_2 Coefficients of a Polynomial Fit

A_s Surface Area

AAE Average Absolute Error

ABR Air-to-Biomass Ratio

$ABR_{delivered}$ Delivered Air-to-Biomass Ratio

ABR_{total} Total Air-to-Biomass Ratio

ASH Percentage of Ash

FC Percentage of Fixed Carbon

HHV Higher Heating Value

HHV_{Bio} Higher Heating Value of Biomass

HHV_{char} Higher Heating Value of Charcoal

k Ratio of Specific Heats

K_G Deflagration Index

m Mass

M_w Molecular Weight

$m_{air,init}$ Mass of Air Initially Present

$m_{air,pri}$ Mass of Primary Air Delivered

m_{ash} Dry Mass of Ash

$m_{Bio,Dry}$ Mass of Biomass After Drying

$m_{Bio,Wet}$ Mass of Biomass Before Drying

m_{cc} Dry Mass of Carbonized Charcoal

m_{char} Initial Dry Mass of Charcoal

m_{H2O} Mass of Moisture

MC_{DB} Moisture Content Percentage on a Dry Basis

MC_{WB} Moisture Content Percentage on a Wet Basis

N Number of Moles

P Pressure

P^* Choked Pressure

P_{max} Maximum Pressure

PD Power Density

PE Percentage Error

R Gas Constant

R Resistance

T Temperature

V Voltage

V Volume

V_{Lost} Volume of Escaped Gas

V_{void} Void Volume

VM Percentage of Volatile Matter

y_{char} Charcoal Yield

y_{fC} Fixed-Carbon Yield

Z Compressibility Factor

Chapter 1

Introduction

1.1 Background

The technique of Flash Carbonization^{TM} is a novel method of charcoal production. In this procedure a packed bed of biomass is placed within a vessel at elevated pressure, a flash fire is ignited within the bed, and the biomass is converted to biocarbon (i.e. charcoal) quickly and efficiently. The Flash Carbonization^{TM} process was developed by Dr. Michael J. Antal, Jr. and his assistants at the Renewable Resources Research (R^3) Laboratory[1]. Most of the previous research related to the development of this process employed various incarnations of a device referred to as the "laboratory-scale" (or "lab-scale") Flash Carbonization^{TM} reactor (see Figure 1.1).

The technology of Flash Carbonization^{TM} has now matured to the point where it is possible to deploy the process on a commercial scale. To demonstrate the feasibility of this transition, a pilot plant has been constructed on the campus of the University of Hawaii at Manoa (see Figure 1.2). The adaptation of the technology behind the lab-scale reactor to the larger pilot plant, hereafter referred to as the "demonstration reactor" (or "demo-reactor"), is a primary theme of this thesis. Specifically, ignition behavior and air delivery requirements of the process will be explored in detail.

1.2 Objective of Thesis

The objective of this thesis is to merge a variety of work preformed to support the scale-up of the Flash Carbonization^{TM} process. In the initial chapter "Production of Charcoal from Biomass: An Overview" the fundamentals of charcoal production will be examined, traditional charcoal manufacturing techniques briefly explained, and the improvements

[1]Located on the campus of the University of Hawaii at Manoa, the R^3 labaratory is a division of the Hawaii Natural Energy Institute (HNEI).

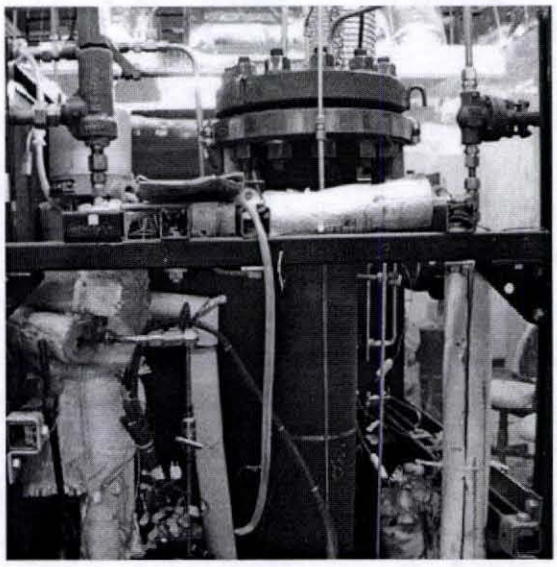

Figure 1.1 The laboratory-scale Flash Carbonization^{TM} reactor.

Figure 1.2 The demonstration-scale Flash Carbonization^{TM} reactor.

offered by the Flash Carbonization^{TM} process described. This chapter will be followed by a description of the device used to study the Flash Carbonization^{TM} process in a laboratory setting—appropriately entitled "The Laboratory-Scale Flash Carbonization^{TM} Reactor". These two initial chapters should provide the reader with the basic knowledge needed to understand the fairly unique process of Flash Carbonization^{TM}. This foundation of information will then be expanded upon in the subsequent chapters.

"Airflow, Compressibility, and Deviations from Ideal Gas Behavior in the Accumulator System" details the first original study conducted for this thesis. In this chapter, the reader will see how this work expanded the understanding of the air delivery requirements of the lab-scale process, and explained the mysterious behavior of the rotameters used to monitor airflow. The following chapter, entitled "Deflagration Fundamentals" is essentially a literature review designed to provide a background for the next chapter—"Violent Ignition Behavior of Pressurized Packed Beds of Biomass: A Factorial Study". This ignition study was conducted in order to experimentally examine the sudden drastic pressure rise which has been observed to occur during the ignition phase of the process[2]. In the final chapter a few brief examples will be given to demonstrate how the information gained through the experiments described in the previous chapters was applied, along with some additional calculations, to size various components of the demonstration reactor.

[2]This type of ignition behavior occurs only in select feedstock types, as will be discussed in the following chapters.

Chapter 2

Production of Charcoal from Biomass: An Overview

2.1 Introduction

Biomass is a broad term used to encompass a wide variety of materials including crop and forest residues, animal byproducts, and some municipal wastes. In the United States, biomass currently supplies approximately three percent of the total energy consumed per year, and recently surpassed hydropower as the largest domestic source of renewable energy [1]. Globally, biomass provides approximately eleven percent of the world's supply of primary energy [2]. The numerous advantages of using biomass as an energy source include sustainability, CO_2 neutrality, waste reduction, and reduced dependence on fossil fuels. This chapter will attempt to provide a broad overview of the field of biomass-to-energy conversion, with a specific focus on the advantages of bio-carbon (charcoal). Basic concepts related to biomass fuel use and charcoal manufacturing will be discussed, a global perspective on charcoal use will be briefly presented, and the traditional methods of charcoal production will be contrasted with the Flash Carbonization™ process.

2.2 The Biomass Resource in the United States

In a recent report created jointly with the U.S. Department of Agriculture, the U.S. Department of Energy (DOE) estimated that ~368 million dry tons of biomass could potentially be removed in a sustainable[1] fashion from U.S. forest land for energy use, and that an additional ~998 million dry tons could be continually removed from agricultural

[1] It should be noted that "sustainability" is a very important concept for any biomass resource development plan. In order for biomass combustion to be a truly CO_2 neutral process, an equal amount of biomass must be re-planted for every unit of biomass removed for fuel use. Additionally, the machinery used for harvesting and processing the biomass should be powered by biofuel.

land. This figure associated with agricultural biomass is somewhat surprising when one considers that currently more than seventy-five percent of the biomass consumption in the U.S. is derived from forest sources. However, the authors of the DOE report predict that the much higher level of management intensity inherent to agricultural land use, if properly administered, could lead to a biomass resource of great potential. To put these numbers in perspective, the amount of biomass currently available from agricultural lands is ~194 million dry tons/year, of which corn stover is the largest single source at ~75 million ton/year [1].

2.3 Derivation of Fuels from Biomass

Most basic forms of biomass have very low bulk energy density compared to fossil fuels [2]. Therefore, transporting a given volume of biomass (i.e. one truck full of wood) is not nearly as effective (on an energy basis) as transporting the same volume of fossil fuel (i.e. the same truck full of coal). These inefficiencies lead to increased transportation and processing costs per unit of energy generated. Due to this fact, a wide variety of techniques have been developed to convert raw biomass sources into more compact forms of energy. These bio-fuels—such as ethanol, biodiesel, and charcoal—approach energy densities comparable to those of fossil fuels. Additionally, the increased fuel uniformity achieved by these processing techniques allows bio-fuels to be used in a much wider variety of combustion devices than the raw biomass feedstock. Figure 2.1 shows a summary of some of the feedstock and processes used to create an assortment of these bio-fuels. Each of these methods has advantages and disadvantages beyond the scope of this work. The following discussion will focus on the process of pyrolysis, and specifically the production of charcoal as the preferred product of this process.

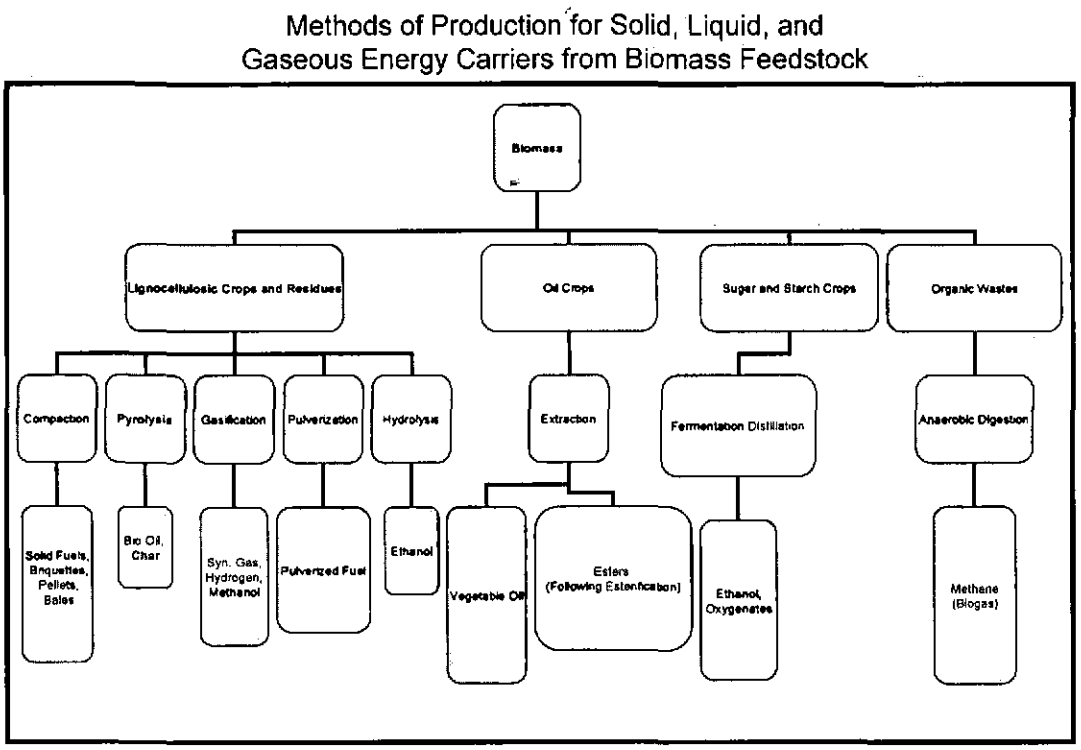

Figure 2.1 Processes used to create a variety of bio-fuels from biomass (Adapted from [2]).

2.4 Basic Terminology and Definitions Related to Charcoal Production

2.4.1 Moisture Content

Because plants rely on water to survive, the mass of moisture present in a biomass sample is usually a significant portion of the overall sample mass. However, due to changes in ambient conditions (i.e. temperature, humidity), the amount of moisture present in the sample can change fairly easily. These factors, as well as the structure of the tissues composing the specific biomass in question, combine to determine the rate, and amount, of moisture released from a biomass sample by transpiration and evaporation [2]. Frequently, due to this variation in moisture, the sample mass can not be regarded as a constant value for any significant period of time. Therefore, a supplementary moisture content analysis is often preformed whenever a mass measurement of a sample is made.

The moisture content of a sample of biomass is determined by drying the sample in an oven until no more moisture remains (the mass of the sample stops changing). Specifically, the method followed in the R^3 laboratory is based on ASTM E 1756-95 [3]. This process involves the following steps: First, the beaker which will contain the sample is placed in an oven at 105°C for at least an hour. The beaker is then removed from the oven and allowed to cool in a desiccator for at least one hour. The mass of the empty beaker is recorded using a balance accurate to one hundredth of a gram (Mettler Toledo PB3002). The sample is placed inside the beaker, and the combined mass value is obtained. The sample and the beaker are placed into the oven for at least three hours but not longer than seventy-two hours. Following this period, they are placed in a desiccator and allowed to cool for one hour. The combined mass is then recorded. This process is repeated with one hour heating and cooling increments until the mass stops changing. The difference between the initial and the final mass values is equal to the mass of the moisture removed from the feed. Using this value, moisture content values can be reported on either a dry or a wet basis as shown in Equations 2.1 and 2.2 [2].

$$MC_{WB} = \frac{m_{H2O}}{m_{Bio,Wet}} \times 100\% \tag{2.1}$$

$$MC_{DB} = \frac{m_{H2O}}{m_{Bio,Dry}} \times 100\% \tag{2.2}$$

Where m_{H2O} is the mass of moisture removed, $m_{Bio,Wet}$ is the mass of the biomass before drying, and $m_{Bio,Dry}$ is the mass of the biomass after drying.

2.4.2 Proximate Analysis

Proximate analysis is an analytical technique used to separate a charcoal sample into three components—volatile matter (VM), ash (ASH) and fixed carbon (FC). The proximate analysis procedure employed in the R^3 laboratory follows ASTM method ASTM D 1762-84 [4]. In this analysis, the charcoal sample is heated in a covered crucible to 950 °C and held at this temperature for six minutes. The mass lost by the sample during this period is attributed to escaping volatile matter, while the solid mass remaining in the crucible is referred to as "carbonized charcoal". The percentage of VM may then be determined by using Equation 2.3. This procedure is followed by ash content analysis, in which the remains of the sample are placed in an uncovered crucible, heated to 750 °C, and held at this temperature for six hours. The material which remains in the crucible following this extended period of heating is defined to be ash as shown in Equation 2.4. The fixed carbon content of the charcoal is the portion of the sample removed during this six hour period as indicated by Equation 2.5.

$$VM = \frac{(m_{char} - m_{cc})}{m_{char}} \times 100\% \tag{2.3}$$

$$ASH = \frac{m_{ash}}{m_{char}} \times 100\% \tag{2.4}$$

$$FC = 100\% - VM - ASH \tag{2.5}$$

Where m_{char} is the initial dry mass of charcoal, m_{cc} is the dry mass of carbonized charcoal (remaining after the six minutes of heating at 950 ^{o}C), and m_{ash} is the dry mass of ash (which remains following combustion of the carbonized charcoal at 750 ^{o}C).

Note that the definition of a high quality charcoal varies based on the desired final use. For example, charcoal appropriate for cooking typically contains 20-30% volatile matter, while charcoal intended for metallurgical purposes often contains 10-15% (or less) volatile matter [5]. Proximate analysis provides a fairly quick and easy method to analytically characterize charcoal samples. Ideally, a charcoal manufacturing process would be able to produce charcoal suitable for a variety of applications by controlling the volatile matter, fixed carbon, and ash contents of its product.

2.4.3 Various Definitions of Yield

Although, to some extent, it is hard to directly compare charcoal manufacturing techniques due the difficulties in defining a universally "good" product, it is still beneficial to develop some common metrics for overall process efficiency. Beyond the proximate analysis discussed above, two yield values are commonly used to characterize a charcoal manufacturing process. The first value, the charcoal yield, y_{char}, as defined in Equation 2.6, may be employed to give a quick understanding of the efficiency of a given charcoal making process. Unfortunately, because charcoal is not a well defined chemical compound, this definition is very vague. Some charcoals are nearly pure carbon, while others have only been partially pyrolyzed, and still contain significant amounts of oxygen and hydrogen [6]. A more useful value is the fixed-carbon yield, y_{fC}, which takes into account the compositions of the sample—determined from proximate analysis—as shown in Equation 2.7. Note that fixed-carbon yield demonstrates the efficiency of conversion from the ash-free feedstock into the fixed-carbon of the final charcoal product [7]. Finally, if the higher heating values of the feedstock

and the charcoal are known, the energy conversion efficiency, η_{char}, may be calculated using Equation 2.8 [5].

$$y_{char} = \frac{m_{char}}{m_{Bio,Dry}} \tag{2.6}$$

$$y_{fC} = y_{char}\frac{FC}{100\% - ASH_{Bio}} \tag{2.7}$$

$$\eta_{char} = y_{char}\frac{HHV_{char}}{HHV_{Bio}} \tag{2.8}$$

Where HHV_{char} and HHV_{Bio} are the higher heating values of the charcoal and biomass respectively and ASH_{Bio} is the percentage of ash in the biomass feedstock[2].

2.5 Combustion and Pyrolysis

2.5.1 General Information

Although, as discussed previously, a wide variety of biomass to bio-fuel conversion processes are available, direct combustion of biomass is still responsible for over 97% of the world's bio-energy production [9]. Therefore, a brief description of the complicated multi-phase processes required for biomass combustion to occur is worth mentioning here. Additionally, a cursory understanding of biomass combustion is essentially a prerequisite for anyone seeking to understand Flash Carbonization™ systems.

It is important to recognize that three primary steps occur any time a solid biomass fuel is consumed by combustion [2, 10]. First, the moisture is driven out of the biomass through evaporation. Secondly, pyrolytic reactions generate fuel gases, tarry liquids, and char. Finally, the fuel gases are combusted[3]. These three steps are all occurring simultaneously

[2]See the appendix for a discussion of estimating HHV from proximate analysis. ASH_{Bio} is determined using ASTM E 1755-95 [8].

[3]Although separating combustion reactions from pyrolysis reactions in an actual system is very difficult if oxygen is present, a clear distinction between these two processes from a theoretical point of view is desirable. Therefore we will define combustion as rapid exothermic oxidation [11]. In contrast, pyrolysis will be defined as the transformation of a compound into one or more other substances by heat alone (i.e. without oxidation) [12].

in any biomass combustion system. The key to understanding this process is that the fuel gasses burn and release the majority of the heat produced by the process. Heat is usually consumed during the drying and volatilization (pyrolytic) processes[4] [9]. As the overall process continues, the liquid produced by pyrolysis evaporates and combusts. Similarly, most of the components of the solid char (i.e. carbon) may also eventually be combusted. Following complete combustion of a biomass fuel, the components of the biomass which cannot burn easily (primarily minerals) remain as ash.

The air delivered during the Flash Carbonization™ process allows for combustion of some volatile gases to occur. This limited combustion produces sufficient heat to assist the pyrolytic reactions in propagating throughout the bed of biomass. However, if too much air is delivered, some of the desired charcoal product will eventually be consumed. Therefore, the rate of air delivery is carefully controlled, and the desired amount of volatile components of the biomass can be removed, leaving only a fairly uniform, high-yield[5], bio-carbon. Thus the Flash Carbonization™ process is alternatively referred to as flaming, or air-assisted, pyrolysis. Also note that the rate of air delivery ensures that combustion always occurs in an oxidant lean environment and at fairly low temperatures.

2.5.2 Emissions Produced During Combustion and Pyrolysis of Biomass

Ideally the products of biomass combustion are only carbon dioxide and water. Equation 2.9 shows a simplified model for the stoichiometric combustion of cellulose[6].

$$C_6H_{10}O_5 + 6O_2 \rightarrow 6CO_2 + 5H_2O \tag{2.9}$$

Additionally, one equation used to represent the pyrolysis of cellulose is Equation 2.10 [5].

$$C_6H_{10}O_5 \rightarrow 3.74C + 2.65H_2O + 1.17CO_2 + 1.08CH_4 \tag{2.10}$$

[4]This is a simplification. Wood pyrolysis transforms from endothermic to exothermic at temperatures above ~280 °C. Increased pressure causes the total heat of cellulose pyrolysis to shift from endothermic to exothermic [5].

[5]In this case the term "high-yield" refers to fixed-carbon yield.

[6]Cellulose may be used as a representative compound for a wide variety of biomass feedstocks [13].

Alternate forms of Equation 2.10 include carbon monoxide as one of the products. Note that in the case of the oxidant starved combustion which occurs during the Flash Carbonization^{TM} process, we expect carbon monoxide as well as unburned hydrocarbon products such as methane to be present in the exhaust stream. To put it another way, the fuel rich combustion case approaches pure pyrolysis with decreasing availability of oxygen.

Therefore, from an emissions standpoint, particulate matter (PM_{10}, $PM_{2.5}$), carbon monoxide, and volatile organic compounds (VOCs, including unburned hydrocarbons) are the criteria pollutants of concern when charcoal is manufactured. The same pollutants are produced when charcoal is combusted for fuel uses. Oxides of nitrogen (NO_x) and oxides of sulfur (SO_x) are not usually a major problem for well designed charcoal manufacturing processes. The temperatures involved in the process are usually too low to produce thermal NO_x, and the amount of fuel bound sulfur and nitrogen is negligible in most biomass feeds [5, 14]. As expected, when gas samples of the exhaust from the lab-scale Flash Carbonization^{TM} reactor were analyzed by gas chromatography the species detected included H_2, CO, CH_4, N_2, O_2, CO_2 and some unidentified organic compounds [7]. When the catalytic afterburner is provided with sufficient secondary air, the Flash Carbonization^{TM} process emits significantly less pollution than traditional charcoal production methods [15][7].

2.6 A Global View of the Charcoal Industry

Of the techniques mankind has developed to convert biomass into more useful forms of fuel only the process of the charcoal production reaches back to prehistoric times [17]. However, despite the thousands of years man has worked to improve charcoal manufacturing methods, current industrial technologies remain slow, dirty, and inefficient. This section will describe why charcoal derived from biomass is an important commodity in both developed

[7] Drastic reductions in CO, H_2, and CH_4 have been documented when the proper amount of secondary air is provided to the catalytic afterburner. Levels of pollutants produced by the Flash Carbonization^{TM} process per unit mass of charcoal have been found to be significantly less than the accepted EPA emission factor for charcoal production [16]. The catalytic afterburner is described in the following chapter.

and developing nations, and briefly explain some of the common methods of charcoal manufacturing currently employed around the world.

2.6.1 Charcoal's Role in Developed Nations

In most industrial applications, especially in developed nations, charcoal must compete with natural coal, petroleum coke and lignite. The advantages of charcoal over these alternatives include: low sulfur content, high carbon to ash ratio, relatively few and unreactive inorganic impurities, specific pore structure with large surface area, good reduction ability, and little to no smoke produced during combustion [18]. Because of these unique properties, charcoal is often used as a metallurgical reductant [6, 5]. For example, in Brazil during 1991 over one million tonnes of wood charcoal were consumed to smelt iron ore [19]. In the form of activated carbon, charcoal is used for a wide variety of air and water filtration systems [20]. In domestic settings, charcoal is used as a cooking fuel, as a soil amendment, and as a digestive aid [21, 5].

2.6.2 Charcoal's Role in Developing Nations

In the developing world charcoal serves as a primary fuel, chiefly used for cooking, and is preferred by many consumers over alternatives such as firewood and agricultural residues because charcoal is clean, safe, and easily storable for long periods of time [18]. Additionally, the levels of indoor air pollution (i.e. fine particulate) produced from charcoal cook stoves are considered to be less harmful than those produced by firewood use [22, 23, 24, 25]. For example, it was recently estimated that a rapid shift in the primary fuel choice from wood to charcoal could prevent 2.8 million premature deaths—due to lower respiratory infections and chronic obstructive pulmonary disease—in Africa alone by the year 2030 [26].

2.6.3 Traditional Methods of Charcoal Production

The oldest and simplest methods for producing charcoal are the charcoal pit and the earthmound kiln. A charcoal pit is recessed into the earth, while an earthmound kiln is built up around a pile of biomass (see Figure 2.2). Both of these technologies involve covering

Figure 2.2 A traditional charcoal earthmound kiln.

the feedstock with soil in a specific fashion in order to allow a controlled amount of air to enter during carbonization. The earth covering serves to keep out excess oxygen and to insulate against heat loss. Although extremely simple from a technological standpoint, both of these processes require a great deal of operator experience, and in developing nations the "secrets" of proper use of these techniques is often passed down from father to son. Slightly more modern small scale charcoal producers employ portable kilns created by modifying discarded oil drums in a variety of ways [18]. Unfortunately, fixed-carbon yield values are not available for the majority of these processes, so it is difficult to attempt head-to-head comparisons with more advanced technology.

Larger scale techniques include kilns made of concrete or brick. Internally heated processes of this type include the Missouri kiln, the Argentine Kiln, and the Brazilian Beehive Kiln. These devices usually employ thermocouples mounted at several places within the kiln which allow operators to determine how to properly adjust the airflow. Charcoal yields, y_{char}, from a Missouri kiln are typically on the order of 20-30% and require an operating cycle of 25-30 days [27]. A wide variety of factory scale charcoal production techniques currently exist. Most of these techniques, such as the Reichert Process, have operating cycles on the order of 20 hours with charcoal yields on the order of 33-38% [27, 18].

2.7 Advantages of the Flash Carbonization^{TM} Process

Unfortunately, due to the fairly slow, low-yield, traditional methods described above charcoal production is known to contribute to deforestation in many tropical countries, and intensify global warming [22, 28]. In contrast to the majority of processes described previously, the novel process of Flash Carbonization^{TM} is highly efficient. Themochemical equilibrium calculations set a limit on the maximum yield of carbon that can be obtained from any given type of biomass feedstock [5]. The process of Flash Carbonization^{TM} produces fixed-carbon yields which approach—and in some cases obtain—this thermochemical equilibrium limit, after reaction times of as little as 20 to 30 minutes [13]. This is most likely due to the elevated operating pressures unique to this process[8]. It is theorized that, when exposed to elevated pressure, the unstable tarry vapors produced by pyrolysis are more likely to decompose on the surface of existing charcoal, producing a type of secondary charcoal. This phenomenon is believed to be responsible for the increase in fixed-carbon yields (at the expense of tar production) observed at elevated pressures [27]. Additionally, the fact that elevated pressures have been experimentally observed to favor exothermicity and a reduction in onset temperature of pyrolysis for a variety of biomass feedstock helps explain the success of the Flash Carbonization^{TM} technique [5]. Typical yields from the Flash Carbonization^{TM} process may be expressed as charcoal yields ranging between 29.5 and 40.0%, or as the more useful fixed-carbon yield values ranging from 27.7 to 30.9% [13][9].

Although interesting from a scientific perspective, these increased yields are not perceived as the primary advantage of the Flash Carbonization^{TM} process. Instead, the true benefit lies in the reduction in processing time when compared to all other existing methods. This is due to the fact that, providing the biomass feedstock is plentiful, length of carbonization time and labor cost, not yields, are what govern the economics of charcoal

[8]For example, as pressure was increased from 0.4 MPa to 3.3 MPa, the fixed-carbon yield of macadamia nutshell charcoal was found to increase from 31.9 to 35.7% (y_{char} increased from 40.5 to 51.0%). This result was observed in a precursor of the Flash Carbonization^{TM} system [19].

[9]For feeds such as Leucaena wood, oak wood, corncob, and macadamia nutshells.

production [5]. In this area, the Flash Carbonization™ process shows its true merit. Because of the high combustion rate of the secondary vapors in the presence of oxygen at elevated pressure, and mass-transfer limitations which inhibit oxygen from reacting with the surface of the carbon, Flash Carbonization™ exhibits conversion times that far surpass any competing process without loss of process efficiency [13].

Chapter 3

The Laboratory-Scale Flash Carbonization^{TM} Reactor

3.1 Description of Apparatus

3.1.1 Overview

As shown in Figure 3.1 the lab-scale reactor consists of a pressure vessel into which a canister containing biomass is lowered. Once the pressure vessel is sealed, an electric heater is employed to ignite the contents of the canister. Primary airflow for the process is supplied from the air accumulator system. A catalytic afterburner may be attached to the outlet of the process to reduce pollutants in the exhaust stream. When desired, secondary air from a separate compressed air cylinder can be provided to improve the performance of the catalytic afterburner.

Using the lab-scale reactor, the Flash Carbonization^{TM} process has been used to produce fixed-carbon yields that attain the thermochemical limit [6, 13]. Alternatively, charcoal with other desirable properties can be produced for specialized applications. Examples include low ash charcoal, which is desirable for metallurgical applications, and low resistivity charcoal that could potentially be used as a fuel in a carbon fuel cell [29]. A complete understanding of the laboratory-scale reactor offers many insights into the basics of the Flash Carbonization^{TM} process. Therefore, a detailed description of this device will be presented in this chapter.

3.1.2 Details of the Air Accumulator

The air accumulator, which is used as the source of primary air, is composed of a system of three high-pressure vessels (see Figure 3.2). These vessels are connected as shown

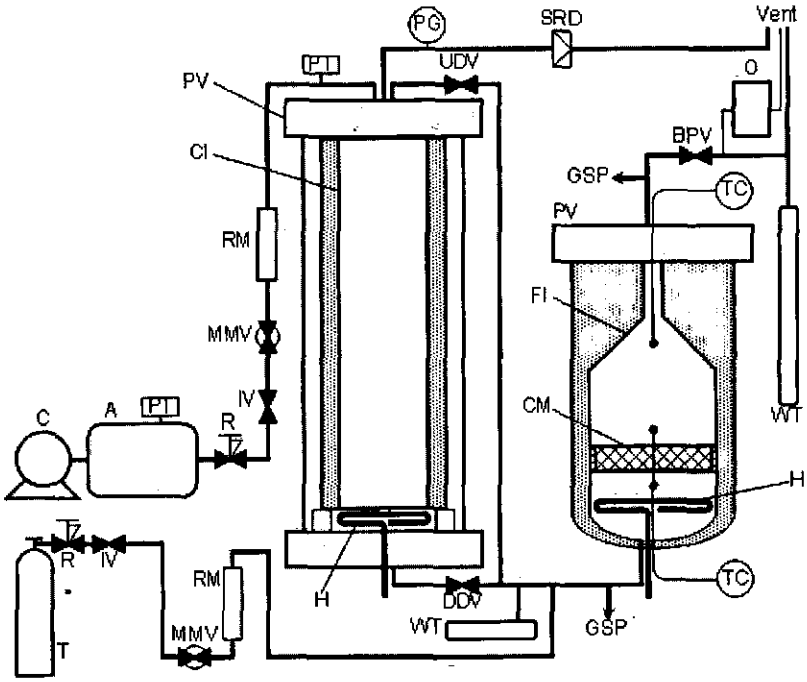

A, air accumulator; BPV, back-pressure control valve; C, compressor; CI, canister with insulation; CM, catalyst monolith; DDV, downdraft valve; FI, funnel with insulation; GSP, gas sampling port; H, electric heater; IV, isolation valve; MMV, micrometer valve; O, oxygen analyzer; PG, pressure gauge; PT, pressure transducer; PV, pressure vessel; R, regulator; RM, rotameter; SRD, safety rapture disk; T, air tank; TC, thermocouple; UDV, updraft valve; WT, water trap.

Figure 3.1 Overall schematic diagram of the lab-scale flash carbonization reactor and the catalytic afterburner (Figure created by Dr. Teppei Nunoura).

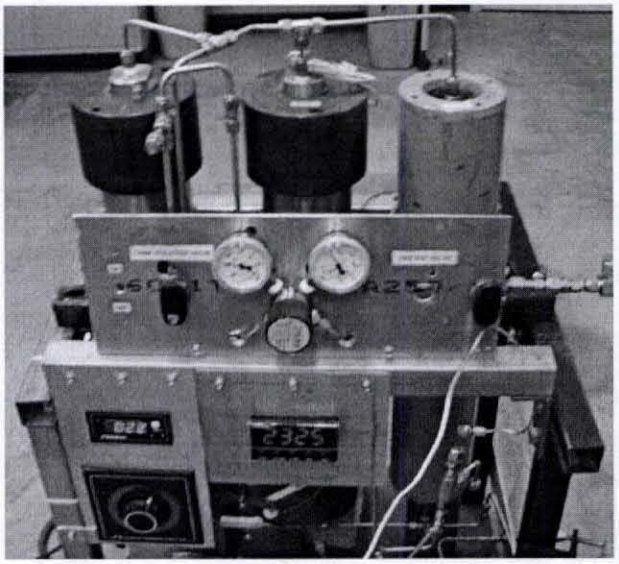

Figure 3.2 The accumulator system used to deliver primary airflow in the lab-scale reactor.

schematically in Figure 3.3. Valves allow for individual sections of the system to be pressurized as desired. The micrometer valve facilitates precise control of airflow. The pressure regulator ensures a constant pressure drives the flow. The maximum safe operating pressure of the accumulator system is 34.58 MPa (5000 psig).

3.1.3 The Carbonizer

The term "carbonizer" is used to designate the pressure vessel in which the Flash Carbonization^{TM} process occurs (see Figure 1.1). In the lab-scale Flash Carbonization^{TM} reactor, the vessel is rated at a maximum operating pressure of 6.10 MPa (870 psig) and consists of a pipe[1] welded to two flanges. These flanges may be sealed using gaskets and 12 bolts per flange. The top flange must be removed to facilitate loading of biomass into the carbonizer, and resealed prior to the beginning of each experiment[2].

The biomass feedstock is placed within an insulated stainless steel canister with an inner diameter of 9.5 cm and a length of 97.5 cm. The feedstock rests on a 1 mm thick stainless

[1]This pipe is 133 cm (52.4 in) in length with an inner diameter of 14.7 cm (5.79 in). The volume of the lab-scale carbonizer is therefore $\sim$0.0226 m^3.

[2]See the safe operating procedure manual of the lab-scale reactor (included in the appendix of this work) for more details.

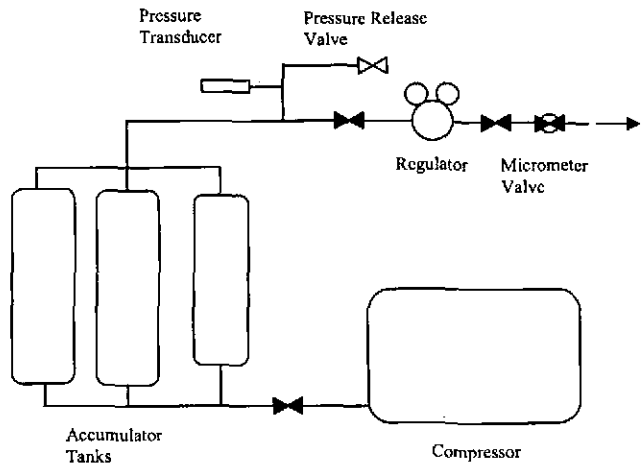

Figure 3.3 Detail of the accumulator system.

steel grate at the bottom of the canister. This canister is lowered into the pressure vessel and rests on a spacer above the electric heater. Once the canister is loaded, the distance from the bottom grate of the canister to the electric heater is 3 cm. An air-tight lid, equipped with an inlet air fitting, is mounted on the top of the canister. This lid is connected to the top flange of the pressure vessel by a short flexible tube. This configuration allows the primary airflow to be directed into the canister, and assures that the airflow will be forced to flow through the canister from top to bottom[3].

3.1.4 The Catalytic Afterburner

The purpose of the catalytic afterburner is to reduce the amount of criteria pollutants produced by the Flash Carbonization^{TM} process in order to satisfy federal and state emission requirements. The exhaust gas which exits the carbonizer enters the bottom of the afterburner, flows through the catalyst, and exits from the top. As a result of the presence of the afterburner, a variety of exhaust species (primarily CO, VOCs, and PM) are combusted and transformed into more benign products. Secondary air may be added in order to assist this process. It should be noted that during a Flash Carbonization^{TM} experiment, the catalytic afterburner operates at the same pressure as the carbonizer. An electric resistance

[3]The Flash Carbonization^{TM} reactors are also occasionally referred to as "downdraft carbonizers" due to this flow orientation.

heater, similar to the ignition heater in the carbonizer, is employed to preheat the catalyst prior to initiating a Flash Carbonization™ experiment.

Two catalytic afterburners currently exist. The first model was developed for eventual use in the demonstration reactor, but was tested with the lab-scale system for an extended period of time. This afterburner, which will be referred to as the "large afterburner", is shown in Figure 3.4. The large afterburner was recently moved to the demonstration reactor and a "small afterburner" was constructed. Both afterburners employ the same type of catalyst, which is composed of a mixture of palladium and platinum suspended in a binding agent, and supported on a monolith structure made from mullite extrudate. In the large afterburner, the catalyst is used in the original configuration supplied by manufacturer (Condar Company, CC-001), which can be described as cylindrical, honeycomb-type monolith disks. The diameter of one of these disks is 14.3 cm, the height is 3.81 cm, and the monolith has square channels with a density of 3.88 cells per square centimeter. To construct the large afterburner, eleven of these disks were set in a galvanized steel cylinder and funnel and then wrapped in insulation. This assembly was housed inside a pressure vessel as shown in Figure 3.1. In the small afterburner, one of these disks was crushed into smaller pieces and assembled into a packed bed configuration. The monolith pieces were placed within a stainless steel mesh pill and the pill housed within a 2 in (5.08 cm) hastelloy pipe as shown in Figure 3.5. Either of these afterburners can be removed or added to the lab-scale system fairly easily. Some lab-scale experiments described in future chapters were conducted without any afterburner (during the period when the small afterburner was being constructed).

3.1.5 The Electric Heaters

The electric resistance heater used to ignite the feed (ARi BXX-19B-45-5T) is located at the bottom of the carbonizer pressure vessel. This heater has been bent into a flat-spiral configuration and mounted to the bottom flange as shown in Figure 3.1. The distance from the electric heater to the bottom of the packed bed of biomass is 3 cm. This model of heater

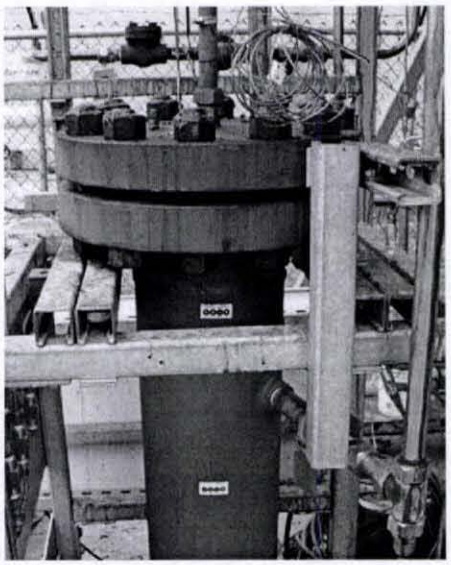

Figure 3.4 The large afterburner, designed for use with the demonstration reactor.

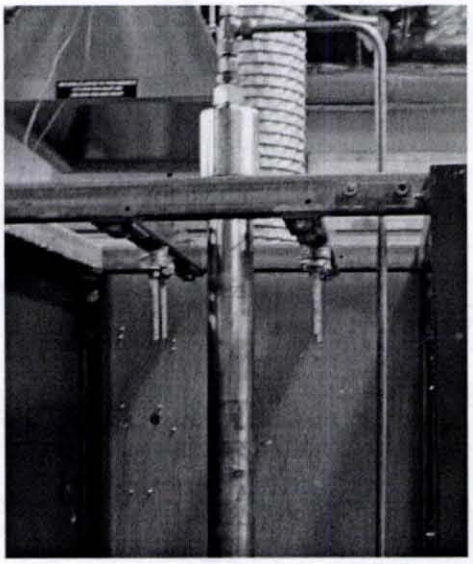

Figure 3.5 The small afterburner, designed for use with the lab-scale reactor.

is identical to the model of heater used in the demo-scale Flash Carbonization™ reactor[4]. Similar heaters are employed to preheat the catalyst monolith in the various incarnations of the catalytic afterburner as discussed above[5].

3.1.6 Variable Autotransformers

A variable autotransformer (also referred to as a VariAC) is a device which, when supplied a given AC input voltage, allows the user to vary the output voltage. There are two sizes of variable autotransformers currently employed in the lab. The first, (STACO 3PN1010, hereafter referred to as the "Small VariAC") provides the user with the ability to transform an input voltage to a variable lower voltage value. The second (Powerstat 1296D, hereafter referred to as the "Large VariAC") is similarly capable of stepping the voltage down, but may also be employed to boost the input voltage above its initial value. Both VariACs employ percentile dials to allow the user to control the output voltage. As indicated in Table 3.1, the Large VariAC is designed to accept an input voltage of 240 Volts, and has the ability to increase the voltage up to 280 Volts. Currently, we have the Large VariAC connected to a 208 Volt source. A ratio comparing the rated values to the operational values was used to establish that the Large VariAC is able to provide a maximum output voltage of 242.7 Volts. The large VariAC is used to deliver power to the primary ignition heater. The small VariAC is used to control the power delivered to the catalytic afterburner heater.

3.1.7 The Oxygen Meter

The sensor employed to monitor the concentration of oxygen gas present in the exhaust stream of the Flash Carbonization™ process is the Bacharach Oxor II. This device, which is based around an electrochemical cell, is capable of monitoring O_2 concentrations between 0-25% with an accuracy of plus or minus 0.8%. The response time of this device is ninety percent of the final value within 40 seconds. The maximum rated temperature for probe exposure is 538 °C. The exhaust sampling line of the lab-scale Flash

[4]For more details see Table 7.4 and the demonstration reactor chapter.
[5]The model number of the heater used in the large afterburner is ARi BXX-19B-50-11T.

	Small VariAC STACO 3PN1010	Large VariAC Powerstat 1296D
Operational Values		
Input Voltage	120 Volts	208 Volts
Output Voltage	0-120 Volts	0-242.7 Volts
Fuse Amperage	10 Amps	40 Amps
Rated Values		
Input Voltage	120 Volts	240 Volts
Output Voltage	0-120 Volts	0-280 Volts
Fuse Amperage	12 Amps	40 Amps

Table 3.1 Comparison of two variable autotransformers available in the lab.

Carbonization^{TM} reactor runs from the exhaust pipe of the catalytic afterburner to the sensor. This configuration requires that the exhaust valve to be open for the oxygen sensor to provide any information. Therefore, during the ignition phase of the process (when the exhaust valve remains closed) oxygen concentration data cannot be taken. Once the exhaust valve is opened (following the initiation of primary air delivery), values of O_2 concentration in the effluent of the process may be recorded. See the following section for more details of how a typical experiment is conducted.

3.2 Standard Experimental Approach

Prior to a normal Flash Carbonization^{TM} experiment, the canister containing biomass is lowered into the reactor pressure vessel. The compressor is employed to charge the accumulator tanks to approximately 31.13 MPa (4500 psig). The compressor is then shut off, and the pressure regulator on the air accumulator is set to a value on the order of 3.55 MPa (500 psig). Air is delivered from the accumulator to the reactor until the system has been charged to the desired operating pressure (usually within the range of 1.14 MPa to 2.17 MPa (150 to 300 psig)). Airflow is then halted and the system is monitored for 10 minutes to verify no leakage is occurring.

To begin the experiment, power is supplied to the electric heater and a flash fire is ignited within the packed bed of biomass. Approximately two minutes after the heater is switched

on, a steady flow of primary air is delivered from the accumulator[6]. Over the course of the experiment, the accumulator pressure falls from its initial value to approximately 13.79 MPa (2000 psig). As the flash fire propagates upward through the bed, the biomass feedstock is efficiently transformed into a high-yield biomass charcoal. A typical experiment using the lab-scale reactor lasts somewhere between twenty and sixty minutes. The exact reaction time required depends strongly on feedstock type and primary air flow rate. For each feedstock used, an air-to-biomass mass ratio (ABR) is established as explained in the following section.

3.3 Air-to-Biomass Ratios

Two types of air-to-biomass ratios will be discussed. The first, the delivered ABR, does not include the amount of compressed air initially present in the canister prior to initiating air delivery. The second type of ABR, the total ABR, includes both the air initially present in the canister and the air delivered during the experiment. These two types of ABRs are shown in Equation 3.1 and Equation 3.2 respectively.

$$ABR_{delivered} = m_{air,pri}/m_{bio} \tag{3.1}$$

$$ABR_{total} = \frac{m_{air,pri} + m_{air,init}}{m_{bio}} \tag{3.2}$$

Where $m_{air,pri}$ is the mass of the primary air delivered, $m_{air,init}$ is the mass of air initially present in the canister, and m_{bio} is the dry mass of the biomass in question. For example, delivered ABR values established by previous researchers include 1.16 kg/kg for corncob and 1.28 kg/kg for macadamia nutshell [13].

The amount of air delivered strongly effects how well the biomass is carbonized. ABR values for experiments in which the feedstock is over-carbonized would tend to be larger

[6]The inlet air flow rate is not exactly constant. In fact, due to compressibility effects, the mass flow rate increases slightly throughout the run. The details related to this phenomenon, and its effect on ABR values, will be explained in the chapter "Compressibility and Deviations from Ideal gas Behavior in the Accumulator System".

than values established for under-carbonized runs. Also note that the ABR values are only valid for a given set of operating parameters. For example, even if all other variables of a Flash Carbonization^{TM} run remain constant, if the operating pressure is increased, the total ABR value decreases [7]. The representative ABR value established for each specific feedstock is assumed to be derived from the most successful run to date for that feedstock and a given set of reactor operating parameters[7].

3.4 Properties of Common Feedstock Types

The types of feedstock which have been successfully subjected to the Flash Carbonization^{TM} process include: a wide variety of biomass (i.e. woods, nutshells, cobs, hulls), pure chemicals (i.e. fructose, cellulose), and petrochemical waste products (tires). Only two of the most successful agricultural waste feeds—macadamia nutshells and corncobs—will be discussed here. Examples of these wastes, and the carbons produced following Flash Carbonization^{TM}, are shown in Figures 3.6, 3.7, 3.8, and 3.9. Ultimate analysis of representative corncob and macadamia nutshells are shown in Table 3.2, typical yield and proximate analysis values of the charcoal produced by these feedstock are shown in Table 3.3 [13]. Macadamia nutshell holds special promise as a feedstock because an abundance of this feed is produced as agricultural waste in the Hawaiian Islands. Similar arguments may be made with respect to the vast amounts of corncob available in other parts of the United States (as mentioned in the previous chapter). Additionally, for corncob, the fixed-carbon yield can obtain the thermochemical equilibrium limit [13]. A cross-section of a typical corncob is shown in Figure 3.10. Noticeable compositional differences exist between the relatively dense woody ring and the less-dense coarse chaff, fine chaff and pith. Chemically, corncobs are primarily composed of cellulose ($\sim$ 41%) and hemicellulose ($\sim$ 36%) [30]. These details will be relevant to the forthcoming discussion of the ignition properties of the Flash Carbonization^{TM} process.

[7] The most successful run is usually determined by comparing the fixed-carbon yield for a variety of runs with similar feedstock and operating conditions, then selecting the run with the highest value.

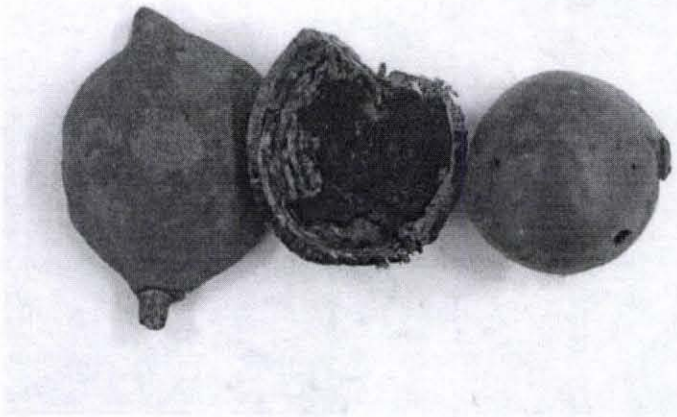

Figure 3.6 Typical macadamia nutshell feedstock.

Figure 3.7 Typical macadamia nutshell charcoal.

	Ultimate Analysis (% dry mass basis)						HHV
Feed Type	C	H	O	N	S	ash	(MJ/kg)
Corncob	43.42	6.32	46.69	0.67	0.07	2.3	17.4
Macadamia Nutshell	52.28	5.65	42.33	0.29	0.06	0.58	20.7

Table 3.2 Ultimate analysis of typical corncob and macadamia nutshell [13].

	Proximate Analysis (%)			y_{char}	y_{fC}	HHV
Feed Type	VM	FC	ASH	(%)	(%)	(MJ/kg)
Corncob	13.6	83.7	2.7	33.1	28	30.9
Macadamia Nutshell	9.8	89.3	0.9	34.5	30.9	33.3

Table 3.3 Proximate analysis of charcoal produced from typical corncob and macadamia nutshell [13].

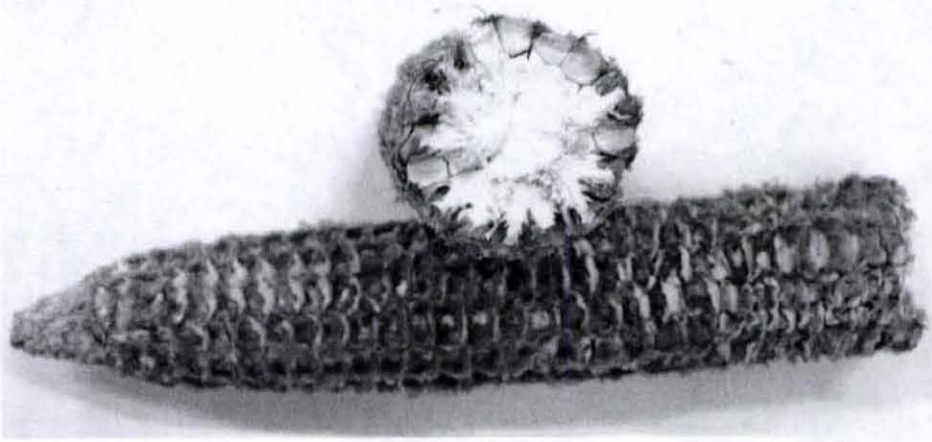

Figure 3.8 Typical corncob feedstock.

Figure 3.9 Typical corncob charcoal.

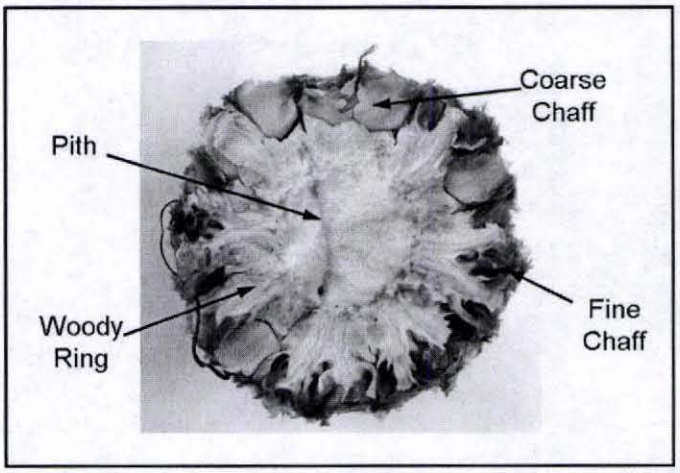

Figure 3.10 Cross-sectional view of a typical corncob.

Chapter 4

Airflow, Compressibility, and Deviations from Ideal Gas Behavior in the Accumulator System

4.1 Introduction

As we have seen in previous chapters, proper control of air delivery is vital to all methods of charcoal production. In the Flash Carbonization™ process properly prescribed levels of primary and secondary air delivery are critical not only to control the carbonization process but also to eliminate pollutants in the catalytic afterburner. Additionally, in order to accurately evaluate the ignition properties of the Flash Carbonization™ process, it is necessary to fully understand the initial amount of air present in the reactor. Therefore, a variety of studies were undertaken to determine how to accurately monitor and regulate airflow in the lab-scale reactor. The effect of compressibility in the accumulator system on air delivery was evaluated, and the previous method of determining air-to-biomass ratios (ABRs) improved. In this chapter a few fundamental gas flow concepts will be discussed, followed by the results and implications of the air delivery studies.

4.2 Gas Fundamentals

4.2.1 The Ideal Gas Law

One form of the ideal gas equation of state often used to describe the behavior of gases is shown in Equation 4.1.

$$PV = mRT \tag{4.1}$$

Where P is absolute pressure, V is volume, m is mass, R is the gas constant of the gas examined, and T is absolute temperature [31]. As we shall see in this chapter and in future chapters, this fundamental relationship is a very useful tool, which forms the basis for a wide variety of calculations.

4.2.2 Correcting Measurements to Normal Temperature and Pressure

When performing gas measurement experiments it is often necessary to simultaneously examine data taken at different conditions. To facilitate comparison between different data sets, all values must be converted to a common reference state. Two commonly used states are Standard Temperature and Pressure (STP) and Normal Temperature and Pressure (NTP). STP is defined as a temperature of 273.15 K and a pressure of 101.325 kPa (14.696 psia). The condition of NTP (also referred to as Standard Ambient Temperature and Pressure) is defined as a temperature of 298.15 K and a pressure of 101.325 kPa (14.696 psia) [32]. For example, to correct a measured volume of gas, which was recorded at room conditions, to NTP Equation (4.1) can be manipulated to arrive at the following expression.

$$V_{NTP} = \frac{V_{Room} P_{Room}}{T_{Room}} \frac{T_{NTP}}{P_{NTP}} \tag{4.2}$$

Unless specifically stated otherwise all reported gas data in this work has been corrected to NTP.

4.3 Gas Flow Measurement Devices

4.3.1 The Wet Gas Meter

The "wet test" or "wet gas" meter employed for airflow tests in the R^3 lab is the Shinagawa Wet Gas Meter W-NK-0.5A. This device is a net-volume integrating flowmeter that consists of a rotating drum immersed in a seal fluid through which the sample gas is passed. The wet gas meter allows volume measurements to be taken irrespective of the specific gravity and viscosity of the gas examined. Deionized water is used as a seal fluid to reduce corrosion inside of the meter. The wet gas meter's primary function is to measure the total volume

of gas that flows through it. However, the meter can also be used in conjunction with a stopwatch to measure volumetric flow rate.

The volumetric flow rates normally employed in Flash Carbonization™ experiments are much larger than the maximum flow rates the wet gas meter can tolerate[1]. Therefore, direct measurement of airflow rate during flash carbonization experiments was not possible with this device. However, gas flow experiments conducted at lower flow rates were successfully employed to study the accumulator system individually. Prior to conducting these experiments with the wet test meter a comparative calibration was conducted to ensure it was functioning properly. This was accomplished by employing the soap-film method as detailed in the following section.

4.3.2 The Soap-film Meter

The device used for the soap-film method will be referred to as the soap-film meter. It consists of a graduated vertical glass tube through which airflow can be routed. At the bottom of the tube is a soap and water solution contained within a rubber bulb reservoir. When the bulb is squeezed, it releases a soap film into the cylinder, which rises at the same speed as the flowing gas, and may be timed between two fixed points. If high accuracy is critical, photoelectric detectors may be employed to reduce errors associated with timing [33]. However, in the case of the wet gas meter calibration preformed for this work a stop watch was used for the sake of simplicity.

In order to perform the comparative calibration, the wet gas meter and the soap-film meter were connected in series, and a steady flow of air was passed through the system. Fifteen data points were taken. The mean wet gas flow meter value was 4.68±0.034 L/min, while the mean soap-film meter value was 4.73±0.119 L/min. A Student's t-test was performed on this data, and it was found that the null hypothesis could not be rejected. Therefore, the values reported by the wet gas meter and the bubble test meter could not

[1]The volumetric flow rate measurement range for this meter is from 1 to 300 L/h.

be said to differ significantly (90% confidence). This implies that the wet gas meter was functioning correctly.

4.3.3 Rotameters

The simplest rotameter design, which is also referred to as the "ball-and-tube" design, consists of a ball float located inside of a vertically mounted clear tube. The tube is slightly tapered in bore, with the diameter decreasing downwards, so that the airflow travels along the axis of the tube and suspends the float until a point where the downward force created by the weight of the ball is balanced by the upward force of the airflow. The type of rotameters employed in the R^3 lab (Matheson, FM-1050) are of the ball-and-tube design and have two balls in each tube. The first ball is stainless steel and the second is glass.

Although rotameters of this type are useful for qualitatively indicting volumetric flow rates, it is difficult to take accurate flow measurements with these devices in pressurized systems. This is due to the fact that manufacturers commonly supply a calibration table comparing the reading of the rotameter to a given flow rate of a specified gas (i.e. air) at NTP. If the operating pressure of the system is not atmospheric, the rotameter must be re-calibrated. Additionally, a sphere is not considered to be the ideal shape for a rotameter float because the type of flow past a sphere is liable to change suddenly in a narrow Reynolds-number range [33]. The unsteadiness which results from this problem, as well as the ability of the balls to rotate about a horizontal axis, have been observed in the rotameters employed in the R^3 lab. These types of problems contribute to the difficulty in taking accurate measurements with these rotameters.

In addition to the commonly recognized difficulties mentioned above, the use of rotameters in the lab-scale Flash Carbonization^{TM} has additional problems. Unexpectedly, during lab-scale experiments the primary airflow rate indicated by the rotameter increased as the experiment progressed—despite the fact that the rate-of-change of pressure in the accumulator was maintained at a constant value. Initially this was attributed to the rotameter deficiencies mentioned previously. However, after multiple experiments in which

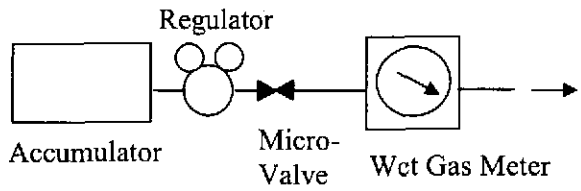

Figure 4.1 Experimental setup employing the wet gas meter. This setup was used to measure the volume of the accumulator, and for measurements related to compressibility.

the indicated volumetric flow rate was observed to consistently increase, an investigation of this phenomenon was initiated. The reasons for this behavior will be explained in the subsequent parts of this chapter.

4.4 Accumulator System Volume Measurement

In order to measure the total volume of the accumulator, the system was initially charged to a low pressure (approximately 75 psig). The wet gas meter was attached directly downstream of the micrometer valve as shown in Figure 4.1. The gas in the accumulator was allowed to escape and the volume of escaped gas V_{Lost} noted. The room temperature T_{Room} and room pressure P_{Room} were also recorded. The temperature at the wall of the accumulator was monitored by a type-K thermocouple during this experiment and was found to always be equal to room temperature.

Equation (4.1) can be manipulated to calculate the equivalent mass of gas m_{Lost} that passed through the wet test meter as follows.

$$m_{Lost} = \frac{P_{Room} V_{WGM}}{R T_{WGM}} \tag{4.3}$$

V_{WGM} is the volume of air that was recorded passing through the wet gas meter. P_{Room} and T_{WGM} are the pressure and temperatures recorded at the wet gas meter. For air, R has a value of $287 \frac{m^3 Pa}{kgK}$ [31]. The volume of the accumulator V_{Accum} can then be found using the following equation.

$$V_{Accum} = \frac{m_{Lost} R T_{Room}}{P_{Lost}} \tag{4.4}$$

Where P_{Lost} is the change in pressure in the accumulator. Using this method the total volume of the accumulator system was found to be 9.33 L.

4.5 Compressibility's Effect on Mass Flow Rate

For the pressure and temperature range commonly employed in the air accumulator[2] interactions between individual molecules have a significant effect on the behavior of air. The resulting intermolecular repulsive forces lead to a lower air density than would be predicted by the ideal gas law. Introducing a compressibility factor Z compensates for this deviation from ideal gas behavior as shown in Equation 4.5 [34].

$$PV = mRTZ \tag{4.5}$$

From this relationship, a method to determine the mass flow rate leaving the accumulator can be developed. First, it is assumed that the accumulator volume is constant, and that the temperature of the gas in the accumulator does not change significantly ($T \approx T_{NTP}$). The compressibility factor can then be said to vary only with pressure. If this is true, rearranging and taking the derivative of the above equation with respect to pressure yields Equation 4.6.

$$\frac{dm}{dP} = \frac{V_{accum}}{RT}\left(\frac{Z - P\frac{dZ}{dP}}{Z^2}\right) \tag{4.6}$$

The motivation for manipulating the relationship in this fashion is that once we have values of Z, P, dZ/dP, dP/dt, and Equation 4.6, we can use Equation 4.7 to determine an approximate mass flow rate.

$$\dot{m} = \frac{dm}{dt} = \frac{dm}{dP}\frac{dP}{dt} \tag{4.7}$$

[2] 31.13-10.45 MPa (4500-1500 psig), close to 300 K.

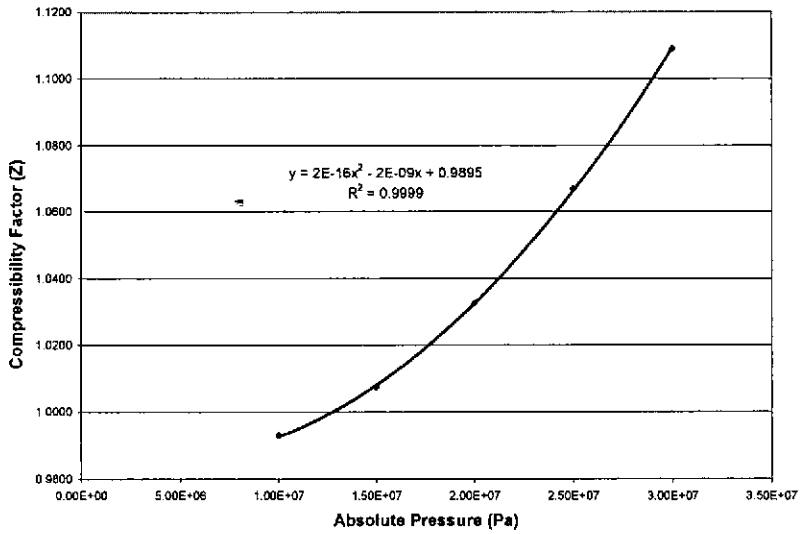

Figure 4.2 A second-degree polynomial fit was applied to accepted values for the compressibility factor of air at 300 K [11].

Note that in previous Flash Carbonization^{TM} experiments dP/dt was held approximately constant in an attempt to hold mass flow rate constant. Also note that a well known constant rate of air delivery promotes reproducibility of experiments and is desirable for modeling considerations.

4.5.1 Curve Fitting of Accepted Compressibility Values of Air

A table of accepted values for the compressibility factor of air was referenced [11]. A second-degree polynomial fit was applied to these referenced values over the pressure range of interest (see Figure 4.2), and an empirical relationships for Z as a function of pressure was developed. A parity plot (see Figure 4.3) demonstrates the validity of this fit. The form of the relationship is shown in Equation 4.8. Differentiating this equation with respect to pressure yields Equation 4.9.

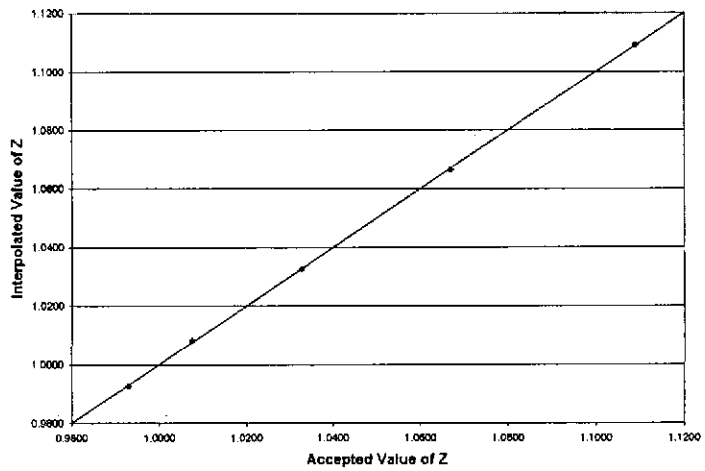

Figure 4.3 A parity plot compares the accepted values for the compressibility factor of air [11] to the interpolated values.

$$Z = a_0 + a_1 P + a_2 P^2 \tag{4.8}$$

$$\frac{dZ}{dP} = a_1 + 2a_2 P \tag{4.9}$$

Combining Equations 4.6, 4.8, and 4.9 yields Equation 4.10. The constant coefficients (a_0, a_1, and a_2) determined by the fit are shown in Equation 4.11. The unit of pressure used for this fit is the Pascal.

$$\frac{dm}{dP} = \frac{V_{accum}}{RT}\left(\frac{a_0 - a_2 P^2}{(a_0 + a_1 P + a_2 P^2)^2}\right) \tag{4.10}$$

$$a_0 = 0.98954 \quad a_1 = -1.523 \times 10^{-9} \quad a_2 = 1.837 \times 10^{-16} \tag{4.11}$$

Substituting back in to Equation 4.7 yields an expression which allows us to calculate the mass flow rate at any accumulator pressure within the normal operating range, providing we choose to maintain a constant known value of dP/dt.

$$\dot{m} = \frac{dm}{dt} = \frac{dP}{dt}\frac{V_{accum}}{RT}\left(\frac{a_0 - a_2P^2}{(a_0 + a_1P + a_2P^2)^2}\right) \tag{4.12}$$

By once again employing the ideal gas law, Equation 4.12 can be manipulated to give an expression for the volumetric flow rate corrected to NTP.

$$\dot{v} = \frac{dV}{dt} = \frac{dP}{dt}\frac{V_{accum}}{P_{NTP}}\left(\frac{a_0 - a_2P^2}{(a_0 + a_1P + a_2P^2)^2}\right) \tag{4.13}$$

As shown in Figure 4.4, the volumetric flow rate of air delivered increases as pressure in the accumulator decreases. Therefore, during a typical Flash Carbonization^{TM} experiment the mass of air-per-unit-time delivered at the beginning of the run is less than the mass of air-per-unit-time delivered near the end of the run. As discussed in the following sections, the failure to account for these compressibility effects led to slight errors in previously reported air-to-biomass ratios. Additionally, the unexpected behavior of the lab-scale rotameters can now be fully explained.

4.5.2 Experimental Validation of Interpolated Compressibility Values

It is now understood that—as a result of compressibility effects in the accumulator system—increased volumetric flow rates occur as a lab-scale Flash Carboniztion^{TM} experiment progresses toward completion. In order to fully illustrate that the increase in rotameter values discussed previously is solely a result of this fact, let us examine a representative lab-scale experiment conducted on February 27, 2004. As shown in Table 4.1, using a measured change in accumulator pressure over a one minute time interval, an approximate mass flow rate can be calculated for each time point (accounting for compressibility as described above). Setting the first value as a point of comparison, a normalizing ratio may

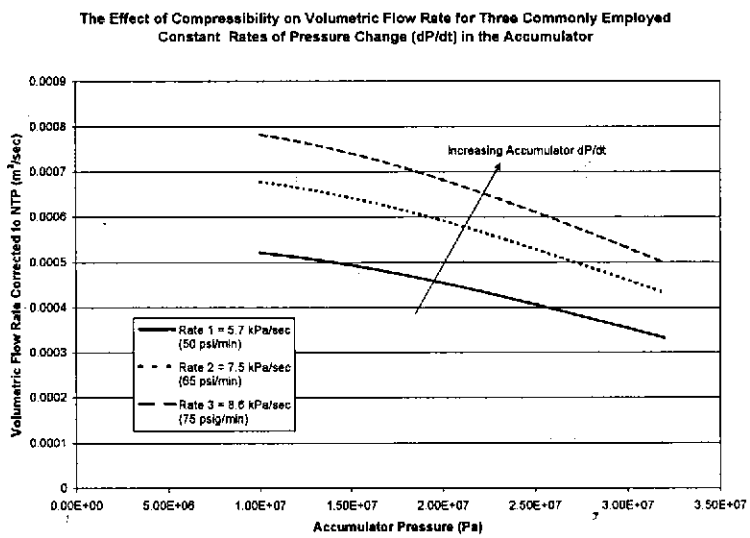

Figure 4.4 Due to compressibility effects, the volumetric flow rate of the air delivered will increase at lower accumulator pressures (assuming dP/dt is held constant). The three constant dP/dt rates shown here are values commonly employed in prior Flash Carbonization^{TM} experiments.

Time Period (min from heater power on)	10-11	28-29	43-44	54-55
Initial Gauge Pressure (psig)	4050	3146	2450	1850
Final Gauge Pressure (psig)	3997	3096	2401	1798
Approximate dP/dt (psi/min)	53	50	49	52
Approx. Mass Flow Rate (kg/s)	4.74E-04	5.21E-04	5.58E-04	6.26E-04
Rotameter Value (glass ball)	31	34	37	42
Normalized Mass Flow Rate	1.00	1.10	1.18	1.32
Normalized Rotameter Value	1.00	1.10	1.19	1.35

Table 4.1 Data from a representative *Flash Carbonization*™ experiment (conducted February 27, 2004). These values demonstrate that the unexpected rise in rotameter values, which initiated this compressibility investigation, can now be explained.

be established for each mass flow rate. When compared to a similar ratio established for the glass ball of the rotameter, we can see fairly good agreement between the rotameter values and the calculated mass flow rate[3]. It is also interesting to note that, although the desired flow rate was 50 psi/min, the actual rate-of-change of pressure in the accumulator varied from 49-53 psi/min. This result is typical, and demonstrates the difficulties associated with maintaining a perfectly constant dP/dt in the accumulator using the micrometer valve.

Additionally, the following experiment was performed to further confirm that the method of interpolating Z values presented above accurately represents the actual properties of air-flow from the accumulator system. Initially, the air accumulator was charged to a value of 29.06 MPa (4200 psig). The wet gas meter was connected in the same configuration used to measure the volume of the accumulator (see Figure 4.1). The air was allowed to escape the accumulator in increments of 1.38 MPa (200 psi) until a final value of 13.89 MPa (2000 psig) was reached. The volume and temperature of the gas were recorded at the wet gas meter. A stopwatch was used to insure the volumetric flow rate did not exceed the acceptable limit of the wet gas meter.

It was found that, as expected, the volume of air lost for each 1.38 MPa (200 psi) increment increased as the overall accumulator pressure decreased. By assuming a value of Z at the midpoint of the pressure values recorded, values of Z for all other data points may

[3]The glass ball appears to give more accurate results than the steel ball in this case. The normalizing ratios are employed because the rotameter has not been calibrated for the operating pressure of this run.

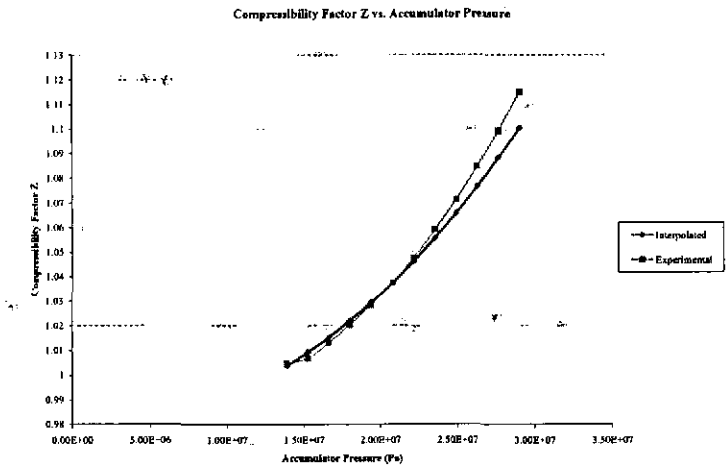

Figure 4.5 A comparison of interpolated and experimentally determined values of air's compressibility factor for the pressure range commonly employed in the accumulator system.

be calculated from this data. These experimental values are compared to the interpolated values in Figure 4.5. Note that Figure 4.5 shows fairly good agreement between the interpolated and experimentally determined values of Z for the majority of data points examined.

4.6 Lab-scale Reactor and Canister Void Volume Measurement

One advantage of accurately knowing the amount of air delivered for any given change in accumulator pressure is the ability to easily estimate the apparent void volume of the entire lab-scale Flash Carbonization^{TM} system. Although the void volume varies—depending on what type of biomass is used as a feedstock, and whether or not an afterburner is attached to the system—an approximate value is still a useful number to know. With this in mind the following measurements were taken prior to the lab-scale Flash Carbonization^{TM} experiment conducted on April 12, 2005[4]. The pressures in the accumulator and the lab-scale reactor

[4]The feed loaded into the canister for this run was corncob (0.82 kg) and a metal beaker containing Inulin.

Pressure in Accumulator	Pressure in Lab-Scale System
2603 psig	1 psig
2217 psig	150 psig
2093 psig	200 psig
1853 psig	300 psig

Table 4.2 Reactor and accumulator pressures used to calculate an approximate system void volume for the lab-scale Flash Carbonization^{TM} reactor.

system (without the afterburner) were recorded at four different states as shown in Table 4.2. Using the method described above to account for compressibility effects, the mass of air which left the accumulator was determined. Using this mass value and the known temperature and pressure of the lab-scale system, a void volume value was determined for each state. The mean of these three values ($V_{void,lab}$=23.2 L) will be used to approximate the void volume of the lab-scale reactor (when the canister is filled with corncob) in future discussions.

A void volume of the lab-scale canister must be determined for each Flash Carbonization^{TM} experiment in order to know the amount of air initially available to react with the biomass, $m_{air,init}$. From this value, and assuming a known amount of delivered air, a total ABR value may be calculated (see Equation 3.2). The canister void volume calculation is accomplished by determining the apparent packed bed density of the biomass feedstock. This value varies depending on the feedstock employed in the experiment. Estimates of apparent packed bed densities for a variety of feedstock types have been determined by previous R^3 lab researchers. Once the apparent packed bed density of the feed is known, a void volume for canister, $V_{void,c}$, may be determined by subtracting the volume occupied by the feed from the known volume of the empty canister.

4.7 Previous Method of Determining ABR Values

The method employed by previous researchers in the R^3 lab to determine air-to-biomass ratios was developed without accounting for compressibility effects in the accumulator system. Examples of ABR values with errors of this type are those reported in the paper "Flash Carbonization of Biomass" [13]. Because the source of this error is directly related to

the amount of air delivered from the accumulator during the experiment, we will focus on the delivered ABR values instead of the total ABR values. The previous method of calculating the initial amount of air present in the system needs no correction because it was based on the fairly low operating pressures of the lab-scale reactor, for which compressibility effects are negligible. To put it another way, the total ABR values are still in error, but only due to the errors in the air-delivered component[5].

Previously, to establish delivered ABR values, the initial pressure and temperature[6] of the accumulator system was recorded prior to each Flash Carbonization™ experiment. Once the run was concluded, the final accumulator temperature and pressure were also recorded. Using these values and an older estimate of accumulator volume[7], the total mass of air delivered was determined using the ideal gas law. When divided by the dry mass of the fuel, a delivered air-to-biomass ratio was established as shown in Equation 4.14.

$$ABR_{deliv,old} = \frac{m_{air,deliv}}{m_{bio}} = \frac{m_{air,i} - m_{air,f}}{m_{bio}} = \frac{\frac{P_i V_{old}}{RT_i} - \frac{P_f V_{old}}{RT_f}}{m_{bio}} \tag{4.14}$$

Where the subscripts i and f designate the initial and final states of the accumulator respectively.

4.8 Updated Method of Determining ABR Values

By applying the knowledge gained from studying the effects of compressibility in the accumulator system, a more accurate way to calculate ABR values has been established. The first improvement was to measure the volume of the accumulator system in a more rigorous fashion as discussed above[8]. Secondly, by including a value of Z (determined using Equation 4.8) for both the initial and final state of the accumulator system, the delivered

[5] Recall, $ABR_{total} = \frac{m_{air,deliv} + m_{air,init}}{m_{bio}}$.

[6] As recorded at the outer wall of the accumulator system.

[7] The volume of the accumulator system was previously estimated to be 8.23 L using experiments similar to the ones described in the "Accumulator Volume Measurement" section of this chapter. However, in these previous experiments high accumulator pressures (~3000 psig) were used to make this measurement and compressibility effects were not accounted for.

[8] The improved value for accumulator volume is 9.33 L.

Feedstock	LW	LW	LW	OW	OW	CC	MS
Run Date	020214	020930	020311	020221	020327	020404	020510
Dry Mass of Biomass (kg)	1.231	0.898	1.170	1.183	1.247	0.437	1.100
Initial Guage Pressure (psig)	3041	3183	3078	3124	3107	3032	3175
Final Guage Pressure (psig)	1651	1537	2161	2203	2081	2270	1069
Old Delivered ABR (kg/kg)	0.76	1.22	0.53	0.53	0.55	1.18	1.28
New Delivered ABR (kg/kg)	0.78	1.26	0.54	0.53	0.55	1.18	1.35
Percent Error (%)	3.26	3.07	0.73	0.12	0.73	0.21	4.99

Table 4.3 A comparison of the updated and previous methods for determining air-to-biomass ratios. Feedstock types: LW leucaena wood, OW oak wood, CC corncob, MS macadamia nut shell.

ABR value can be reported with greater accuracy. A summary of this approach is shown in Equation 4.15.

$$ABR_{deliv,new} = \frac{\frac{P_i V_{accum}}{RT_i Z_i} - \frac{P_f V_{accum}}{RT_f Z_f}}{m_{bio}} \tag{4.15}$$

4.9 Comparison of the Updated Method to the Previous Method

To compare the results of delivered ABR values calculated using Equation 4.14 and Equation 4.15, it is useful to determine a percentage error value by using Equation 4.16.

$$PE = \left(\frac{ABR_{deliv,new} - ABR_{deliv,old}}{ABR_{deliv,new}}\right)(100\%) \tag{4.16}$$

As shown in Table 4.3 we see that the old method always underestimates the amount of air leaving the accumulator system, and therefore reports a smaller delivered ABR than the new method. As should be expected, the amount of error increases with the amount of air delivered. While the error associated with the old method is not very large (maximum ~5 % for the cases considered), the improved method of calculating ABR values offers increased accuracy for minimal additional computational effort.

Chapter 5

Deflagration Fundamentals

5.1 Introduction

Perhaps the most dangerous form of combustion, the threat of explosion is present in many industrial and scientific applications. The potential for costly structural damage and loss of human life associated with even small incidents makes the field of explosion control and prevention a very large and complex area of study. An in-depth understanding of the parameters related to explosions is vital to ensure safe design and operation of any process in which an explosion could potentially occur.

Unfortunately, explosion behavior is exceedingly difficult to predict, and currently no universal model for explosion phenomena has been developed. Therefore, engineers entering the field of explosion prevention and control can quickly be overwhelmed by the wide variety of theoretical, semi-empirical, and empirical studies available, most of which are valid only for very specific conditions [35, 36, 37, 38, 39]. Due to the fact that, under certain circumstances, the ignition properties of the Flash Carbonization™ process resembles an explosion, the goal of this chapter is to provide an overview of one subsection of the field of explosions—the study of deflagrations in closed vessels—and to summarize the basic information available in the literature regarding this topic. In later chapters we will compare and contrast these types of deflagrations to the ignition behavior of the Flash Carbonization™ process.

5.2 Classification of Explosions

In order to fully classify explosions as a unique type of combustion phenomenon[1], an effort must be made to illuminate the characteristics which separate explosions from normal fires. The major distinction between fires and explosions is the rate of energy release. In a normal fire energy is released relatively slowly from the fuel. In an explosion the release of energy occurs suddenly, typically on the order of microseconds. Additionally, the consequence of an explosion is a rapidly moving pressure or shock wave, resulting from the rapid expansion of gases, which is large enough in magnitude to be potentially harmful [40].

Explosions can be classified based on the speed at which they propagate as either deflagrations or detonations. The reaction front of a deflagration proceeds at a speed less than the speed of sound. The reaction is propagated primarily by conduction and diffusion of energy and free radical species into the unreacted fuel oxidant mixture. A detonation proceeds at a speed greater than the speed of sound, and propagates through compressive heating of the unreacted mixture. In general, detonations are more dangerous than deflagrations because they produce higher peak overpressures [41]. The focus of this chapter is deflagrations; detonations will only be mentioned in passing. This limited focus is due to the fact that steps may be taken to mitigate the potentially harmful results of a deflagration, primarily through the use of venting techniques. In contrast, it is impossible to successfully vent a detonation [42, 43]. Additionally, under some conditions, the ignition behavior of the Flash Carbonization™ process closely resembles slow deflagration behavior.

5.3 Experimental Techniques for Evaluating Deflagrations

The most common experimental setup used to study deflagrations is shown in Figure 5.1 and Figure 5.2. This apparatus consists of a 20-liter sphere connected to a gas supply system. Prior to a test the sphere is evacuated, and a desired gas mixture and initial pressure is set. The gas concentration values are converted to partial pressures, and solenoid operated

[1]Explosions also occur without combustion. An example of a mechanical explosion occurs when an automobile tire blows out. Rapid phase changes can also create explosions, such as when a vessel containing a liquefied gas stored above its boiling point is ruptured.

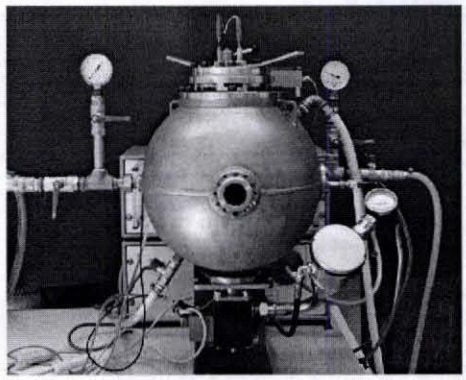

Figure 5.1 A 20-liter sphere used to test the deflagration properties of gaseous mixtures.

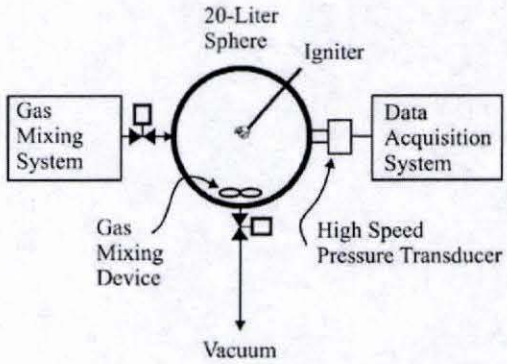

Figure 5.2 Schematic representation of the test apparatus shown in 5.1 [41].

valves—controlled by feedback from a high speed pressure transducer—inject the proper amount of gas to establish the initial experimental conditions.

A magnetic stirrer is used to ensure a homogonous mixture. Following a short delay to allow turbulence to dissipate once the mixer is stopped, the mixture is ignited through the vaporization of a thin strip of wire (similar to a fuse) or by spark ignition [44]. The pressure behavior of the system as a function of time is then recorded.

5.3.1 Results of Deflagration Experiments

A typical pressure vs. time curve resulting from the experiment described above is shown in Figure 5.3. Multiple experiments of this type may be conducted to determine the upper and lower flammability limits of the mixture in question. Two very important parameters

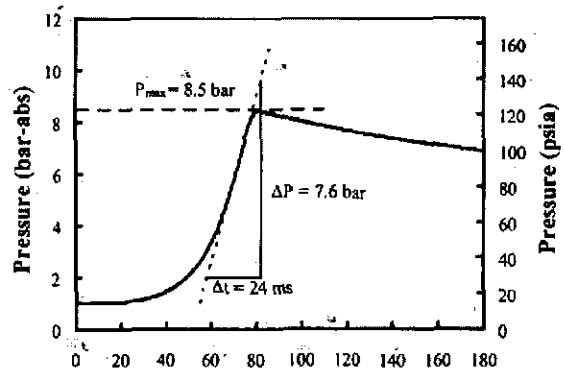

Figure 5.3 A typical Pressure vs. Time (ms) curve for a deflagration in a 20-liter sphere test apparatus [41].

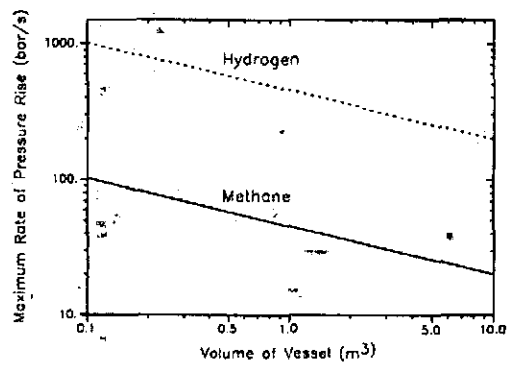

Figure 5.4 The cubic law indicates that a constant deflagration index K_G may be established [40].

used to characterize the behavior of combustible gas systems result from this type of pressure data. The first, P_{max}, describes the maximum pressure observed. The second is the maximum slope of the curve $(dP/dt)_{max}$. Unlike the maximum explosion pressure, which is not significantly affected by changes in vessel volume, $(dP/dt)_{max}$ does depend on the size of the vessel.

However, as shown in Figure 5.4, a plot of the log of the maximum rate of pressure change versus the log of the test vessel volume frequently produces a straight line with a slope of -1/3. This trend is known as the "cubic law" [40]. The cubic law leads to the establishment of a value referred to as the deflagration index, K_G. For a given gas mixture and set of initial conditions, K_G is a constant defined by the following equation.

	Maximum Pressure P_{max} (barg)			Deflagration Index K_G (bar-m/sec)		
Chemical	NFPA 68	Bartknecht	Senecal	NFPA 68	Bartknecht	Senecal
Hydrogen	6.9	6.8	6.5	659	550	638
Methane	7.05	7.1	6.7	64	55	46

Table 5.1 Reported optimum (greatest) values for deflagration indices and maximum pressures of hydrogen and methane in air from three sources. There is good agreement for values of P_{max}, but the deflagration index is more difficult to consistently measure (Adapted from [41]).

$$K_G = (dP/dt)_{max} V^{1/3} \tag{5.1}$$

K_G is a very important parameter for the design of safety systems; a larger K_G value indicates a more violent explosion, with less time available for venting measures to take effect. Unfortunately, K_G is not a physical property of the fuel in question. Instead this value is sensitive to the composition of the mixture, the mixing within the vessel, the shape of the reaction vessel, and the energy of ignition source. Therefore, if the K_G value is to be used as a design parameter it is very important that experimental conditions mimic those of the intended application as close as possible (the spherical test vessel shown above may not be appropriate) [40]. In fact, the value of K_G commonly differs between researchers [44]; some of these values are shown in Table 5.1. However, K_G values determined in identical test vessels can be compared to indicate which gas mixture exhibits the most dangerous explosion characteristics.

5.3.2 Effect of Initial Conditions

There are many parameters which affect the outcome of a deflagration. An increase in initial pressure leads to a linear increase in both P_{max} and $(dP/dt)_{max}$. However, an increase in initial temperature creates an inverse change in the maximum pressure attained. As shown in Figure 5.5, the initial composition of the mixture also has a significant influence on the pressure characteristics of the system. Normally, the optimum (largest) values of P_{max} and $(dP/dt)_{max}$ are observed near stoichiometric concentrations. However, the

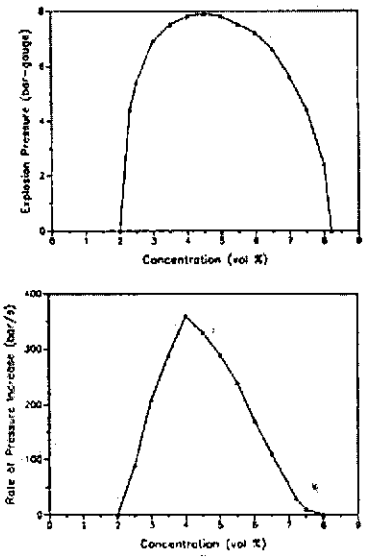

Figure 5.5 The effect of concentration of the fuel on P_{max} and $(dP/dt)_{max}$ [40].

optimum values for both of these indices do not necessarily occur at exactly the same concentration. Initial turbulence in the gas mixture leads to a somewhat higher maximum pressure and significantly higher rates of pressure rise. In addition, turbulence is created during a deflagration as gases move past any obstacles present in the enclosure. This helps facilitate a phenomenon known as deflagration to detonation transition [40].

5.4 Deflagration to Detonation Transition

It is possible for a deflagration to develop a large enough velocity head (ramming pressure) to transition to detonation behavior. This behavior occurs when sufficient energy accumulates in the deflagration pressure wave to create a high level of adiabatic compression. This compression leads to autoignition and detonation. As shown in Figure 5.6, this can be observed by irregularities in the curve when the pressure indices are plotted vs. concentration. Under the experimental conditions used to create Figure 5.6 the propane/air mixture begins to transition to detonation for a mixture which is approximately 5 percent propane by volume [45]. Deflagration to detonation transitions are most common in pipelines due to the geometric properties of pipes and channels [41].

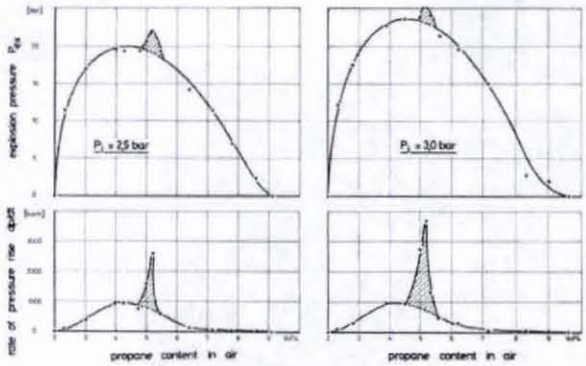

Figure 5.6 Characteristics of a fuel which shows the beginning of deflagration to detonation transition at certain concentrations [45].

Figure 5.7 Silo explosions are an example of the highly combustible properties exhibited by many dusts.

5.5 Dust Deflagrations

A dust is defined as a finely divided solid 0.016 in or less in diameter. The dusts of most solid combustible materials, if dispersed in air and exposed to an ignition source, can burn extremely rapidly leading to an explosion [41]. Dust explosions are most common in the flour milling, grain storage and coal mining industries. Grain explosions in silos can be especially devastating as shown in Figure 5.7. The deflagration index for dust, K_{St}, is defined in an identical fashion to K_G. However, experimental determination of the explosion characteristics of dusts involves some slight modifications to the experimental procedure discussed above. This topic is covered in the following references [45, 41, 42].

Chapter 6

Violent Ignition Behavior of Pressurized Packed Beds of Biomass: A Factorial Study

6.1 Introduction

In laboratory-scale Flash Carbonization^{TM} experiments some fuels have been observed to ignite violently, resulting in a sudden drastic pressure rise ($\Delta P \sim$1 MPa within 2-3 seconds). This type of behavior has been observed for corncob and a variety of wood feedstocks, with corncob demonstrating the most violent behavior of any feed yet examined. Other feedstock types, such as macadamia nutshells, do not exhibit this type of ignition behavior. Additionally, this sudden pressure rise has not been observed for experiments conducted at reactor operating pressures below 1.14 MPa. Because this event could potentially be hazardous, a study of this phenomenon was undertaken in preparation for the scale-up of the Flash Carbonization^{TM} process.

6.2 Factorial Experimental Design

In order to examine this violent ignition behavior, an experimental design technique referred to as the "two-level full factorial method" was employed. This method is especially useful for indicating basic trends and showing interactions. Each variable or "factor" to be considered is assigned two levels, the higher value is designated with the "+" symbol, while the lower value is indicated with the "-" sign. The total number of experiments necessary is equal to 2^k, where k is the number of factors to be examined. In this study the influence of the following three factors are examined: reactor chamber pressure, feed moisture content, and supplied heater power. Additionally, each experimental condition was duplicated once, making this approach a 2^3 full factorial design with replication [46]. Primary advantages of

this method include: construction of plots that clearly display main effects and interactions between effects, and ease of statistical analysis.

6.3 Establishing the Factors

6.3.1 Moisture Content

The feed moisture levels employed in this study were achieved using two different pretreatments—oven-drying (-) and air-drying (+). Air-dried feed was simply removed from the storage container and allowed to equilibrate with the laboratory environment for one day prior to carbonization. Oven-dried feed was placed in a mechanical convection oven (Lindberg/Blue M01440A-1) at a temperature of 105 °C for a minimum of two days prior to carbonization. Following this pretreatment, the cobs appeared noticeably dehydrated; the exterior of the cob darkened somewhat from a reddish-orange color to a light brown, and the overall size of the cob decreased slightly. Samples subjected to oven-drying are designated "dry", while samples subjected to air-drying will be referred to as "wet". The moisture content of both dry and wet feedstock was determined as discussed in previous chapters. The mean moisture content (wet-basis) of the dry feedstock employed in this work was 1.5±0.67 %, while the wet feed had a mean moisture content of 11.4±0.42 %. The feed moisture content values for each of the experiments individually is shown in Table 6.1. The mass of the feedstock was recorded for each run immediately prior to the loading of the canister.

6.3.2 Pressure

Two different initial pressure levels were examined in this study—the "low" (-) value employed was 1.48 MPa (200 psig) and the "high" (+) value was 2.17 MPa (300 psig). These two values were selected based on prior experimental experience suggesting that these levels would produce significantly different system responses. Reactor chamber pressure was monitored using a high-speed pressure transducer (Omega PX602) connected to a SCXI

Run #	Date	Conditions[a]	Moisture Content(%) Wet Basis	Dry Basis
1	1/27/05	- - -	1.4	1.4
2	4/25/05	- - -	1.0	1.0
3	2/18/05	+ - -	1.5	1.5
4	4/12/05	+ - -	3.1	3.2
5	3/9/05	- + -	11.1	12.5
6	5/18/05	- + -	11.9	13.5
7	10/18/04	+ + -	11.5	13.1
8	4/5/05	+ + -	10.8	12.1
9	3/2/05	- - +	1.1	1.1
10	5/16/05	- - +	1.3	1.3
11	6/20/05	+ - +	1.3	1.3
12	5/24/05	+ - +	1.2	1.2
13	6/14/05	- + +	11.1	12.5
14	1/14/05	- + +	11.7	13.2
15	6/2/05	+ + +	11.2	12.6
16	3/22/05	+ + +	11.9	13.5

[a]See Table 6.2 for a description of these conditions

Table 6.1 Moisture content on both a dry and wet basis for the experiments conducted for the ignition study.

data-logging system (National Instruments) which was set to sample at a rate of 100 signals per second during the ignition phase of the experiment.

6.3.3 Heater Power

As discussed previously, by changing the settings of the VariAC a range of voltages may be supplied to the ignition heater in the carbonizer. Using a set voltage value, and the known resistance of the electric heater element at room temperature (5.4 Ω at 25 C), an initial value of apparent electrical power value may be calculated. For this study, two apparent electrical power levels of 1.8 kWe and 1.4 kWe were employed. From the known heated surface area of the heater (170.97 cm^2) these values may also be reported as 10.52 W/cm^2 and 8.19 W/cm^2. These heater power settings will be referred to as "high" (+) and "low" (-) respectively. Note that in past Flash Carbonization^{TM} experiments similar electric heaters have failed when the level of voltage supplied was too large. The high value of heater power

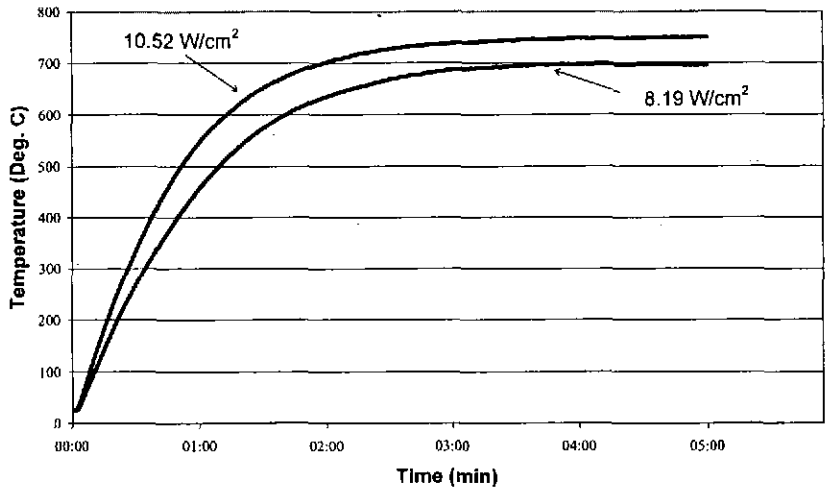

Figure 6.1 Temperature profiles of the electric heater at the two power levels examined. Note that these tests were conducted in open air.

was chosen to prevent this type of burnout, and the low value was chosen to ensure that ignition occurred within the first two minutes of every run (to allow for comparisons to prior work). As shown in Figure 6.1, in open air tests conducted at atmospheric conditions, these two heater power settings produce a maximum difference in heater temperature of ~90 °C within one minute, and stabilize to a final temperature difference of ~50 °C in roughly three minutes. A summary of the three factors examined in this study—initial reactor pressure, moisture content, and supplied electric heater power—is shown in Table 6.2.

6.4 Other Experimental Details

6.4.1 Basics

As mentioned in previous chapters, a wide variety of biomass feedstocks have been subjected to the Flash Carbonization™ process. However, for this study corncob was the sole feed

Factor	Level	
	-	+
A. Reactor Pressure	1.48 MPa	2.17 MPa
B. Moisture Content	Oven-dried	Air-dried
(Mean Values on a Wet-Basis)	(1.5 ± 0.67%)	(11.4 ± 0.42%)
C. Heater Power	8.19 W/cm^2	10.52 W/cm^2

Table 6.2 High and low levels for the three factors examined in the ignition study.

used. This limited choice of feedstock is due to the fact that, as mentioned above, the sudden pressure rise observed during the ignition phase of corncob experiments is most dramatic of any feedstock encountered thus far. The experimental apparatus employed in this study is similar to the setup described in the lab-scale reactor chapter. Therefore, only details relevant to the ignition process will be mentioned here. The catalytic afterburner was not attached to the system for these experiments.

To conduct a typical experiment for this study ~0.8 kg of corncob was placed within the canister. The lowest portion of the canister (approximately 15 cm in depth) was filled with cob which has been broken apart into smaller pieces, approximately 3 cm long by 1 cm in width and depth. The remainder of the canister was filled with whole corncobs. The practice of creating a bottom layer of broken pieces of corncob is a carryover from the method used by this laboratory to conduct prior corncob experiments. This procedure is believed to assist in the ignition of the reaction by increasing the amount of surface area of feed in close proximity to the electric heater.

6.4.2 Truncated Experiments

In most experiments preformed for this study, the Flash Carbonization^{TM} process was allowed to continue until the bed was fully carbonized in a fashion similar to the method described in previous chapters. However, during some experiments, the electrical heater was turned off immediately following the sudden pressure rise. The reactor was then rapidly purged with nitrogen gas to preserve the biomass bed in the state at which it existed immediately following the violent ignition. These truncated experiments were conducted in an attempt to visually examine the effects the violent ignition has on the feed. For these

Run #	Date	Feedstock	Mass of Corncob[a] (kg)
1	1/27/2005	Corncob, Pistachio Nutshell	0.79
2	4/25/2005	Corncob, Glucose	0.75
3	2/18/2005	Corncob, HMF, Fructose	0.80
4	4/12/2005	Corncob, Inulin	0.82
5	3/9/2005	Corncob, Inulin, Lignin	0.81
6	5/18/2005	Corncob, Sucrose[b]	0.82
7	10/18/2004	Corncob, Sucrose[c]	0.85
8	4/5/2005	Corncob, Macadamia Nutshell, Oat Hulls	0.56
9	3/2/2005	Corncob, Lignin, Indulin	0.75
10	5/16/2005	Corncob, Sucrose	0.84
11	6/20/2005	Corncob	0.88
12	5/24/2005	Corncob	0.84
13	6/14/2005	Corncob	0.89
14	1/14/2005	Corncob, Tire	1.01
15	6/2/2005	Corncob	0.88
16	3/22/2005	Corncob, Kraft Lignin	0.86

[a]Moist mass
[b]Ammonium phosphate doped
[c]Boron doped

Table 6.3 Masses of corncob for the ignition runs (and a list of the additional materials added to these runs for purposes not associated with this study).

runs, the mass of the feedstock after the experiment (following one day of stabilization to allow equilibration with laboratory conditions) was recorded, and a difference from the initial value was calculated. As shown in Table 6.3, occasionally a small amount of additional feedstock was added to the canister for special interests not associated with this study.

6.5 Method of Characterizing the Ignition Response

6.5.1 A Typical Response

A typical pressure-time curve is shown in Figure 6.2, a detail of the ignition period is shown in Figure 6.3[1]. The sudden pressure increase, which begins at approximately 56 seconds in this case, is attributed to the ignition of the biomass feedstock. The flame initiates at the bottom of the packed bed, near the location of the electric heater, and propagates quickly to the top of the bed—rapidly blackening the outer layer of each individual corncob—within a period of approximately five seconds (a simple mechanism describing this process will be proposed in subsequent sections). The sudden rise in pressure associated with this ignition

[1]This data is from the run conducted June 2, 2005 (Run #15).

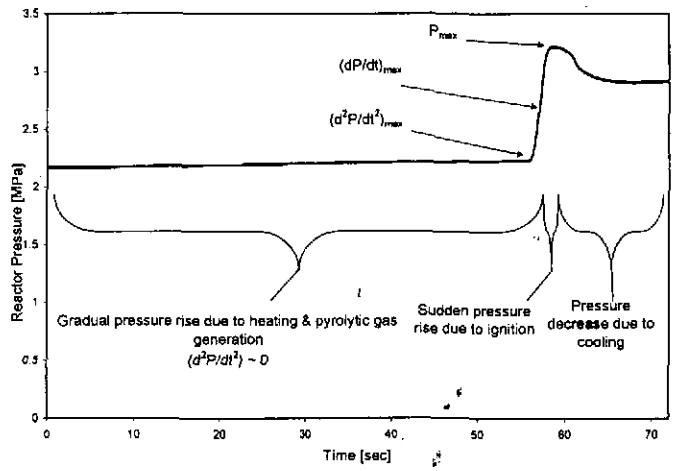

Figure 6.2 A typical pressure profile observed during the violent ignition phase of the Flash Carbonization^{TM} process (0 sec = ignition heater on).

is preceded by a much more gradual pressure rise, and followed by a decrease in pressure. This gradual pressure rise is likely due to the heating of the compressed air initially present in the reactor chamber, and the generation of some gaseous products due to pyrolytic reactions. Similarly, the pressure decrease, which follows the period of violent combustion, is associated with cooling of the gases in the system.

6.5.2 Defining the Response Parameters

From a plot of the type shown in Figure 6.2 three parameters, or system responses, of importance may be determined. The basis of the first parameter is the maximum pressure achieved, P_{max}. This peak pressure may be used to properly select future reaction vessels, and to determine set-points for automated venting devices. However, to facilitate comparisons between runs conducted at different initial pressures, it is often more convenient to represent P_{max} as a change-in-pressure value, ΔP_{max}. This value is established by simply taking the difference between P_{max} and the initial pressure. The second parameter

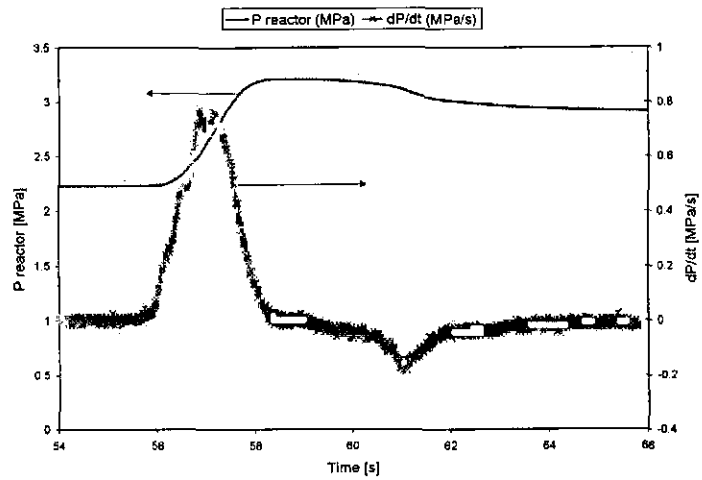

Figure 6.3 Typical values of pressure and (dP/dt) during the violent ignition phase of the Flash Carbonization^{TM} process (0 sec = ignition heater on).

of interest is the maximum rate of pressure rise, $(dP/dt)_{max}$, which can be viewed as characterizing the violence of the combustion phenomenon. The larger the maximum slope of the pressure vs. time curve, the less time available for safety measures—such as venting devices—to act. An approximate value of (dP/dt) was determined from the pressure data using the forward difference equation shown in Equation 6.1.

$$\frac{dP}{dt} = \frac{P_{n+20} - P_n}{t_{n+20} - t_n} \tag{6.1}$$

Where P represents a pressure data point, t a time data point, and the subscript denotes the index of the point in question. Because the sampling data rate was 100 signals per second, the time interval in the denominator of Equation 6.1 is equivalent to 0.2 seconds. The third parameter of interest is the period of time prior to the onset of ignition. This system response—which will be referred to as "time-to-ignition"—is measured from the moment of electric heater activation to the beginning of the sudden pressure rise. The

beginning of the pressure rise, which will also be referred to as the "point of ignition", is defined as the time at which the second derivative of the pressure vs. time curve reaches its maximum value. It should be noted that some elements of the method described above have been adapted from the field of gas and dust explosion protection as discussed in the previous chapter. Specifically, the first two parameters mentioned, $(dP/dt)_{max}$ and P_{max}, are identical to the parameters used to characterize the sudden rise in pressure produced by gaseous and dust deflagrations in closed vessels. Because these parameters are borrowed from this specialized field of study, a brief discussion of the similarities and differences between gaseous/dust deflagration behavior and the ignition of the large pieces of solid biomass fuel in the Flash Carbonization^{TM} process is warranted.

6.6 Comparison to Deflagration Behavior

As discussed in the preceding chapter, the experimental methods for studying the pressure rises produced by dust and flammable vapor deflagrations in enclosed vessels are fairly well established. In order to examine a desired gas or dust mixture, known amounts of the fuel and oxidant are ignited within a specialized spherical pressure vessel, and the pressure response of the system is recorded by a high speed pressure transducer [45, 44]. With the exception of the shape of the vessel, this experimental procedure is fairly similar to the one used for this ignition study. However, note that the typical time to reach the maximum pressure in a gaseous deflagration or dust explosion is on the order of 25 ms and the peak pressure generated is on the order of eight times the initial absolute pressure [41]. Even during the most violent ignitions of the Flash Carbonization^{TM} system the maximum pressure is reached much more slowly than in a deflagration ($\sim$2-3 sec from ignition to P_{max} in a typical Flash Carbonization^{TM} experiment) and the maximum pressures observed are at maximum only $\sim$1.6 times the initial absolute pressure of the system. Also note that the expected maximum rate of pressure rise in a grain deflagration of corncob grit is reported to be on the order of 21 MPa/s [47], while the maximum $(dP/dt)_{max}$ recorded in this study was 1.21 MPa/s. Regardless of the differences which exist between the violent ignition behavior

observed in the Flash Carbonization™ process and explosive deflagration behavior, the parameters mentioned previously, $(dP/dt)_{max}$ and P_{max}, are still useful for studying the Flash Carbonization™ ignition process.

6.7 Results of the Ignition Tests

Table 6.4 shows the results of the experiments conducted for this study. Recorded values of $(dP/dt)_{max}$ varied from 0.34 MPa/s to 1.21 MPa/s. For all runs, ignition occurred within 69 seconds (after power was delivered to the heater), and the values of ΔP_{max} ranged from 0.42 MPa to greater than 1.31 MPa. Unfortunately, the safety devices which protect the laboratory reactor from hazardous overpressures are designed to maintain the reactor pressure below 3.48 MPa. The first line of overpressure protection is a solenoid activated, pneumatically powered, ball valve (Marwin 7333RGS), controlled by the reactor pressure transducer. When pressures in excess of 3.48 MPa are achieved, this pneumatic valve opens, and the reactor chamber pressure decreases. Due to this necessary venting, when the violent ignition of the feed would have created pressures in excess of this upper system pressure value (runs #4 and #12) P_{max} was not accurately recorded.

6.8 Interpreting the Factorial Experimental Design

The influences of the three primary factors on the mean values of the system responses are shown graphically in Figure 6.4. In the case of $(dP/dt)_{max}$, an increase in initial pressure created an increase in the maximum rate of pressure rise. Additionally, moving from a wet feed to a dry feed similarly increased the violence of the ignition. For the case of ΔP_{max}, parallel trends to those of $(dP/dt)_{max}$ exist—an increase in initial pressure or a decrease in moisture content led to a greater maximum change-in-pressure value. Unfortunately, no clear trend exists for the time-to-ignition data. The mean ΔP_{max} values shown in Figure 6.4b include the runs in which venting prevented accurate determination of ΔP_{max}. To determine the mean values shown, a value of 1.31 MPa was substituted for all unknown ΔP_{max} values. These values are preceded by a greater-than sign to indicate this uncertainty.

Run#	Date	Factor A[a]	B[b]	C[c]	Response $(dP/dt)_{max}$ (MPa/s)	P_{max} (MPa)	ΔP_{max} (MPa)	Time-to-Ignition(sec)
1	1/27/05	-	-	-	0.37	1.96	0.48	21
2	4/25/05	-	-	-	0.46	2.12	0.64	56
3	2/18/05	+	-	-	0.81	3.09	0.92	44
4	4/12/05	+	-	-	1.05	>3.48[d]	>1.31	69
5	3/9/05	-	+	-	0.34	1.9	0.42	52
6	5/18/05	-	+	-	0.35	2.01	0.53	56
7	10/18/04	+	+	-	0.44	2.78	0.61	18
8	4/5/05	+	+	-	0.41	2.62	0.45	34
9	3/2/05	-	-	+	0.39	1.96	0.48	29
10	5/16/05	-	-	+	0.46	2.14	0.66	46
11	6/20/05	+	-	+	0.96	3.42	1.25	46
12	5/24/05	+	-	+	1.21	>3.48[d]	>1.31	47
13	6/14/05	-	+	+	0.43	1.99	0.51	40
14	1/14/05	-	+	+	0.36	1.94	0.46	40
15	6/2/05	+	+	+	0.77	3.21	1.04	56
16	3/22/05	+	+	+	0.57	2.98	0.81	37

[a] Initial Pressure "+"=2.17 MPa "-"=1.48 MPa
[b] Moisture Content "+"=Air Dried (11.4±0.42%) "-"=Oven Dried (1.5±0.67%)
[c] Heater Power "+"=10.52 W/cm^2 "-"=8.19 W/cm^2
[d] Necessary venting prevented accurate measurement of P_{max}

Table 6.4 Reaction conditions and experimental results of Flash Carbonization™ ignition experiments.

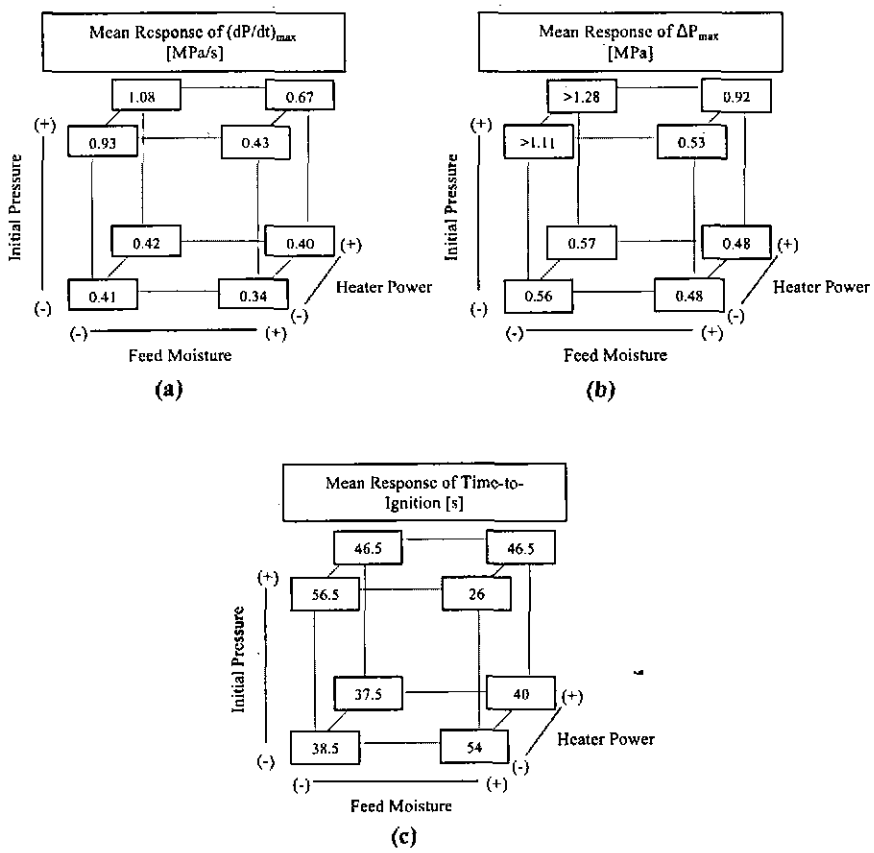

Figure 6.4 Graphical representation of mean full factorial results for (a) the maximum rate of pressure rise, (b) the maximum change in pressure, and (c) the time prior to ignition.

Table 6.5 quantitatively shows the influence of the three primary factors, their interactions, and the associated standard errors, for both the maximum rate of pressure rise and the time-to-ignition responses. Two primary factors, initial reactor pressure (A), and feed moisture content (B), as well as the interaction of these two factors (AB), have significant influence on $(dP/dt)_{max}$ (99% confidence interval). Note that the response of ΔP_{max} was not evaluated because of the two experiments in which venting prevented accurate recording of P_{max}. No trend appears to exist in the time-to-ignition data. Table 6.5 was constructed using the fundamentals of factorial experimental design, analysis of variance (ANOVA) techniques, and the F-statistic. Recall that the F-statistic employs mean square values from an ANOVA table to determine whether the null hypothesis can be accepted or rejected for each factor or interaction. Under the hypothesis that the influence of a main effect or interaction is zero, the corresponding F-value should be close to 1 (since both the numerator and the denominator of the F-value are estimating only the error variance in this case). However, if the null hypothesis is false, the numerator mean square will tend to be larger than the error mean square, and a large F-value will result. Based on this reasoning, F-values larger than a specified F-critical value lead to the rejection of the null hypothesis for a chosen confidence interval [48].

In the case of $(dP/dt)_{max}$, it can be determined that the interaction between the initial pressure and feed moisture content is significant (F-value>F-critical, 99% confidence). Therefore, although the primary factors of both initial reactor pressure and feed moisture content clearly influence $(dP/dt)_{max}$, they should not be examined separately [46]. Instead, the effect of these two factors ought to always be considered simultaneously in order to properly anticipate the maximum rate of change in pressure of the system. Heater power, as well as all of the interaction terms in which heater power is involved, cannot be said to significantly affect $(dP/dt)_{max}$.

Table 6.5 shows that statistically no trend can be said to exist in the time-to-ignition data, reinforcing the conclusion reached graphically above. The lack of a clear influence of heater power on any of the system responses may be due to inadequate differences between

	(dP/dt)max		Time-to-Ignition	
	Effect±Standard Error (MPa/s)	F-Value[a]	Effect±Standard Error (sec)	F-Value[a]
Primary Factors[b]				
A	0.38±0.05	52.26	1.38±6.58	0.04
B	-0.25±0.05	22.71	-3.13±6.58	0.23
C	0.11±0.05	4.44	-1.13±6.58	0.03
Two-Factor Interactions				
AB	-0.21±0.05	15.13	-12.13±6.58	3.39
AC	0.08±0.05	2.42	6.38±6.58	0.94
BC	0.03±0.05	0.42	4.38±6.58	0.44
Three Factor Interactions				
ABC	0.01±0.05	0.05	10.88±6.58	2.73

[a]F-Critical (99% confidence) = 11.26
[b]A=Initial Pressure, B=Moisture Content, C=Heater Power

Table 6.5 The influence of the three primary factors, and their interactions, on the maximum rate of pressure rise and the time-to-ignition.

the high and low values of heater power selected for this study. Upon closer examination of Figure 6.1, it appears possible that the two temperature profiles do not deviate drastically enough within the first minute—the time period in which almost all ignitions occurred—to create significantly different system responses. However, recall that the heater power choices were initially selected with the goals of maintaining safe operating levels to prevent element burnout on the "high" side of this factor, and of maintaining acceptable ignition times on the "low" side. It was therefore unexpected to determine that the heater power factor, at the two levels considered, does not demonstrate a significant effect on the time-to-ignition response. However it is known that heater power does affect the rate at which carbonization proceeds following ignition. Because the effects of electrical heater power on the carbonization process have been perfected by the extensive studies detailed in prior work [13], it is unlikely that heater powers lower than the "low" value considered in this study will be used for future laboratory scale experiments of the Flash Carbonization^{TM} process, and therefore the heater power factor will not be examined further at this time.

Overall, by examining the results of the factorial experimental design, it is clear that an increase in pressure leads to more vigorous ignition—likely through increased local oxygen concentration available for combustion—which leads to increased ΔP_{max} and $(dP/dt)_{max}$. Additionally, an increase in feed moisture content leads to decreased combustion due to absorption of heat through vaporization of the water present in the feed. Note that both of these trends mirror those of dust explosions [49]. This factorial design approach has allowed us to experimentally quantify the parameters of interest for the lab-scale Flash Carbonization^{TM} system, and to determine that the interaction between moisture content and pressure is significant.

6.9 A Simple Model

As mentioned previously, occasionally a run was stopped immediately following the sudden pressure rise, and nitrogen delivered, in an attempt to preserve the feedstock at the state in which it exists immediately following ignition. In order to examine the sudden pressure rise from a theoretical standpoint, we will consider one such truncated experiment (Run #11 in Table 6.4) as a representative example. The results of this model will indicate that the change of moles in the gas phase may contribute significantly to the pressure rise, and that heat and mass transfer limitations of the system prevented the continued propagation of the initial violent combustion, prior to either the fuel or the oxidizer being fully exhausted.

From elemental analysis (see Table 3.2) it is known that, for the type of corncob employed in this study, the weight percentages of carbon, hydrogen, and oxygen are as follows C:H:O = 43.42:6.32:46.69. Therefore, the apparent composition formula of corncob may be written as $CH_{1.747}O_{0.806}$ (unit MW = 26.66), and a simple representation of the complete combustion of corncob with a stoichiometric amount of oxygen is shown in Equation 6.2.

$$CH_{1.747}O_{0.806} + 1.034O_2 \rightarrow CO_2 + 0.874H_2O \tag{6.2}$$

Assuming that the water in the products remains in the vapor phase, this equation implies that for every molar unit of corncob consumed, an increase of 0.840 moles occurs

in the gas phase of the system. By manipulating the ideal gas equation of state, the total molar amounts of gas present in the system both initially and immediately following the sudden ignition may be determined from Equations 6.3 and 6.4.

$$N_i = \frac{P_i V_{void}}{RT_i} \tag{6.3}$$

$$N_f = \frac{1}{T_f}\left(\Delta P_{max}\frac{V_{void}}{R} + N_i T_i\right) \tag{6.4}$$

Where ΔP_{max} is the change in system pressure measured during the ignition, R is the universal gas constant, V_{void} is the void volume of the reactor system (filled with a full corncob canister), N is the number of moles of all gaseous species, and T is the temperature of the system. The subscripts i and f indicate the initial and final states respectively. Recall that, when filled with a full canister of corncob[2], the void volume of the entire laboratory scale Flash Carbonization^{TM} system is known to be $2.32\text{x}10^{-2}\pm0.09\text{x}10^{-2}$ m^3. For the experiment in question ΔP_{max} was equal to 1.25 MPa. The initial and final temperatures were taken from a thermocouple mounted on the exhaust line, close to the bottom of the reactor. The exhaust was vented immediately following the ignition, and the final temperature of the system (T_f ~172 °C) was estimated from the mean temperature at the exhaust line in the first three minutes of this venting (temperature sampling rate of 10 samples per min). The initial temperature was measured by the same thermocouple to be 23 °C. It should be noted that this thermocouple is not actually inside of the reactor, and therefore gives only an approximate idea of the range of temperatures within the reactor following ignition.

For the run in question, Equations 6.3 and 6.4 indicate that initially there was a total of 20.46 moles of gas (air) in the system, and following the sudden pressure rise there was 21.45 moles of gas. By subtracting the initial total molar amount of gas from the final total amount, a total increase of 0.99 moles is calculated. From Equation 6.2 we know that for

[2]It should be noted that this value changes slightly between runs with similar feedstock and more drastically with different feedstock types.

every 0.840 moles of excess gas produced, one mole of corncob is consumed. Therefore, Equation 6.5 may be used to describe the ignition of the representative experiment.

$$1.18CH_{1.747}O_{0.806} + 4.30O_2 + 16.16N_2 \rightarrow 1.18CO_2 + 1.03H_2O + 3.08O_2 + 16.16N_2 \quad (6.5)$$

Note that, following the sudden pressure rise, we expect to see an oxygen concentration of 14.36% by volume. As anticipated, when the reactor was vented immediately following ignition, the oxygen analyzer detected a fairly high level of oxygen (~15% initially, which decreased as combustion continued and N_2 was delivered) present in the exhaust stream of the process. This fairly high oxygen concentration following ignition is typical, and when the biomass is examined after such an abbreviated experiment it is clear that only a small amount of the feed has been consumed. In fact, the biomass from this run appeared only lightly blackened as shown in Figure 6.5. In this representative case, after nitrogen was delivered, the system depressurized, and the feed removed from the canister, a total change in feedstock mass of 138.46 g was measured. Although this value does not compare too closely to the 31.44 g predicted by Equation 6.5, note that it is likely that the combustion reaction continued for a brief period of time—but at a slower rate—following the violent ignition, after the heater was shut off, and prior to the nitrogen gas delivery. Additionally, as can be seen in Figure 6.5, a good amount of fine charcoal dust is produced during a truncated experiment. The amount of this dust which cannot be collected (i.e. lost during unloading of the canister and setup for the picture) certainly accounts for some of the difference between the experimentally recorded mass values and that predicted by the model.

Additionally, recall that for the combustion of simple hydrocarbon gases in air, an increase in pressure of the system is almost solely a result of the increased temperature of the products [11]. For example, no increase in moles of gas in the system occurs when methane is combusted with a stoichiometric amount of air, but very high temperatures—

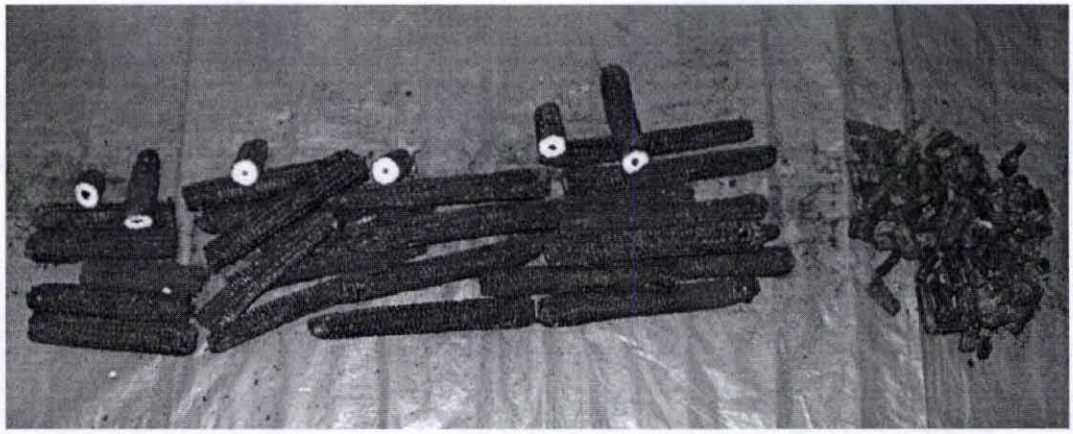

Figure 6.5 The visual appearance of the corncob after a truncated experiment. This particular picture is of the run used to develop the basic model (Run #11 conducted June 20th, 2005). Other truncated runs produced similar results.

and therefore large changes in pressure— result from this reaction. In contrast, following the combustion of solid biomass during the type of violent ignition examined in this study, this model indicates that the increase in the number of total moles of gases in the system has a significant effect on the pressure of the system, although pressure rise still occurs primarily through the increase in system temperature. For example, if this reaction had proceeded isothermally, say at a constant temperature of 97.5 ^{o}C (the mean value of the initial and final temperatures) the pressure rise would have been ~0.13 MPa. Therefore, the generation of excess product gases is responsible for approximately ten percent of the total pressure rise in the system, a much greater percentage contribution than in systems involving the combustion of gaseous hydrocarbons.

This conclusion is highly sensitive to the final temperature value, T_f. The very large thermal gradients in this highly dynamic system following ignition make T_f the largest source of uncertainty in Equation 6.4. Although no thermocouples were present inside of the reactor for any experiments conducted for this study, previous workers have monitored the ignition temperatures of a bed of corncob subjected to the Flash Carbonization^{TM} process [13]. Figure 6.6 gives an idea of the large differences in temperature observed at different locations inside of the canister. Possible values of T_f

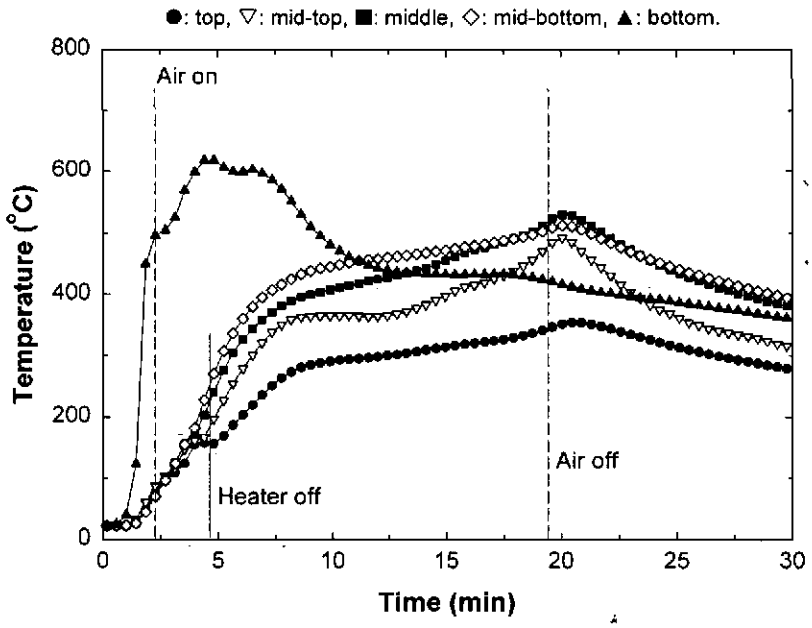

Figure 6.6 Measured centerline temperature profiles during a typical corncob experiment (conducted for a previous study) [13].

for the specific representative case for this study (Run #11) can be seen by plotting the final number of moles in the gas phase against a range of possible values for T_f as shown in Figure 6.7. This sort of plot sets the boundaries of possible T_f values. A minimum value of T_f occurs in the isothermal case—where the pressure rise is solely a result of molar increase in the product gases—which occurs at a T_f of 23 °C. Similarly if the pressure rise is only due to change in temperature, the final moles in the gas phase are equal to the initial number of moles, and the maximum value of T_f is 192 °C. From this analysis our approximate experimental value of 172 °C seems to be a plausable estimate of T_f.

An energy balance may be employed in order to further check if the value of T_f used in the above section is reasonable. As a first assumption, the properties of corncob will be approximated by those of cellulose. For stoichiometric combustion of cellulose 467 kJ of heat are released for every mole of O_2 combusted [13]. As shown in Equation 6.5, in the case being considered 1.22 mol of O_2 is assumed to be consumed. Therefore, 570 kJ of heat would be released. If we assume all of the heat goes to heating the gas in the

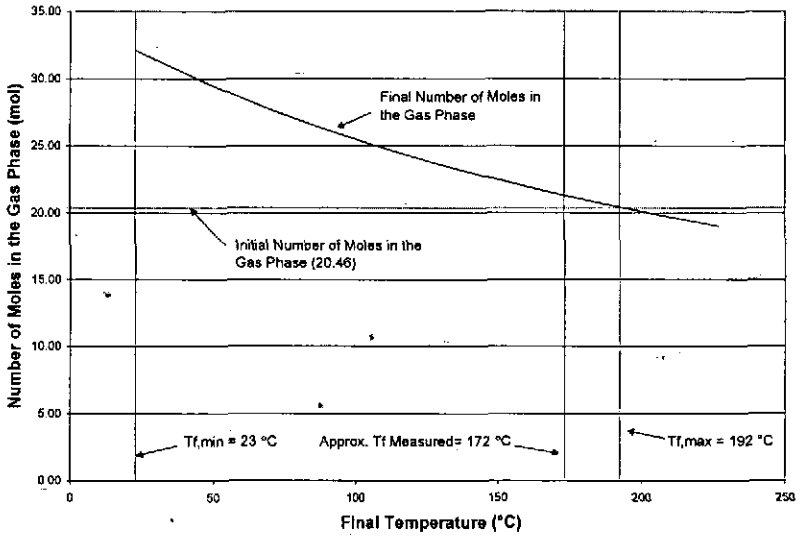

Figure 6.7 The effect of final temperature on the calculated final number of moles in the system (Run #11 conducted June 20th, 2005).

system and that the specific heat[3] of the final gas mixture may be approximated by that of N_2 (C_{p,N_2}=0.02958 kJ/(mol·K)) [50], the following equation may be used to calculate the change in temperature.

$$\Delta T = \frac{570\ kJ}{(21.45\ mol)(0.02958\ kJ/(mol \cdot K))} = 898\ K \tag{6.6}$$

If we assume that the heat is also dissipated into the biomass ($C_{p,cell}$=1.38 kJ/(kg·K) [13]) the following equation would be true.

$$\Delta T = \frac{570\ kJ}{[(21.45\ mol)(0.02958\ kJ/(mol \cdot K)) + (0.88\ kg)(1.38\ kJ/(kg \cdot K))]} = 308\ K \tag{6.7}$$

Finally if we assume the heat is dissipated into the gas, the biomass and an unknown amount of iron[4], we can use Equation 6.8 to predict the amount of iron which must be heated to produce ~150 °C change in temperature.

$$m_{Fe} = \frac{1}{0.5\ kJ/(kg \cdot K)} \left(\frac{570\ kJ}{150\ K} - 0.634\ kJ/K - 1.21\ kJ/K \right) = 3.91\ kg \tag{6.8}$$

From this rough calculation it is clear that the energy generated by combusting the corncob would be sufficient to raise the system temperature somewhere close to the approximate value of T_f used in the above discussion. Although these calculations involve a high degree of uncertainty, they serve to generally explain the sudden pressure rise observed during the violent ignition of the Flash Carbonization™ process, and indicate that heat and/or mass transfer, as opposed to the complete exhaustion of fuel or oxidant, is the limiting factor preventing combustion from continuing at the vigorous rate it initially exhibits.

[3] All specific heats in this analysis are assumed to be constant.

[4] Which represents the steel in the canister and the pressure vessel. $C_{p,iron}$=~0.5 kJ/(kg·K) [11].

6.10 Implications of Visual Evidence

The pictures shown in Figures 6.5 and 6.8 visually support the conclusions reached above. It appears that during the ignition of the Flash Carbonization^{TM} process, the exterior of the corncob[5] is fully combusted or partially carbonized by the initial violent reaction. This process creates a carbonized exterior layer surrounding the outside of the cob, which may limit mass transfer and inhibit the reaction from continuing at the same vigorous combustion rate responsible for the initial sudden pressure rise. When compared to other common types of biomass fuels (i.e. woods, nutshells), corncob's layer of fine chaff intuitively appears well suited to this sort of quick combustion. Interestingly, the pith in some cob samples was also partially or fully carbonized during the ignition phase of the run. As mentioned in the chapter entitled "The Laboratory-Scale Flash Carbonization^{TM} Reactor", the pith is similar chemically to the chaff, and is noticeably less dense when compared to the woody ring. At higher pressures it is plausible that a significant amount of air can penetrate through the fairly porous pith, reducing mass transfer limitations, and creating a condition which would increase the amount of fuel available for the initial violent combustion. Therefore, it is not surprising that this section of the cob is also partially reacted during the initial ignition, despite being located in the center of the cob. In general it may be said that an increase in pressure leads not only to increased local O_2 concentration, but also, in the case of porous feeds, to increased surface area available for reaction. This argument is supported by the fact that the piths of the cob pieces were observed to be less carbonized in the abbreviated experiments conducted at the lower pressure level. As the Flash Carbonization^{TM} process continues, it is likely that the chaff and the pith are fully carbonized prior to the complete carbonization of the woody ring. Thus, carbonization occurs from both the inside and the outside of the corncob simultaneously. The resulting increased amount of simultaneously reacting surface area of this fuel may explain why the most violent initial system pressure rises are observed in corncob experiments. For a denser, less porous feedstock, such as macadamia nutshell, the ability of the pressurized air to make additional surface area

[5]The majority of fine chaff and some coarse chaff (see Figure 3.10).

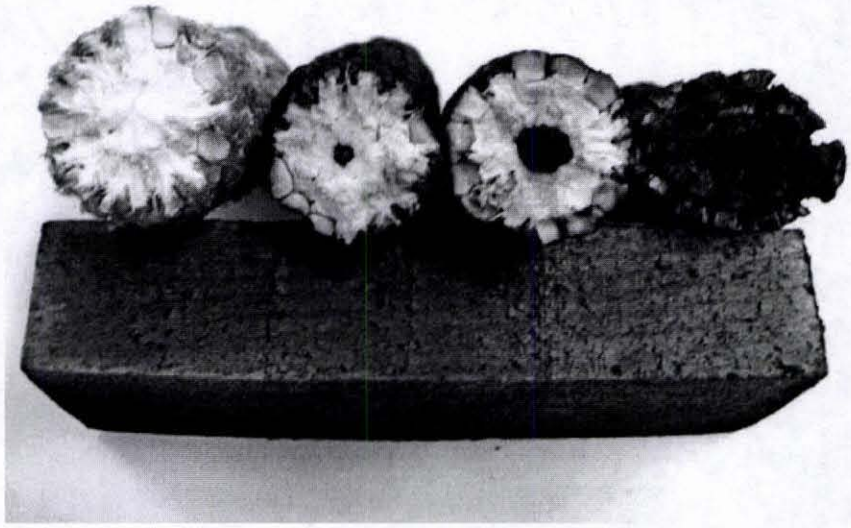

Figure 6.8 The progression of corncob carbonization. From left to right: an un-carbonized cob, a cob subjected to the ignition stage only (pith partially carbonized), cob subjected to the ignition stage only (pith fully carbonized), fully carbonized cob.

available for reaction would be reduced. Consequently, it would be more difficult for ignition to occur in the violent fashion observed in corncob experiments. Similar arguments could be made to explain the relatively short reaction time required for the complete Flash Carbonization^{TM} of this corncob when compared to other feedstock types.

Chapter 7

The Demonstration-Scale Flash Carbonization^{TM} Reactor

7.1 Introduction

The demonstration reactor (see Figure 1.2) is similar to the laboratory-scale systems in most respects. However, the few exceptions to the preceding statement have made the task of assembling the demo-reactor quite challenging. The most obvious difference is the scale—the pressure vessel used for the carbonizer in the demonstration system has an inner diameter of 0.91 m (36 in) and a height of 2.74 m (108 in)[1]. An additional difference is that the demonstration reactor does not have an accumulator system, but instead relies on a compressor to deliver air directly to the process. A third factor is that, because no power from the electrical grid is available at the site of the demo-reactor, all electronic equipment must be run off of a gasoline-powered electric generator. A schematic of the demonstration reactor is shown in Figure 7.1. This chapter will describe how the knowledge gained from the studies detailed in previous chapters has been applied to select components of the demo-reactor, and how elements of the Flash Carbonization^{TM} process have been adapted to fit this commercial scale pilot plant.

7.2 Relief Vent Sizing

7.2.1 Introduction and Relationship to the Ignition Study

As a result of the ignition study described in the preceding chapter, we now have a fairly good idea of what sort of $(dP/dt)_{max}$ values can be expected from violent ignitions in the

[1]Therefore the volume of the demo-reactor carbonizer is ~1.80 m^3, about eighty times greater than the lab-scale counterpart. This ratio is actually a bit of an underestimate due to the hemispherical top and bottom of the demo-reactor carbonizer were not accounted for in this approximate volume calculation.

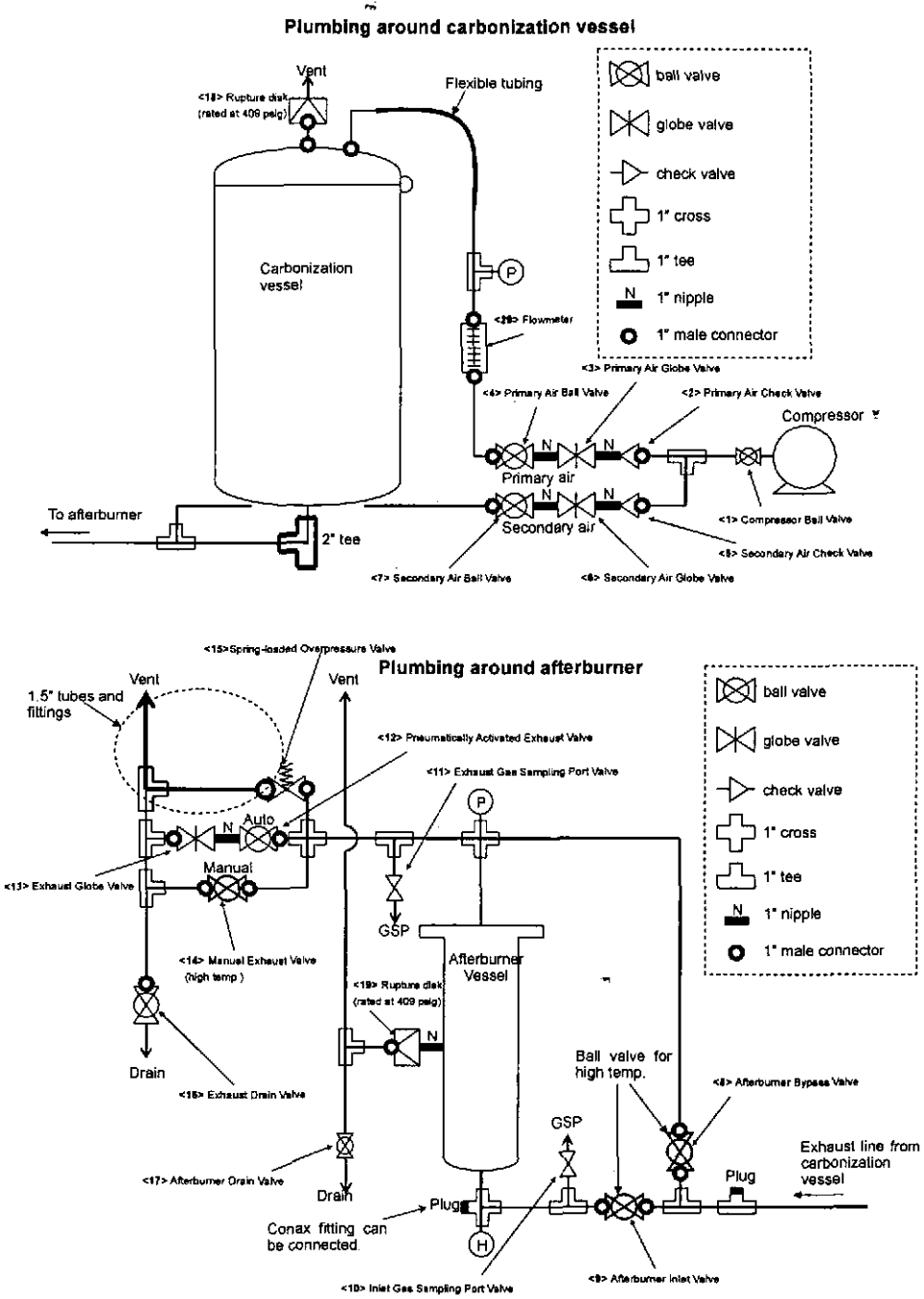

Figure 7.1 A schematic of the demonstration reactor (Figure created by Dr. Teppei Nunoura).

laboratory scale reactor. In this section this information will be used to examine the pressure relief requirements of the demonstration reactor. While it is encouraging to note that, in the case of gaseous and dust deflagrations, when all other parameters are held constant, an increase in vessel size leads to a decrease in $(dP/dt)_{max}$ (see Equation 5.1), at this time we do not have sufficient experimental information to determine what type of scaling law[2], if any, would be applicable to the sudden violent pressure rise observed during the ignition of the Flash Carbonization^{TM} process. Instead, we currently assume that the $(dP/dt)_{max}$ values which could potentially occur in the demonstration reactor system are on the order of those observed in the laboratory-scale system[3].

7.2.2 Description of Rupture Disks

The desired method of venting hazardous overpressure in the demonstration reactor involves the installation of rupture disks[4] similar to the one shown in Figure 7.2. These disks consist of a lightweight metal that will, when activated, disintegrate or be ripped open and blown away, allowing pressure in the system to decrease. Currently two of these types of devices are installed on the demonstration reactor in the locations shown in Figure 7.1. Both of these disks have a rated set pressure of 2.92 MPa (409 psig)—when the system pressure exceeds this value these disks will burst and the system will vent. This phenomenon has already occurred once during preliminary tests of the demonstration reactor system. Both disks ruptured and the overpressure was successfully vented without any damage to the system. A photograph showing the results of this occurrence is shown in Figure 7.3. Although it was encouraging that the current safety system operated as intended, as a result of the ignition study detailed in the prior chapter, and the following calculations, we currently plan to increase the amount of overpressure protection by adding additional rupture disks.

[2]For further information see the "cubic law" description in the chapter entitled "Deflagration Fundamentals".

[3]Therefore, the highest value of $(dP/dt)_{max}$ observed in the ignition study, 1.21 MPa/s, will be used for the following analysis.

[4]Also referred to as burst diaphragms.

Figure 7.2 A typical rupture disk.

Figure 7.3 Following the burst of the rupture disk mounted on the top of the demonstration reactor (housed in the hexagonal casing), a plume of smoke and a shower of tarry vapors vented quickly, resulting in the dark stain shown in this photograph.

7.2.3 A Model for Rupture Disk Venting

Flow of gas through a rupture disk is described using an orifice equation similar to the one shown in Equation 7.1 [40]. Specifically this equation models adiabatic discharge of an ideal gas through a frictionless nozzle, when the flow is choked, from a large chamber where velocity is effectively zero [11].

$$\dot{m} = AP_o\sqrt{\left(\frac{2}{k+1}\right)^{(k+1)/(k-1)}\left(\frac{kM_w}{RT_o}\right)} \tag{7.1}$$

Where $\dot{m}$ is the exit mass flow rate, P_o and T_o represent the pressure and temperature at the stagnation conditions inside of the large chamber, A is the cross-sectional area of the orifice, k is ratio of specific heats for the gas in question, M_w is the molecular weight of the gas, and R is the universal ideal gas constant. The choked flow condition may be checked using Equation 7.2 [40].

$$P^* = P_o\left(\frac{2}{k+1}\right)^{k/(k-1)} \tag{7.2}$$

Where P^* represents the greatest downstream pressure which permits maximum flow through the orifice for a given P_o value[5]. In the case we will consider, the pressure of the surroundings to which the rupture disk vents will be atmospheric (101.325 kPa) . Additionally, because the exhaust gas would be composed primarily of nitrogen (a diatomic gas) we assume a value of k=1.4 [51]. Therefore, as long as P_o >191.80 kPa the flow will be choked and we may employ Equation 7.1. If we also assume that the temperature inside of the chamber (carbonizer vessel) does not change during venting, we may use the following version of the ideal gas law to relate a rate of change-in-pressure to a rate of change-in-mass.

$$\dot{m} = \frac{dP}{dt}\frac{VM_w}{RT_o} \tag{7.3}$$

[5] P^* is referred to as the choked pressure.

Equating Equations 7.1 and 7.3 and solving for vent area yields Equation 7.4.

$$A = \frac{dP}{dt}\frac{V}{P_o}\left(\frac{M_w}{RT_o}\right)^{1/2}\left(k\left(\frac{2}{k+1}\right)^{(k+1)/(k-1)}\right)^{-1/2} \tag{7.4}$$

In order to model a worst case scenario, we make the following assumptions: venting occurs at the rated pressure of the rupture disks currently installed on the demo-reactor[6] of (2.92 MPa), the exhaust gas has a molecular weight similar to that of air (28.97 kg/kmol) [52], and that the largest $(dP/dt)_{max}$ observed in the ignition study (1.21 MPa/s) must be vented. This example may be considered a worst case situation for a variety of reasons. First, consider the fact that, in the ignition study, (dP/dt) was never observed to sustain large values for any significant period of time (see Figure 6.3). Additionally, when a full canister of biomass is present in the demo reactor the volume available to be filled with gas will decrease, which should decrease the required vent area as indicated by Equation 7.4. Finally, because of the knowledge gained as a result of the ignition study, the low-moisture-content/high-operating-pressure situations which created the largest $(dP/dt)_{max}$ values in the laboratory will intentionally be avoided in demonstration reactor experiments. In fact, as a result of this study it is unlikely that the demonstration reactor will ever be operated above 1.48 MPa (200 psig).

Equation 7.4 may be plotted as a function of gas temperature, T_o, as shown in Figure 7.4. Examining this figure we note that, if venting occurred at a T_o equal to room temperature (298 K), a maximum vent area of 3.72x10^{-3} m^2 would be required. Although ignition resulting in a sudden pressure rise at this temperature is highly unlikely, the pair of one inch[7] rupture disks currently installed on the demo-reactor have a combined vent area of only 7.05x10^{-4} m^2. This area is not sufficient to vent the desired dP/dt even at the highest gas temperature considered[8]. Therefore, the current protection is not sufficient to handle

[6]Recall that the demo-reactor has a volume of 1.8 m^3.

[7]The inner diameter of a nominal one inch pipe used on the demo-reactor is 0.834 inches (0.0211 m). This value was used to calculate the vent area of the one inch rupture disk lines.

[8]A high temperature value of ~700 °C was observed to occur during Flash Carbonization™ experiments by prior researchers working with an alternate version of the lab-scale reactor. This previous model of the lab-scale reactor was equipped with thermocouples inside of the carbonizer [13].

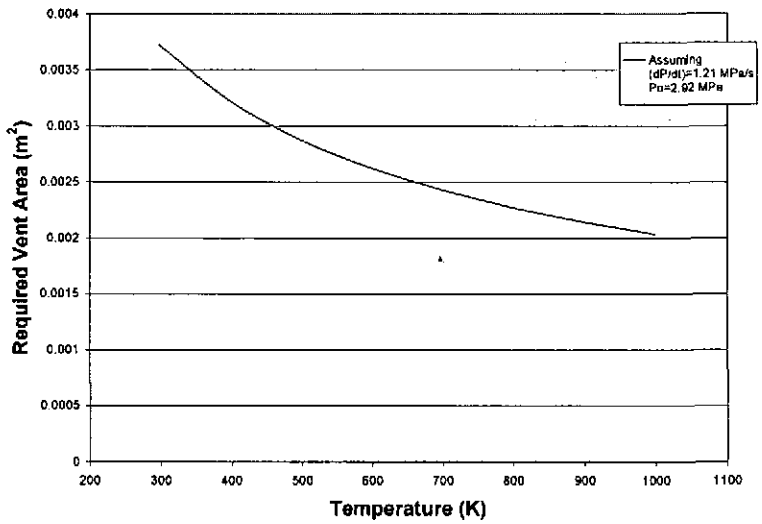

Figure 7.4 Required vent area as a function of gas temperature.

the venting requirements of this worst case scenario. As a result of this study the best method of adding additional rupture disks is currently being evaluated.

7.3 Demonstration Reactor Rotameter Evaluation

7.3.1 Introduction

An experiment was conducted in an attempt to evaluate the accuracy of the rotameter (Flow-Alert™ Flow Switch HLIT 219) currently installed on the demonstration reactor. This rotameter is of the variable area based piston-and-spring configuration, as opposed to the ball-and-tube devices employed on the lab-scale reactor. The techniques used for this study are similar in some respects to those discussed in the chapter "Airflow, Compressibility, and Deviations from Ideal Gas Behavior in the Accumulator System"[9].

[9]However, because no accumulator system is used at the demo-reactor, no part of the system experiences pressures high enough to warrant consideration of the compressibility factor, Z.

7.3.2 Experimental Procedure

In preparation for this experiment, the two valves which isolate the afterburner from the carbonization vessel were fully closed, and the compressor[10] (Ingersoll-Rand 2475F15GIR) was turned on. As soon as the primary-air ball valve was opened and the compressor began delivering air, the following values were recorded every twenty seconds: system pressure, temperature of the pipe wall at the inlet of the rotameter, and the volumetric flow rate indicated by the rotameter. As shown in Figure 7.5, following an initial jump, the system pressure was observed to increase linearly with time. The temperature at the wall of the pipe also increased throughout the run, although in a less uniform fashion than system pressure. Noticeable fluctuations in the temperature value, due to convection, occurred whenever a strong gust of wind was observed.

7.3.3 Analysis of Results

Using the ideal gas law, an average change in moles of gas, ΔN, was calculated for each 20 second period using Equation 7.5.

$$\Delta N = N_2 - N_1 = \frac{V}{R}\left(\frac{P_2}{T_2} - \frac{P_1}{T_1}\right) \tag{7.5}$$

These molar flow rate values were translated to equivalent volumetric flow rates[11] at normal temperature and pressure. Using the recorded data, and the temperature and pressure correction factors supplied by the manufacturer, a corrected volumetric flow rate was calculated for each indicated rotameter value. A plot of the indicated, corrected, and calculated volumetric flow rate values as a function of time is shown in Figure 7.6.

Clearly, there is not a good agreement between the corrected rotameter value and the values calculated using the ideal gas law. There is some error in the ideal gas calculation due to the underestimate of the system volume; an increased system volume value would

[10] A variety of compressors have been tested for this application, the final selection has not yet been made.
[11] In standard cubic feet per minute (SCFM), centered at the midpoint of each 20 second time interval.

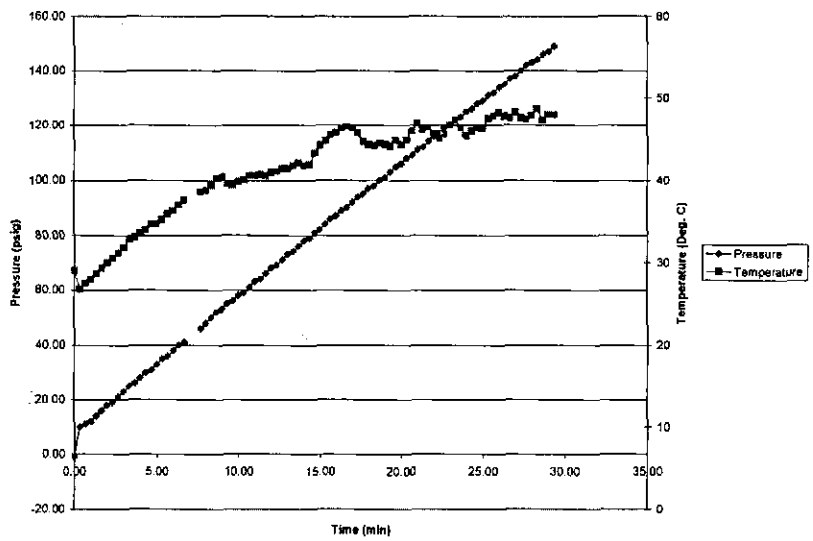

Figure 7.5 Temporal response of pressure and temperature in the demonstration reactor. After an initial jump, system pressure increased linearly. The temperature also increased, but not in as smooth a fashion.

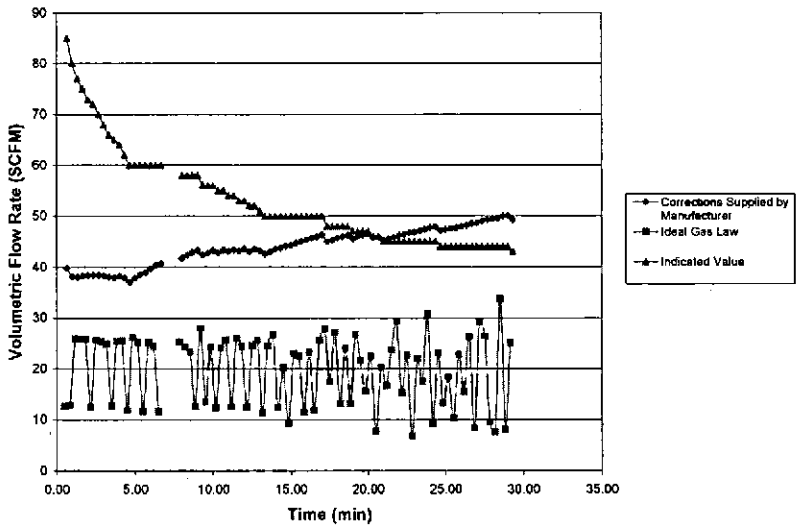

Figure 7.6 The volumetric flow rates calculated by the ideal gas law appear to be more accurate than the values obtained using the manufacturer's corrections for the rotameter values.

cause the ideal gas flow values to increase[12]. However, when the flow rates in Figure 7.6 are compared to the value the compressor is rated to deliver (25 SCFM), the ideal gas calculation appears to be more accurate than the corrected rotameter values. This result suggests that the rotameter is malfunctioning. This hypothesis is supported by the fact that the rotameter occasionally sticks and must be hit on the side to resume functioning.

Possible reasons for erroneous rotameter readings include: the presence of the primary air valve fairly close to the rotameter, back pressure created during runs in which we attempted to maximize secondary air, and general fatigue due to weathering and lack of use. It is stated in the rotameter manual that high magnitude pressure spikes, created by fast-acting (i.e. ball) valves, can damage the internal components of the meter, resulting in inaccuracies or malfunctions. Alternatively, these inaccuracies may be a result of instances where too much secondary air was employed. If, as a result of this increased secondary air flow, the pressure in the carbonization chamber was greater than that before the inlet of the rotameter, a backpressure would result. This situation would cause the rotameter to act as a check valve, which the manual states can cause an excessive pressure differential. Large differentials of this sort can damage internal meter components. As a result of this study, it was determined that the rotameter is currently only useful to indicate flow in a very qualitative sense, and that it should be replaced by a more robust model.

7.4 Adapting the Ignition and Electrical Systems

Properly selecting the electric heaters used to initiate the reaction in the demo-reactor was an important step in the scale up of the Flash Carbonization™ process. The primary criteria for selection of the new electric heaters was that they reach 700 °C fairly quickly. Once the electric heaters were selected, an electrical generator was sized around these heaters. Note that this work was preformed prior to the ignition study.

[12] A system volume of approximately 4 m^3 creates fairly good agreement with the corrected rotameter values.

	Afterburner Heater	Spring-Coiled Heater
Manufacturer	ARI	ARI
Part Number (Both Custom)	BXX-19B-50-11T	BXX-19B-40-11T
Diameter	3/16 in	3/16 in
Heated Length	50 in	40 in
Cold Length	11 in	11 in
Approx. Surface Area	29.45 in^2	23.56 in^2
Resistance	6.3 Ohms	4.8 Ohms

Table 7.1 Information from two heaters used in experiments conducted to establish the required power density of the demonstration reactor heaters.

7.4.1 Establishing the Required Power Density of the Demonstration Reactor Heaters

In order to determine which electric heaters should be purchased as the source of ignition in the demonstration reactor's carbonizer, we performed the following tests on two heaters which were available in the lab. The first heater had been used previously in the catalytic afterburner and will therefore be referred to as the "afterburner heater". It was bent in a flat spiral-like shape. The second heater will be referred to as the "spring-coiled heater" because it was bent into a helical spring-like shape. The details of these two heaters are shown in Table 7.1.

Thermocouples were attached in similar locations on both heaters (approximately 1" from the tip). The necessary voltages were calculated to achieve equal power densities in both heaters (for two separate power densities 59 W/in^2 and 69 W/in^2)[13]. The heaters were connected to the small VariAC and the desired voltages supplied. The maximum temperature observed and the necessary time to reach the peak value were recorded. The final stabilization temperature remained close to (within 20 ^oC) of the peak value in all experiments. The results of these tests, as shown in Table 7.2, indicate that maximum temperature is almost directly related to power density. The slight differences in the temperatures reached, and in the time needed to reach those temperatures, can be accounted for by the geometric differences of the heaters, precision of the VariAC, and the location of thermocouples.

The power density, PD, of both test heaters was calculated using Equation 7.6 [53].

[13]These values were selected based on listed power densities of heaters we were considering purchasing.

	Afterburner Heater	Spring-Coiled Heater
Power Density = 59 W/in^2		
Voltage Supplied	104.63 Volts	81.68 Volts
VariAC Percent Setting	87.20%	68%
Temperature	643 C	640 C
Time to Temp.	6 min 30 sec	8 min
Power Density = 69 W/in^2		
Voltage Supplied	113.15 Volts	88.33 Volts
VariAC Percent Setting	94%	74%
Max. Temperature	660 C	687 C
Approximate Time to Temp.	6 min	7 min

Table 7.2 Temperature response of the test heaters to different power densities.

$$PD = \frac{V^2}{RA_s} \tag{7.6}$$

Where V is voltage supplied, R is the measured resistance when the heater is cold, and A_s is the approximate surface area of the heated portion of the heater (circumference times length). Note that we expect the resistance of the heater to decrease with increasing temperature, this fact decreases the accuracy of the simple method of approximating power density shown in Equation 7.6. However, this method is still acceptable for our purposes.

The goal of the next set of experiments performed was to determine the minimum voltage (and therefore power density) that would allow each heater to reach 700 °C. For each run, the VariAC was set at an initially guessed voltage. The VariAC was switched on, and the heater was allowed to reach peak temperature. The VariAC was then switched off, and adjustments made before the next run. If the temperature was too low the voltage was increased, if it was too high the voltage was decreased. The voltages needed are shown in the Table 7.3.

The results of these experiments indicate that a power density greater than 76 W/in^2 was desirable for the heaters purchased for the demonstration reactor. With this in mind, a heater with a power density of 94 W/in^2 was selected. The full specifications of this heater

	Afterburner Heater	Spring-Coiled Heater
Final VariAC Setting	97%	77%
Voltage	116.4 Volts	92.4 Volts
Power Density	73.03 W/in^2	75.5 W/in^2

Table 7.3 Voltages needed to reach the desired temperature of 700 °C for two test heaters.

	Heater Purchased
Manufacturer	ARI
Part Number	BXX-19B-45-5T
Power at 115 Volts	2500 Watts
Power Density at 115 Volts	94 W/in^2
Heated Length	45 in
Diameter	3/16 in
Cold Length	5 in

Table 7.4 Specifications of heaters purchased for use in the demonstration reactor.

are shown in Table 7.4. Note that this model of heater was also installed in the carbonizer of the lab-scale reactor.

7.4.2 Electrical System

After establishing which sort of electrical heaters we needed for the demonstration reactor[14], it remained to be determined if the generator we were planning to purchase (VOLTmaster LR150V) would be able to supply the total power needs of the system. Table 7.5 and Figure 7.7 were created in order to ensure that the selected generator would be sufficient. The components whose power needs are listed as "Unknown" are considered to require negligible amounts of power when compared to the demands of the electric heaters, or are never in operation at the same time as the heaters. It should be noted that the rated power of the generator is only slightly more than the maximum power requirements of the system. However, because the exact amount of power needed for the afterburner heater was unknown at the time the generator was purchased, a maximum value was used in these calculations. In practice, a VariAC is used to supply the afterburner heater with less voltage than listed in Table 7.5.

[14]The electrical heaters were assumed to consume the most power of any electrical required for operation of the demo-reactor.

	Voltage	Amperage	Power
During Operation			
3 Primary Ignition Heaters	120 V	22.68 A (Each)	8,164.8 W (Total)
Temperature and Pressure Gauges	120 V	Unknown	Unknown
Vacuum Pump	120 V	3.6 A	432 W
Automatic Release Valve	120 V	Unknown	Unknown
Data Monitoring System	120 V	Unknown	Unknown
Afterburner Heater (with VariAC)	Max 120 V	Max 22.68 A	Max 2721.6 W
Total Power			>11,318.4 W
Total Rated Power of Generator			12,000 W
Maximum Power of Generator			15,000 W
During Setup and Loading			
Hoist	120 V	6.21 A	745.7 W
Hydraulic Pump	Unknown	Unknown	Unknown

Table 7.5 A power balance used to determine if the selected generator will be able to meet power demands.

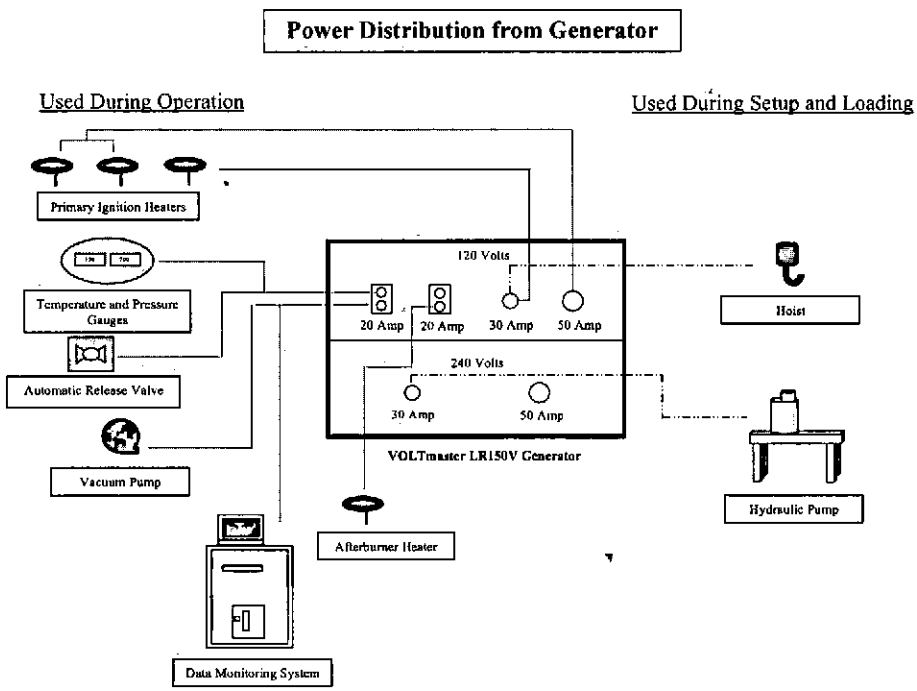

Figure 7.7 Details of the supply of power from the generator to components of the demonstration reactor system.

Appendix A

Developing a Correlation for Higher Heating Value from Proximate Analysis

A.1 Introduction

Higher heating value (HHV) is defined as the amount of heat released when a fuel is burned in stoichiometric proportions of air in a steady-flow process, such that the reactants are initially at a standard reference state (i.e. NTP) and the products are returned to the same standard reference state [51][1].

It is useful to be able to determine the HHV of a charcoal sample using the results of the simple proximate analysis tests conducted in the R^3 lab [4]. A variety of HHV correlations based on this type of test currently exist in the literature. However, subtle differences in the methods used by different researchers to conduct proximate analysis may lead to significant variations in the reported percentage values of fixed carbon (FC), volatile matter (VM), and ash (ASH). Assuming this is true, a correlation established using a small number of data points taken with the proximate analysis methods employed in the R^3 laboratory could potentially predict the higher heating value (HHV) of all our samples with greater accuracy than correlations based on more detailed studies.

A.2 Previous Correlations

Two previous correlations for HHV from proximate analysis available in the literature are those developed by Cordero et. al. [54] and Parikh et. al. [55] (as shown in Table A.1). It should be noted that the equation developed by Cordero was created for lignocellulosics and carbonaceous materials, while the correlation developed by Parikh is valid for a wide

[1] Note that at NTP water is in the liquid phase.

	Correlation for HHV (MJ/kg)
Cordero	HHV = 0.3543FC + 0.1708VM
Parikh	HHV = 0.3536FC + 0.1559VM − 0.0078ASH

Table A.1 Correlations for HHV from proximate analysis developed by previous researchers.

	R3 Lab Correlations for HHV (MJ/kg)
Correlation 1	HHV = 0.3495FC + 0.1725VM
Correlation 2	HHV = 0.3511FC+0.173VM-0.0842ASH
Correlation 3	HHV = 35.10-0.1784VM-0.4292ASH

Table A.2 Correlations for HHV from proximate analysis developed for the R^3 lab.

variety of solid fuels. The study conducted by Cordero employs 24 data points to establish the correlation and 17 points to validate it. The study conducted by Parikh employs 450 data points to establish the correlation and 100 points for validation. In both cases, least squares analysis of the data was the basic tool used to establish the correlation in question. In addition, Parikh developed an algorithm to determine the optimum form of the algebraic equation to be employed. This algorithm considered ten different possible forms of the equation and concluded that, as shown in Table A.1, the best form includes a coefficient for the ASH percentage value. Because the FC value is coupled to the other two variables (recall FC=100%−ASH−VM), this increase in accuracy may simply be the result of having an additional coefficient. If this assumption is true, similar results should be obtained with an equation in an intercept form (i.e. HHV=a+bASH+cVM).

A.3 Developing a New Correlation

To establish a correlation based exclusively on the proximate analysis method used in the R^3 laboratory, a system of simultaneous linear equations was developed based on the six samples we recently had tested by Huffman Laboratories. Using multiple regression techniques, a solution in a least squares sense was established for this over-determined system[2]. Three

[2]The system was solved using Matlab's backslash operator. The backslash operator is an algorithm designed to solve systems of equations of the general form AX=B with improved accuracy using QR decomposition with pivoting [56].

different possible forms of the algebraic equation were considered. The equation of the form which is similar to Cordero (HHV=aFC+bVM) shall be referred to as Correlation 1, Correlation 2 is of the form proposed by Parikh (HHV=aFC+bVM+cASH), and Correlation 3 is of the intercept format (HHV=a+bASH+cVM). The correlations developed as a result of this analysis are shown in Table A.2.

A.4 Analysis of Results

As shown in Tables A.3 and A.4, as well as in Figures A.1-A.5 , our correlations seem to fit our data slightly better than the correlations from the literature. The percent error appears to be on the same order as the previously established correlations, and the maximum absolute error and the average absolute error is the lowest for our three correlations. Where percent error, PE, and average absolute error, AAE, are defined as shown in Equations A.1 and A.2 respectively. Absolute percent error is defined as the absolute value of Equation A.1. The maximum absolute error indicated in Tables A.3 and A.4 includes all of the data points.

$$PE = \left(\frac{HHV_{Predicted} - HHV_{Measured}}{HHV_{Measured}} \right) (100\%) \tag{A.1}$$

$$AAE = \frac{1}{n} \sum_{i=1}^{n} \left| \frac{HHV_{Predicted} - HHV_{Measured}}{HHV_{Measured}} \right| (100\%) \tag{A.2}$$

To some extent these promising results may only be a reflection of the fact that the first six data points were used to create the correlations. However, the graphs shown in Figures A.1-A.5 seem to indicate that our correlations offer a better fit for this data (for example Cordero's values practically all have positive errors). It is also interesting to note that Correlation 3, the intercept form, has the smallest average absolute error. This equation offers a good adjusted R-squared value of 0.974. These facts, as well as the physical motivation mentioned above, leads to the conclusion that Correlation 3 should be the form employed for future work in this lab.

Values of HHV (MJ/kg) and Errors (%)		
Experimental	Cordero	Parikh
33.699	34.046 (+ 1.03)	33.885 (+ 0.55)
32.543	32.940 (+ 1.22)	32.744 (+ 0.62)
32.571	32.671 (+ 0.31)	32.405 (- 0.51)
30.655	31.465 (+ 2.64)	31.145 (+ 1.60)
30.513	30.994 (+ 1.58)	30.589 (+ 0.25)
28.245	28.334 (+ 0.32)	27.754 (-1.74)
33.5	33.762 (+ 0.61)	33.596 (+ 0.12)
31.1	31.583 (+ 1.56)	31.225 (+ 0.41)
30.9	31.978 (+ 3.34)	31.696 (+ 2.42)
33.3	33.313 (- 0.08)	33.097 (- 0.73)
Max. Abs. Error (%)	3.34	2.42
Avg. Abs. Error (%)	1.27	0.89

Table A.3 Calculated values (and the percentage error) of HHV from the different correlations developed by previous researchers.

Values of HHV (MJ/kg) and Errors (%)			
Experimental	Correlation 1	Correlation 2	Correlation 3
33.699	33.608 (- 0.27)	33.693 (- 0.02)	33.686 (- 0.04)
32.543	32.522 (- 0.06)	32.391 (- 0.47)	32.399 (- 0.44)
32.571	32.281 (- 0.89)	32.350 (- 0.68)	32.341 (- 0.71)
30.655	31.104 (+ 1.47)	31.006 (+ 1.15)	31.008 (+ 1.15)
30.513	30.668 (+ 0.51)	30.768 (+ 0.84)	30.754 (+ 0.79)
28.245	28.091 (+ 0.55)	28.049 (- 0.69)	28.041 (- 0.72)
33.5	33.329 (- 0.68)	33.353 (- 0.61)	33.386 (- 0.51)
31.1	31.235 (- 0.44)	31.330 (+ 0.74)	31.317 (+ 0.70)
30.9	31.599 (+ 2.11)	31.513 (+ 1.83)	31.515 (+ 1.84)
33.3	32.901 (- 1.32)	32.973 (- 1.10)	32.965 (- 1.13)
Max. Abs. Error (%)	2.11	1.83	1.84
Avg. Abs. Error (%)	0.83	0.81	0.80

Table A.4 Calculated values (and the percentage error) of HHV from the different correlations developed for the R^3 Laboratory. It should be noted that the first six data points were used to establish these correlations.

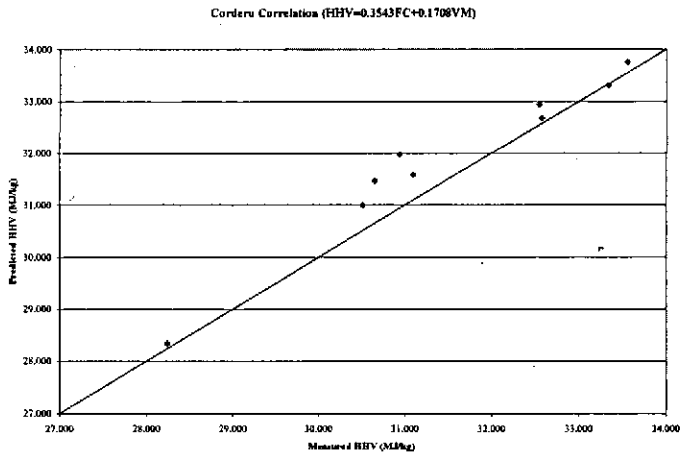

Figure A.1 Comparison between measured and predicted HHV using Cordero's Correlation. Note that almost all error values are positive, indicating a systemic error of some sort.

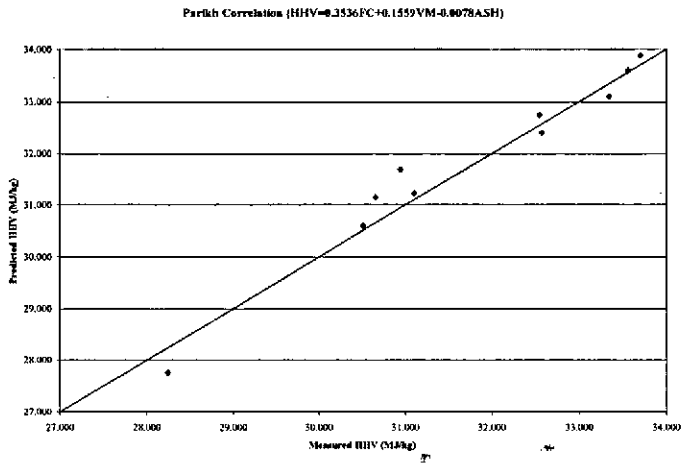

Figure A.2 Comparison between measured and predicted HHV using Parikh's Correlation.

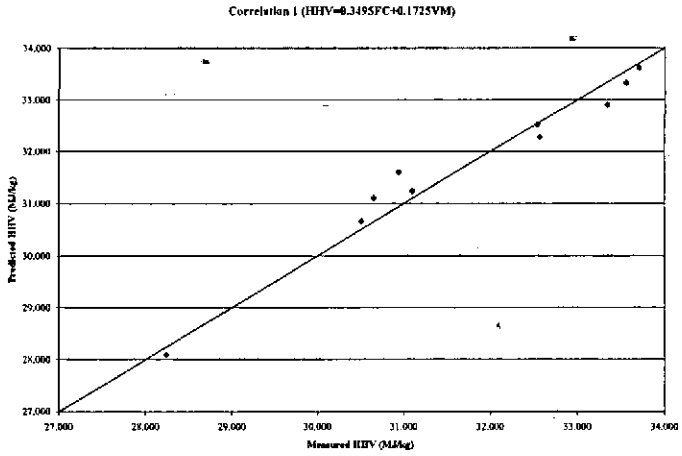

Figure A.3 Comparison between measured and predicted HHV using Correlation 1. Note that six of the plotted values were used to create Correlations 1-3.

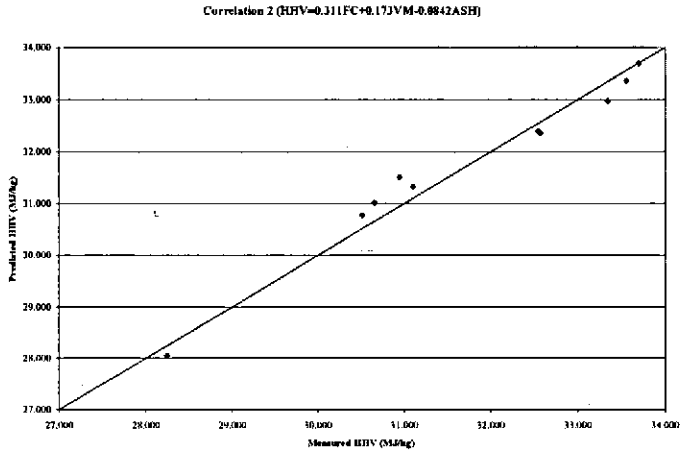

Figure A.4 Comparison between measured and predicted HHV using Correlation 2. As should be expected, correlations which employ three coefficients fit the data better than those with only two.

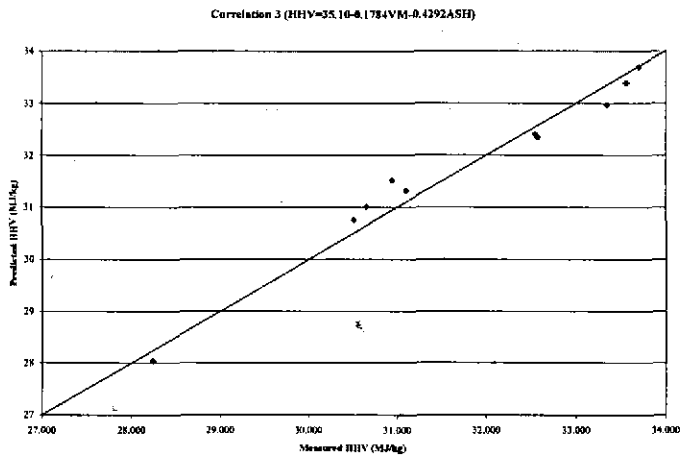

Figure A.5 Comparison between measured and predicted HHV using Correlation 3. Because this intercept form is the most accurate (as well as the most physically practical), it should be employed in future work conducted at the R^3 laboratory.

Appendix B

Safe Operating Procedures for the Laboratory-Scale Reactor

LABARATORY SCALE FLASH CARBONIZATION REACTOR
SAFE OPERATING PROCEDURES MANUAL
CREATED BY: Sam Wade

APPROVED BY: _____ DATE: _____

Table of Contents

INTRODUCTION AND PURPOSE

Currently research is being conducted in the R^3 laboratory at the University of Hawaii in which the process of "Flash Carbonization" is used to produce charcoal from biomass. In this novel procedure a packed bed of biomass is placed within a vessel and exposed to elevated pressures. When a flash fire is ignited within the bed, the biomass is converted to biocarbon (i.e. charcoal) quickly and efficiently.

The apparatus currently used to study this process is referred to as the "lab-scale" flash carbonization reactor (to differentiate it from a commercial-scale demonstration reactor, that is also being developed). As shown in Figure 1 the lab-scale reactor consists of a pressure vessel into which the canister containing biomass is lowered. Once the pressure vessel is sealed an electric heater is employed to ignite the contents of the canister. Primary airflow is supplied from the air accumulator. The exhaust gases from the combustion process are treated to reduce pollutants in the catalytic afterburner. When desired, secondary air from a separate compressed air cylinder can be provided to improve the performance of the catalytic afterburner.

Introduction and Purpose (cont.)

This manual provides the necessary instructions for the safe operation of the lab-scale reactor, including details related to setup, sampling, data acquisition, maintenance, disassembly, and known hazards.

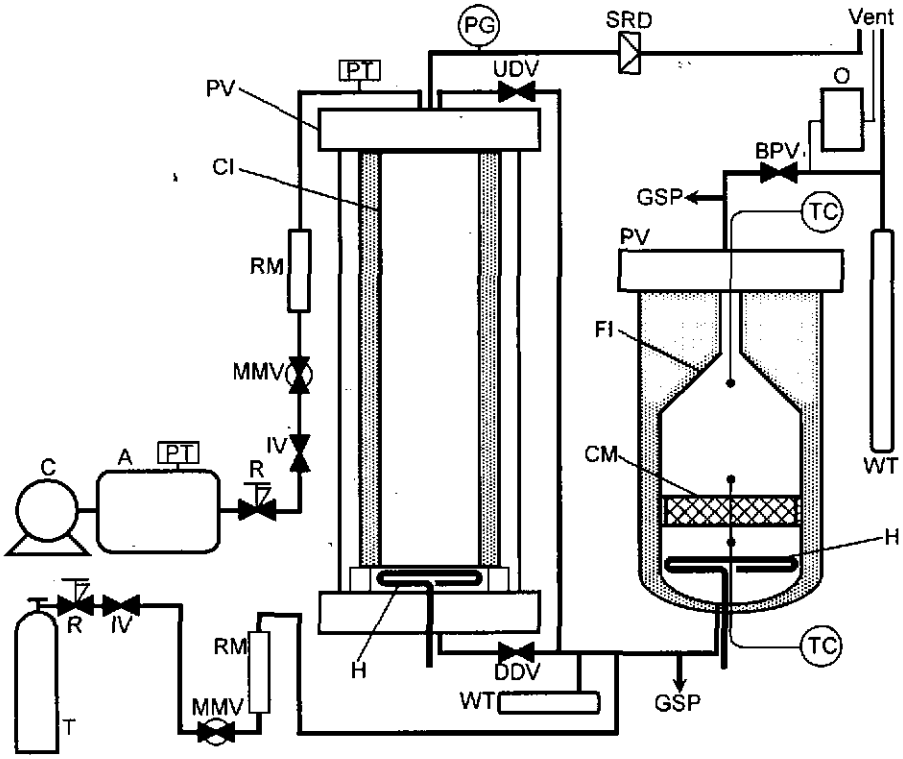

Figure 1. Overall schematic diagram of the lab-scale Flash Carbonization Reactor and the catalytic afterburner. A, air accumulator; BPV, back-pressure control valve; C, compressor; CI, canister with insulation; CM, catalyst monolith; DDV, downdraft valve; FI, funnel with insulation; GSP, gas sampling port; H, electric heater; IV, isolation valve; MMV, micrometer valve; O, oxygen analyzer; PG, pressure gauge; PT, pressure transducer; PV, pressure vessel; R, regulator; RM, rotameter; SRD, safety rapture disk; T, air tank; TC, thermocouple; UDV, updraft valve; WT, water trap.

HAZARDS AND NEAR MISSES

Health Hazards Avoid breathing exhaust gases. Ensure adequate ventilation to prevent asphyxiation and carbon monoxide poisoning. Verify that the exhaust hood is working properly before the start of run. If a strong smell

Hazards and Near Misses (cont.)

of exhaust is detected during the run its source should be located and dealt with in the appropriate fashion. If the leak is severe, air delivery should be terminated and the run aborted.

Carbon monoxide is highly toxic when inhaled. Exposure can cause death. Cumulative exposure to low levels is hazardous and may affect the nervous system. Insure that the carbon monoxide detector is activated prior to the start of the run.

If the catalytic afterburner is not employed, the exhaust gases are flammable. Avoid exposure to potential ignition sources.

Pressurized vessels and pipes could potentially rupture. Safety glasses must be worn at all times.

Electrical connections create the risk of shock or electrocution. Verify all power sources are disconnected before modifications are made to the system wiring. Ensure proper grounding of all equipment. Be continuously aware of all possible electrical hazards.

During the run many components of the system become hot. Avoid contact until sufficient time has passed to allow cooling.

Clogged lines and valves present hazards. Maintenance of the system is critical to prevent buildup (see appendix for details).

Nitrile gloves should be worn when handling charcoal.

Inhalation of charcoal dust is potentially toxic. Respirator masks should be worn whenever significant amounts of small charcoal particles are present.

The liquid collected in the reactor's water traps is potentially hazardous. Nitrile gloves should be worn when this liquid is handled and inhalation of vapors should be minimized.

Near Misses

It is essential that when a new hazard is determined or a near miss occurs it be recorded and the safe operating procedures be updated. The following is a record of dangerous situations that have already been observed and should be avoided in the future.

Hazards and Near Misses (cont.)

Vacutainers have burst during gas sampling. The sampling needle has come close to injuring operators. Always follow the safe gas sampling procedure as detailed in the appendix.

When pistachio nuts were used as a feedstock, a flammable liquid pitch-like substance collected at the bottom of the reactor. This liquid flowed into the exhaust line causing the line to glow red hot. The run was aborted immediately. Pistachio nuts should not be used as a feed.

PROCEDURE

Preparation and Loading

1. Examine Experimental Proposal Form
   - Note purpose of experiment; consider what makes this run different from prior work.
   - Note feed type, pressure and air delivery values, loading and sampling specifics, and any other additional information indicated.
   - Reference the prior work listed for more information.

2. Weigh and load feedstock
   - Read notes regarding specific feedstock to be used (see Appendix).
   - Take proper safety precautions. Depending on feed type this may include wearing dusk mask and gloves.
   - Load desired amount of feedstock into the canister. Maintain a minimum of one inch spacing between top of the feedstock and the top edge of the canister.
   - Weigh empty Nalgene containers (large, white, plastic beakers).
   - Sort feedstock from the canister into three Nalgene containers. One container should correspond to the top portion of the canister, one to the middle, and one to the bottom.
   - Label the containers with feedstock type.
   - Set aside small sample from excess feedstock for moisture content analysis.

Preparation and Loading (cont.)

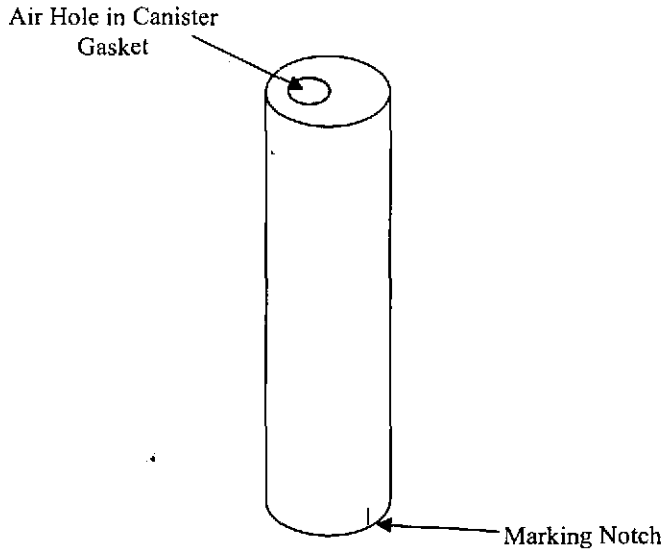

Figure 2. Proper orientation of canister gasket. The air hole in the gasket should be located on the opposite side of the canister from the marking notch.

- Let feedstock come to equilibrium with room conditions by exposing it to the air in the lab for one day.
- On the following day, measure the combined weight of the containers and feedstock using the large balance.
- Record weights, the date, and other important information on the canister record sheet (an example of this sheet is in the Appendix).
- Return the feedstock to the canister.
- Place screen and weights on top of feedstock. Record bed height.
- Ensure air hole is aligned properly as shown in fig. 2. Secure lid.
- Attach wire used to load canister.

3. Reload Canister
   - Lift loaded canister with winch above pressure vessel.
   - Align rails of canister with slots mounted inside of pressure vessel. Ensure air fitting is aligned properly.
   - Lower canister into pressure vessel.

4. Flange assembly.
   - Remove old flange gasket, if possible save gasket for next run.
   - Use gasket scraper to clean remaining old gasket material from flange faces.
   - Prepare new gasket if old gasket is no longer functional.

Preparation and Loading (cont.)

- If new gaskets need to be ordered contact "Industrial Gasket and Supply Co.", a Flexitallic gasket Licensee (phone # (310) 530-1771). Order permanite ring gaskets (sheet # AF2100). These gaskets should be 1/16" thick, have an outer diameter of 8 ¾" and an inter diameter of 6 5/8".

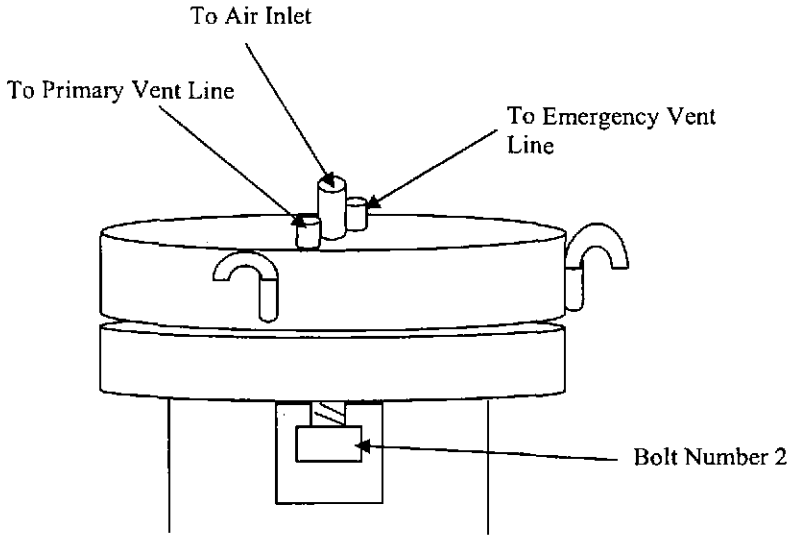

Figure 3. Proper flange orientation as seen from front of reactor.

- Paint graphite paste on bottom of gasket.
- Set gasket in place. Paint one half of the top of the gasket.
- Verify that vent tubes are properly aligned.
- Attach quick connect fitting.
- Paint remaining half of gasket top.
- Lower flange into place.
- Install studs, nuts, and washers to finger tight.
- Bolts 1 and 2 (see figure 4) are the bolts that always remain as guides for the flange.
- Bolts 5,6,11,12 cannot accommodate a bottom washer.

5. Tighten Flange Bolts
   - Use the large adjustable wrench and socket wrench.
   - Follow the bolt tightening order shown in the figure below (this diagram is also located on the exhaust hood).
   - Cycle through the order three times.

Preparation and Loading (cont.)

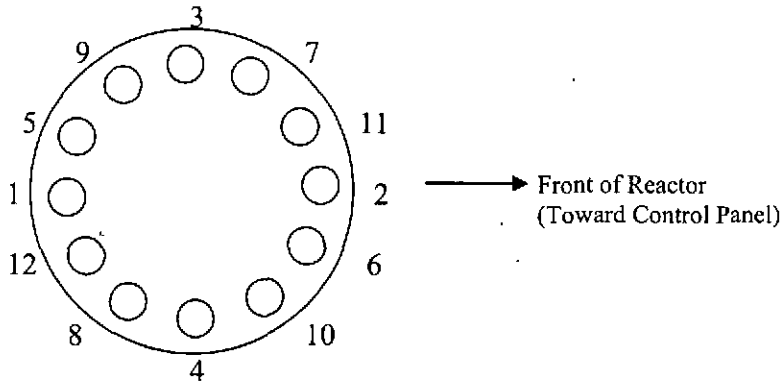

Figure 4. Bolt tightening pattern for the flange on the reactor pressure vessel. Repeat this order three times.

Connections and Settings

1. Ensure ball valve at rear of reactor is closed.

2. Connect two vent lines and one air inlet line at the top of the reactor.
   - Clean all fittings with alcohol prior to connection.

3. Afterburner connections (if afterburner is used).
   - Connect two 1" Swagelok lines to catalytic afterburner.
   - Connect power cable to vacuum pump used in gas sampling, and power for the afterburner heater.
   - Connect the two green 10 gauge wires with the twist lock connector. This wire is connected to the frame of the reactor and then grounded to a cold water pipe.
   - Connect thermocouples.

4. Attach large pipe reservoir for exhaust condensate.
   - Install wood mount to support the reservoir.

5. Connect the power cords for the main heater transformer, the compressor power, and the accumulator cart power. All connections should be made with standard three-prong 120-volt extension cords to the wall outlets.

6. Charge Air Accumulator.
   - Remove moisture from compressor reservoir.
   - Ensure all accumulator valves are closed.

Connections and Settings (cont.)

- Turn on compressor.
- Open accumulator inlet valve.
- Run air compressor until accumulator pressure is approximately 4500 psig.
- Close accumulator inlet valve.
- Turn off compressor.
- Note that the compressor's dipstick should be checked monthly, and the oil replaced when noticeably low or dirty (approximately every six months).

7. Set the ignition heater and catalytic afterburner heater at desired values.
   - Do not turn the heaters on yet.

8. Charge reactor vessel.
   - Set automatic pressure release system to desired pressure. (Note: The maximum value this system should ever be set to is 400 psig. If the set value is exceeded by 11 psi the automatic pressure release valve will open).
   - Open the accumulator outlet valve and allow air from accumulator to flow to the reactor vessel.
   - Wait until the reactor vessel reaches the desired operating pressure.
   - Follow procedure above to recharge accumulator to 4500 psig.

9. Connect data acquisition computer and prepare to record data (see appendix).

10. Verify that the automatic pressure release is enabled and will act if pressure limits are exceeded.

11. Attach Oxygen (O2) meter and Filter.
    - Attach O2 meter to C-clamp on side of reactor.
    - Set the particulate filter on the cart. Fill the reservoir of the filter with ice and water. Connect the inlet and outlet tubing.
    - Attach filter thermocouple.
    - Turn on O2 meter approximately fifteen minutes prior to the start of the run.
    - With the O2 meter inlet port exposed to room conditions, calibrate using small screwdriver until display reads 20.9% (see the figure below).

Connections and Settings (cont.)

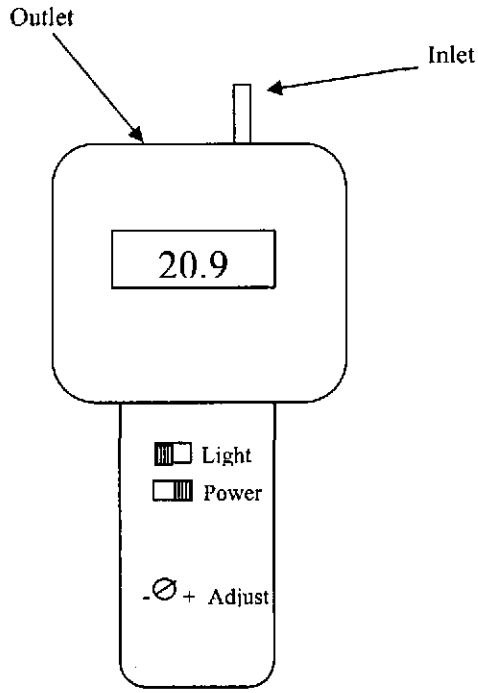

Figure 5. The oxygen meter. When exposed to room conditions the O2 level should be 20.9 %.

- Note that the value indicated by the O2 meter will drift lower as the catalytic afterburner heater warms up. If the afterburner is not being used and the value indicated by the O2 meter changes, repeat the calibration immediately before the run begins.
- Attach the sampling hoses to the O2 meter.
- The black hose attaches to the inlet of the meter, the white hose attaches to the outlet.
- If any problems arise the manual is located where the meter is stored in cabinet 11-5H (see lab layout).

12. Set the primary air micrometer valve to desired value.
    - See prior experiments to determine micrometer valve setting for specific pressure flow rates.
    - This value should be on the order of 10-20 micrometer units.

13. Turn on the variable autotransformer (variAC) that regulates power to the catalytic afterburner heater.
    - Insure the variAC is set at the value indicated on the experimental proposal form.

Connections and Settings (cont.)

- Do not begin run until temperature at the afterburner base is approximately 300 degrees C (this should take approximately 30 min).

14. Begin Taking Data
    - Click "Run Task" within the computer program VI Logger as soon as the catalytic afterburner heater is turned on.
    - Insure that all desired data signals are recording correctly.

Operation

The following is an example of a typical procedure. The actual procedure will vary according to the goals of the current research effort. The experimental proposal form provides details of the exact procedure for each run.

1. At time t=0.
    - Open ball valve at rear of reactor.
    - Turn on power to main heater.
    - Monitor pressure in reactor vessel.
    - Begin recording the oxygen level (as indicated by the O2 meter) every 30 seconds.
    - Maintain desired pressure value by opening down draft valve when necessary. Continue to do so for the rest of the run.

2. At approximately t=2 min.
    - Turn on primary air at the accumulator outlet valve.
    - Open micrometer valve as necessary during the run to maintain a constant change in accumulator pressure per unit time.

3. Pressure may cause automatic release valve to blow.
    - Frequently there is a quick rise in pressure inside the primary reactor vessel immediately following initial combustion. When this pressure rise occurs allow the automatic release valve to blow. This will cause the pressure in the vessel to fall below the desired pressure.
    - Do not attempt to compensate by opening the down draft valve or increasing airflow rate, the desired operating pressure will eventually be restored by the flow of primary air.

Operation (cont.)

4. When the oxygen level falls to approximately 4% begin delivery of the secondary air.
   - Open the secondary air micrometer valve (usually between one and two full rotations initially).
   - If the oxygen level continues to fall increase the flow of secondary air.
   - If the oxygen level rises above 5 percent decrease the flow of secondary air.
   - Continue this process until end of run.

5. Take gas samples as desired if the afterburner is being employed (see appendix).

6. Run the reactor until feedstock has been fully carbonized. Indicators that the run is complete include:
   - The temperatures above the catalyst begin to fall quickly,
   - Oxygen level rises steadily, as indicated by the O2 meter (this is not necessarily a good indicator when secondary air is supplied).
   - The amount of primary air supplied is comparable to that delivered in an earlier, successful run.

Shut Down

1. Stop the flow of primary and secondary air.
   - Close accumulator outlet valve, and secondary air micrometer valve.
   - Record the stop time.

2. Release pressure from reactor vessel
   - Open the downdraft valve and slowly decrease the pressure in the reactor vessel.

3. Let system cool overnight.

Unloading and Disassembly

1. Purge system with nitrogen.
   - Insure gas can flow through the system (downdraft and ball valves open).
   - Connect nitrogen cylinder to primary air inlet.
   - Set regulator on cylinder to approximately 10 psig.

Unloading and Disassembly (cont.)

- Let nitrogen flow through the system for approximately five minutes.

2. Disconnect catalytic afterburner.

3. Disconnect vent tubes and air inlet from the flange.

4. Undo bolts and use hoist to remove flange from reactor vessel.
   - Remove bolts in the same order they were tightened in.
   - Lower flange onto wood blocks on a cart.

5. Lift out canister
   - Place cardboard mat on floor.
   - Use hoist to lift out canister
   - Place canister on cardboard mat.
   - Fix ventilation duct tube over opened reactor.

6. Empty contents of canister.
   - Empty carbonized feedstock onto tarp.
   - Split into three sections (top, middle and bottom).
   - Weigh each section.
   - Set aside sample from each section to determine moisture content.

Appendix

1) **Feedstock Notes**

2) **Gas Sampling**

3) **Data Acquisition**

4) **Required Maintenance Schedule**

5) **Example Canister Record Sheet**

APPENDIX 1: FEEDSTOCK NOTES

Corn Cob

1. Wear gloves when handling cobs.
2. Remove needed amount of cobs from large gray bin labeled "corn cob".
3. Break cobs into uniform pieces using hands and the vice.
4. Sort the cobs by size.
5. Remove and discard any remaining husks.
6. Place a 4-6 inch layer of small pieces in the bottom of the canister to encourage initial ignition.
7. Arrange six of the larger pieces of cob into a cylinder-like shape approximately the same diameter as the canister.
8. Insert layers of cob in this fashion as shown in Figure A.1, using a stick to insure uniform packing.
9. Maintain a minimum of 1" clearance on top of canister.

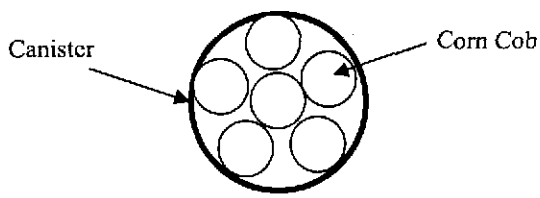

Figure A.1 Top view of canister and one layer of six large pieces of corncob.

Mac Shell

1. Wear gloves when handling macadamia nut shells (mac shells).
2. Separate desired amount of mac shells from the large gray bin labeled "macadamia nut shells".
3. Ensure all shells chosen are broken and no full nuts remain.
4. Pour mac shells into canister.
5. Maintain a minimum of 1" clearance on top of canister.

APPENDIX 2: GAS SAMPLING

The following procedure may be employed to gather gas samples used to evaluate the effect the catalytic afterburner has on emissions. Two gas sampling loops are mounted on the afterburner cart. One loop samples the inlet of the afterburner, and the other the outlet.

1. The initial state of the valves before each sample should be: V1 = closed, V2–V5 = opened, and a cover of the needle is removed (see figure A.2 for valve numbering).
2. Set a vacutainer at the sampling port needle.
3. Turn on the vacuum pump and wait for a while (usually 1 minute).
4. Close V4 and V5.

Appendix 2: Gas Sampling (cont.)

5. Turn off the vacuum pump.
6. Follow one of the procedures below as determined by the operational pressure inside the reactor pressure vessel.
7. If 75 psig ≤ P ≤ 150 psig: Close V3 → Open V1 → Close V1 → Open V3 → Close V3 → Open V5 → Close V5
8. If 150 psig < P ≤ 300 psig: Close V2 and V3 → Open V1 → Close V1 → Open V2 → Close V2 → Open V3 → Close V3 → Open V5 → Close V5
9. Remove the vacutainer.
10. Go back to initial conditions. Note that the procedure is identical for gas sampling before and after the catalytic monolith. When the last sample is finished replace cover on the needle of the sampling port.

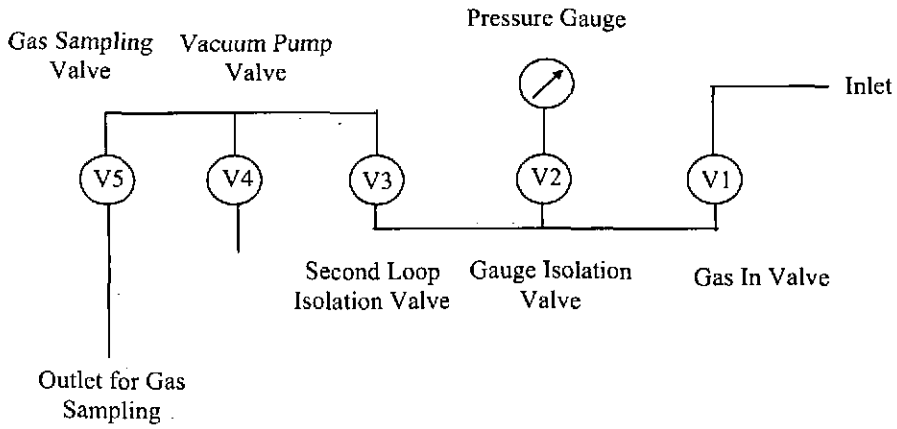

Figure A.2 Gas sampling plumbing diagram. The valve configuration is identical for sampling both before and after afterburner.

APPENDIX 3: DATA AQUASITION

The following procedure details the steps necessary to prepare the laptop computer to record data during a standard flash carbonization experiment.

1. Insert National Instruments Type II PC card (DAQCard-6062E) into the laptop computer.
2. Turn on computer.
3. Connect the two pressure transducers and all desired thermocouples (usually 13-14) to the jack panel mounted on the rear of the cart.
4. Turn on the power on the chassis (where the Amplifier and Terminal Block are mounted see the figure below).
5. Connect the output from the chassis to the PCI card.

Appendix 3: Data Acquisition (cont.)

6. Open the computer program "VI Logger" (a data logging program produced by national instruments).
7. Click on "VI Logger Tasks"
8. Click on "Copy of NI-DAQ Task
9. Ensure the desired channels are being monitored and that the sampling rate is correct. (for more information please see the VI Logger Manual)
10. Click the "Real Time Data" tab to prepare to monitor the data.
11. Open the computer clock by double clicking on the clock in the lower right hand corner of the screen.
12. The screen should now appear as shown in the screenshot below.

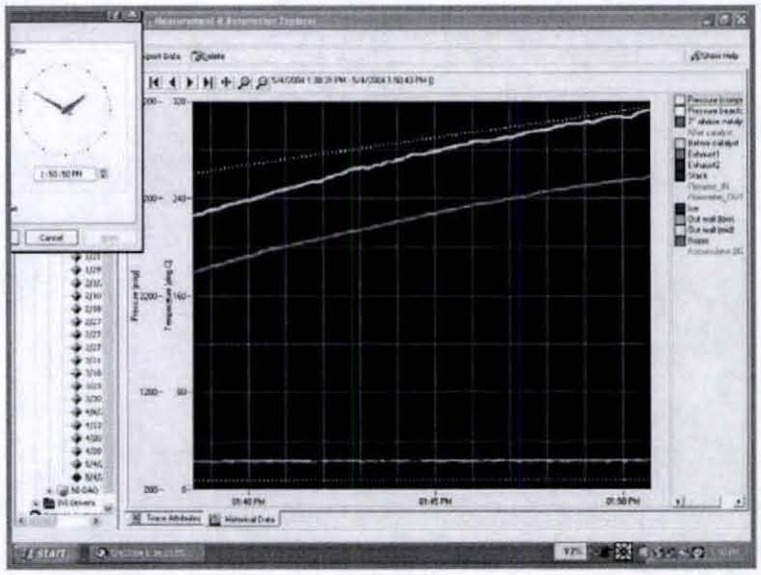

Figure A.3 Screenshot of the computer program "VI Logger" as it should appear when experimental data is being recorded.

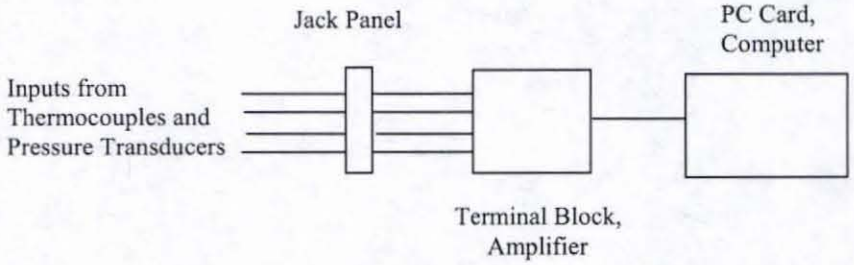

Figure A.4 Schematic of information flow for the data acquisition system.

Appendix 3: Data Acquisition (cont.)

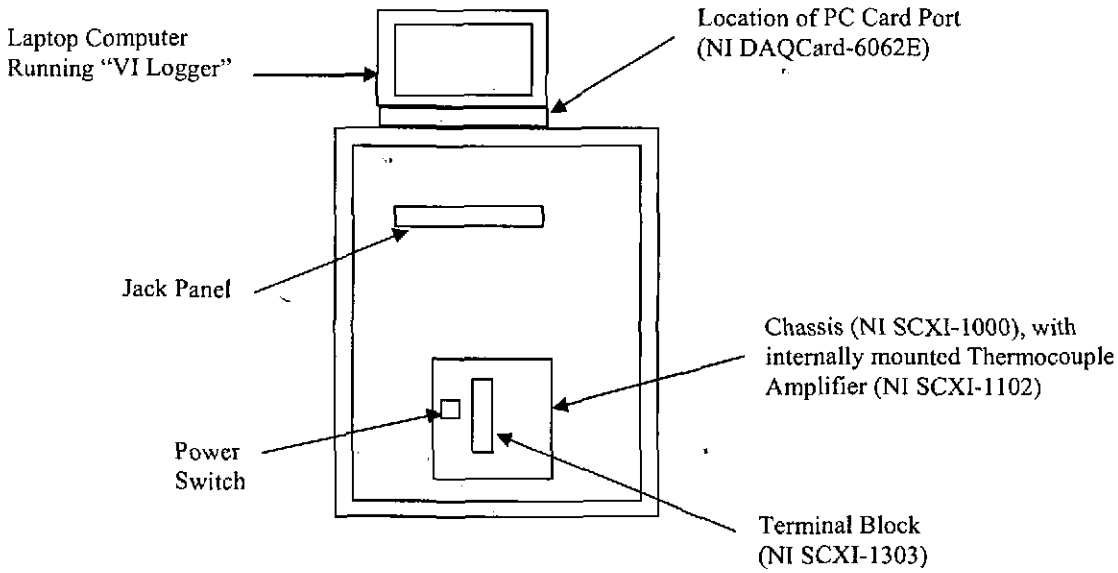

Figure A.5 Schematic of the data acquisition cart.

APPENDIX 4: REQUIRED MAITANENCE SCHEDUAL

The following describes the necessary tasks to maintain the lab scale reactor. Items that have been included in other sections are repeated here for completeness. Records of proper maintenance should be maintained on the "Laboratory Scale Reactor Maintenance Sheet" posted on the front of the reactor.

1. Remove, examine, and clean all plumbing after a period of ten runs.
2. Visually inspect burst diaphragm whenever plumbing is removed (once every ten runs).
3. Test spring release safety valve once every year. Record date tested on the valve.
4. Clean fittings that are frequently removed (such as those on the top flange of the pressure vessel) with alcohol before they are reattached.
5. Exercise the downdraft valve by fully opening and closing it multiple times prior to each run.
6. Empty water traps on the day following each run. Remove the plug at the bottom of the water trap under the exhaust hood and thoroughly clean after every ten runs.
7. Change oil in compressor when dirty or low (at least every six months).

APPENDIX 5: EXAMPLE CANISTER RECORD & REACTOR MAINTENANCE SHEETS

SEE ATTACHED PAGES

Appendix C

Safe Operating Procedures for the Demonstration-Scale Reactor: Cold Flow Test

DEMONSTRATION FLASH CARBONIZATION™ REACTOR
COLD FLOW TEST SAFE OPERATING PROCEDURES MANUAL
CREATED BY: Sam Wade

APPROVED BY: _____ DATE: _____

Table of Contents

INTRODUCTION AND PURPOSE

Currently research is being conducted in the R^3 laboratory in which the process of Flash Carbonization™ is used to produce charcoal from biomass. In this novel procedure a packed bed of biomass is placed within a vessel and exposed to elevated pressures. When a flash fire is ignited within the bed, the biomass is converted to biocarbon (i.e. charcoal) quickly and efficiently.

In order to illustrate the feasibility of employing this process on a commercial scale, a pilot plant has been built on the University of Hawaii Campus. This apparatus is referred to as the "demonstration flash carbonization reactor" (in order to differentiate it from the laboratory-scale reactor with which the process was developed).

Tests will be conducted to ensure that the plumbing of the demonstration reactor has been installed correctly, and that the inlet and exhaust airflow can be controlled as desired. During these tests the electric heaters will not be employed, and no biomass will be ignited. Because there will be no temperature difference between the inlet and exhaust gas, these tests are referred to as "cold flow tests". This safe operating procedures manual provides the necessary instructions for the correct operation of the demonstration reactor during such a cold flow test.

HEALTH HAZARDS

Pressurized vessels and pipes could potentially rupture. Safety glasses must be worn at all times. Pressure gauges and transducers must be monitored at all times. Overpressure protection devices must be properly maintained.

Electrical connections create the risk of shock or electrocution. Verify all power sources are disconnected before modifications are made to the system wiring. Ensure proper grounding of all equipment. Be continuously aware of all electrical hazards.

Hydraulic vessel closure system presents hazards during operation. Ensure safety devices are correctly installed and operational.

Generators, compressors, and leaf-blowers are fueled by gasoline. All possible ignition sources must be kept at a safe distance from these devices.

Use caution when employing the hoist and gantry system. Heavy loads may unexpectedly come loose. Hard hats must be worn at all times.

Working on the movable stair system may be dangerous. Verify the brake system is deployed prior to assent.

Opening and closing of the pressure vessel presents hazards to personnel nearby. The movable stair system must not be occupied while the hydraulic vessel closure system is active.

Unexpected weather conditions may present hazards.

Ear protection is required when compressors, leaf-blowers or generators are being used. Ear protection may interfere with communication between operators. Steps should be taken to verify comprehension.

PROCEDURE

The following is an example of a typical test procedure (including preparation, operation, and shut down). The general procedure should be well understood before any cold flow test is attempted. The actual procedure will vary according to the goals of the current research effort. The Cold Flow Test Experimental Proposal Form provides details of the exact procedure for each run. In the following pages whenever a valve is referred to the symbol **<>** *is used. Valve numbering correspond to the plumbing diagram found in Appendix D.*

Preparation

1. The following valves should be fully closed at the beginning of the test.
   - Primary air ball valve **<4>**
   - Secondary air ball valve **<7>**
   - Afterburner bypass valve **<8>**
   - Inlet gas sampling port valve **<10>**
   - Exhaust gas sampling port valve **<11>**
   - Manual exhaust valve **<14>**
   - Exhaust drain valve **<16>**
   - Afterburner drain valve **<17>**

2. The following valves should be fully open at the beginning of each test.
   - Compressor ball valve **<1>**
   - Afterburner inlet valve **<9>**

3. The following valves should be partially opened to the levels indicated on the cold flow test experimental proposal form.
   - Primary air globe valve **<3>**
   - Secondary air globe valve **<6>**
   - Exhaust globe valve **<13>**

4. The compressor and generator must have adequate amounts of fuel.
   - Verify fuel levels prior to each test.

5. Ensure that all personnel are wearing required personal protection equipment (PPE).
   - This includes safety goggles, ear protection, and hard hats.

6. Connect data logging system to pressure transducer and thermocouple outputs.
   - Details may be found in Appendix C.

7. Start the generator.
   - Verify the ground wire is firmly attached to generator frame.

8. Plug in all electronic devices. This includes:
   - Pressure indicators and data logging computer.
   - Pneumatically activated exhaust valve **<12>** solenoid and controller power.

9. Verify that pneumatically activated exhaust valve **<12>** is properly connected.
   - Gas cylinder (scuba tank) regulator should be set at 100 psig.

10. Set the desired operating chamber pressure using the pneumatically activated exhaust valve **<12>** controller.
    - This value is specified on the Cold Flow Test Experimental Proposal Form.

11. Start the compressor.

Operation

1. Begin to monitor reactor pressure data using the VI Logger Program.
   - Compare pressure data as recorded by the computer with the analog pressure gauge values.
   - Details can be found in Appendix C.

2. Open the primary air ball valve **<4>**.

3. Observe the system as the pressure rises to the desired value as specified on the Cold Flow Test Experimental Proposal Form.

4. If the pneumatically activated exhaust valve **<12>** fails to properly control the pressure, manually vent the chamber using the manual exhaust valve **<14>** before the pressure limit of the compressor is reached (175 psig and above).

5. Monitor the flow rate and vary valve settings as detailed for each individual test.

6. Secondary air supply should be controlled as described for each test.

Shut Down

1. Stop the flow of primary air by closing the primary air ball valve **<4>**.

2. Release pressure from the system.
   - Open the manual exhaust valve **<14>** and slowly decrease the pressure in the reactor system. When reactor gauge pressure falls to zero fully open manual exhaust valve **<14>**.

3. Shut down data logging computer and unplug other electric devices.
   - Fully disconnect computer and store properly.

4. Turn off compressor and generator.

5. Fully shut off gas supply to pneumatically activated exhaust valve **<12>**.

APPENDIX A: COLD FLOW TESTS EXPERIMENTAL PROPOSAL FORMS

The following three cold flow tests are designed to safely bring the carbonization reactor to operating pressure for the first time (test #1) and provide a preliminary evaluation of the inlet valves' ability to control the airflow rates (test #2 and test #3). The general procedure described previously in this manual (including preparation, operation and shut down) should be well understood before the following tests are conducted.

As written the following proposal forms describe each test as a stand-alone experiment. However, ideally these three tests could be run one immediately following the other to avoid fully depressurizing and re-pressurizing the system each time. This sequential testing approach requires only minimum modification to the following experimental procedures and would minimize the time and cost associated with these tests.

Demonstration Charcoal Reactor
Cold Flow Test Experimental Proposal Form

Date:

Test Number: 1

Purpose: To verify the demonstration carbonization reactor can safely be pressurized to the normal operating pressure (150 psig). To determine optimum setting of exhaust globe valve at this operating pressure.

Procedure:

- Ensure all personnel are wearing required personal protection equipment (PPE).
- Start compressor and single phase generator.
- Start data logging computer and the VI logger software.
- Set primary air globe valve **<3>** open five full turns.
- Verify pneumatic exhaust valve **<12>** is supplied with the proper pressure from gas cylinder (~80 psig).
- Set pneumatic exhaust valve **<12>** controller at an operating pressure of 50 psig. Verify that the controller is set for an operating dead-band of 1 psi.
- Fully open primary air ball valve **<4>**.
- Test manual exhaust valve **<14>** to verify it can vent the system pressure in an emergency.
- Let the system pressure rise to the first operating pressure value (50 psig). Record time needed to reach this pressure.
- Check the afterburner bypass line by opening the afterburner bypass valve **<8>** and closing the afterburner inlet valve **<9>**. If the bypass system functions as desired, reopen afterburner inlet valve **<9>**, then close afterburner inlet valve **<8>**.
- Raise the set point of the pneumatic exhaust valve **<12>** controller to 100 psig.
- Allow the system operating pressure to rise to 100 psig. Record time needed to reach this pressure.
- Adjust the exhaust globe valve **<13>** as necessary. Observe behavior of the pneumatic exhaust valve **<12>**. Record indicated flowmeter value.
- Close exhaust globe valve **<13>**.
- Raise the set point of the pneumatic exhaust valve **<12>** controller to 150 psig.
- Allow the system operating pressure to rise to 150 psig and observe behavior of the pneumatic exhaust valve **<12>**. Record the indicated flowmeter value and time to reach this pressure.
- Adjust the exhaust globe valve **<13>**. Record time-open and time-closed values for three cycles at three different settings. Record indicated flowmeter values.
- Record the optimum position for the exhaust globe valve **<13>** and the position of the primary air globe valve **<3>** when the system is operating at 150 psig.
- Close primary air ball valve **<4>**.
- Vent system using manual exhaust valve **<14>**.
- Shut down compressor and all other system components.

Demonstration Charcoal Reactor
Cold Flow Test Experimental Proposal Form

Date:
Test Number: 2

Purpose: To establish the effect of incrementally opening the primary air globe valve **<3>** on flow rate.

Procedure:

- Ensure all personnel are wearing required personal protection equipment (PPE).
- Start compressor and single phase generator.
- Start data logging computer and the VI logger software.
- Ensure temperature data from a thermocouple mounted next to the flowmeter is being monitored.
- Set primary globe valve **<3>** open one full turn.
- Verify pneumatic exhaust valve **<12>** is supplied with the proper pressure from gas cylinder (80 psig).
- Set pneumatic exhaust valve **<12>** controller at an operating pressure of 150 psig.
- The exhaust globe valve **<13>** should be opened to the optimum value determined from test number one.
- Fully open primary air ball valve **<4>.**
- Test manual exhaust valve **<14>** to verify it can vent the system pressure in an emergency.
- Let system pressure rise above 150 psig to test the performance of the pneumatic exhaust valve **<12>**. Observe the behavior of the pneumatic exhaust valve **<12>** for two minutes.
- If the pneumatic exhaust valve **<12>** is functioning properly continue, otherwise abort and vent system pressure by opening the manual exhaust valve **<14>**. Shut off compressor.
- Adjust the trim provided by exhaust globe valve **<13>** to produce proper venting.
- Record the volumetric flow rate of primary air as indicated by the flowmeter (in units of standard cubic feet per minute).
- Open the primary air globe valve **<3>** in increments of one full turn at a time, recording the flowmeter values resulting from each setting. Record any adjustments that need to be made to the exhaust globe valve **<13>**.
- Close primary air ball valve **<4>**.
- Vent system using manual exhaust valve **<14>**.
- Shut down compressor and all other system components.

Demonstration Charcoal Reactor
Cold Flow Test Experimental Proposal Form

Date:

Test Number: 3

Purpose: To establish the effect of incremental opening of the secondary air globe valve **<6>** on the primary air flow rate.

Procedure:

- Ensure all personnel are wearing required personal protection equipment (PPE).
- Start compressor and single phase generator.
- Start data logging computer and the VI logger software.
- Ensure temperature data from a thermocouple mounted next to the flowmeter is being monitored.
- Set primary globe valve **<3>** open five full turns (or to a better setting as indicated by the results of test #2).
- Verify pneumatic exhaust valve **<12>** is supplied with the proper pressure from gas cylinder (80 psig).
- Set pneumatic exhaust valve **<12>** controller at an operating pressure of 150 psig.
- The exhaust globe valve **<13>** should be opened to the optimum value determined from test number one.
- Fully open primary air ball valve **<4>.**
- Test manual exhaust valve **<14>** to verify it can vent the system pressure in an emergency.
- Let system pressure rise to the desired operating pressure (150 psig).
- If the pneumatic exhaust valve **<12>** is functioning properly continue, otherwise abort and vent the system pressure by opening the manual exhaust valve **<12>**. Shut down the compressor.
- Adjust the trim provided by exhaust globe valve **<13>** to produce proper venting.
- Record the volumetric flow rate of primary air as indicated by the flowmeter (in standard cubic feet per minute).
- Set secondary air globe valve **<6>** open one full turn.
- Fully open the secondary air ball valve **<7>**.
- Record the flowmeter value.
- Open the secondary air globe valve **<6>** in increments of one full turn at a time, recording the flowmeter values resulting from each setting.
- Close secondary air ball valve **<7>**.
- Close primary air ball valve **<4>**.
- Vent system using manual exhaust valve **<14>**.
- Shut down compressor and all other system components.

APPENDIX B: COLD FLOW TEST RECORD SHEET

Demonstration Reactor Cold Flow Test Record Sheet

Date:
Desired System Pressure:
Time to Fully Charge System:

Primary Air Globe Valve Setting (# of turns)	Secondary Air Globe Valve Setting (# of turns)	Exhaust Globe Valve Setting (# of turns)	Measured Flow Meter Value (SCFM)	Duration of Pneumatic Valve in Open Position (sec/cycle)	Duration of Pneumatic Valve in Closed Position (sec/cycle)

APPENDIX C: VI LOGGER SETTINGS

The following procedure details the steps necessary to prepare the laptop computer to record data during a standard flash carbonization experiment.

- Insert National Instruments Type II PC card (DAQCard-6062E) into the laptop computer.
- Turn on computer.
- Ensure primary reactor and afterburner pressure transducers are properly connected to the data logging system.
- Ensure all necessary thermocouples are properly connected to the data logging system.
- Turn on the power on the chassis (where the Amplifier and Terminal Block are mounted see the figure below).
- Connect the output from the chassis to the PCI card.
- Open the computer program "VI Logger" (a data logging program produced by national instruments).
- Click on "VI Logger Tasks"
- **Click on the** appropriate task name.
- Ensure the desired channels are being monitored and that the sampling rate is correct. (the sampling rate should be approximately one sample every six seconds)
- Click the "Real Time Data" tab to prepare to monitor the data.
- Open the computer clock by double clicking on the clock in the lower right hand corner of the screen.

APPENDIX D: PLUMBING DIAGRAM OF REACTOR

Plumbing around carbonization vessel

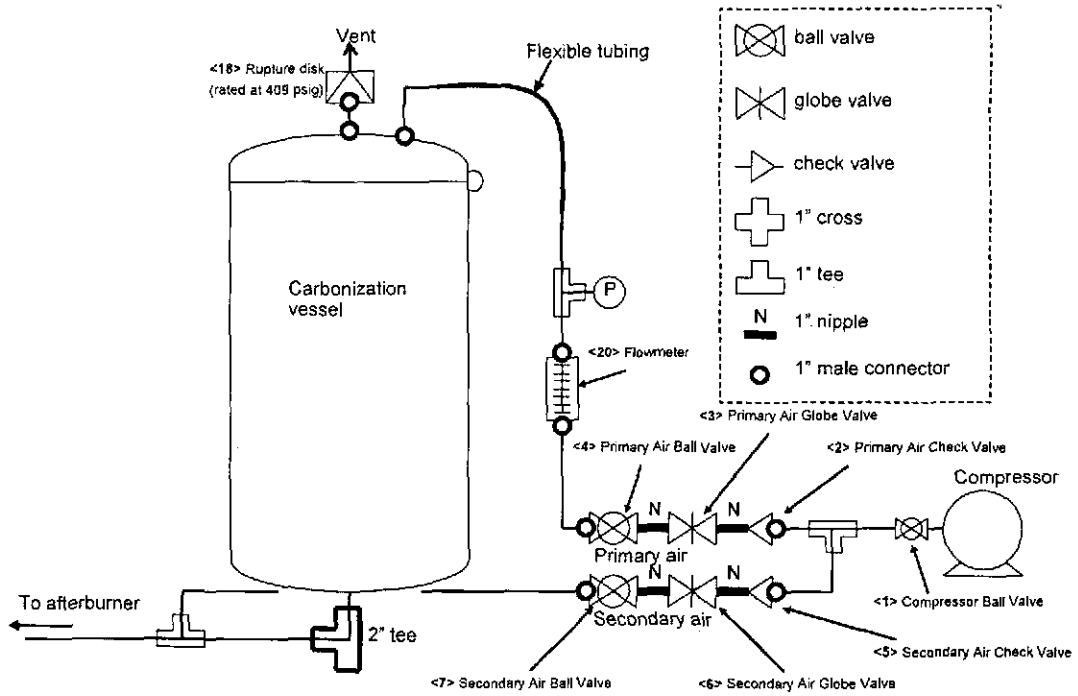

Plumbing around afterburner

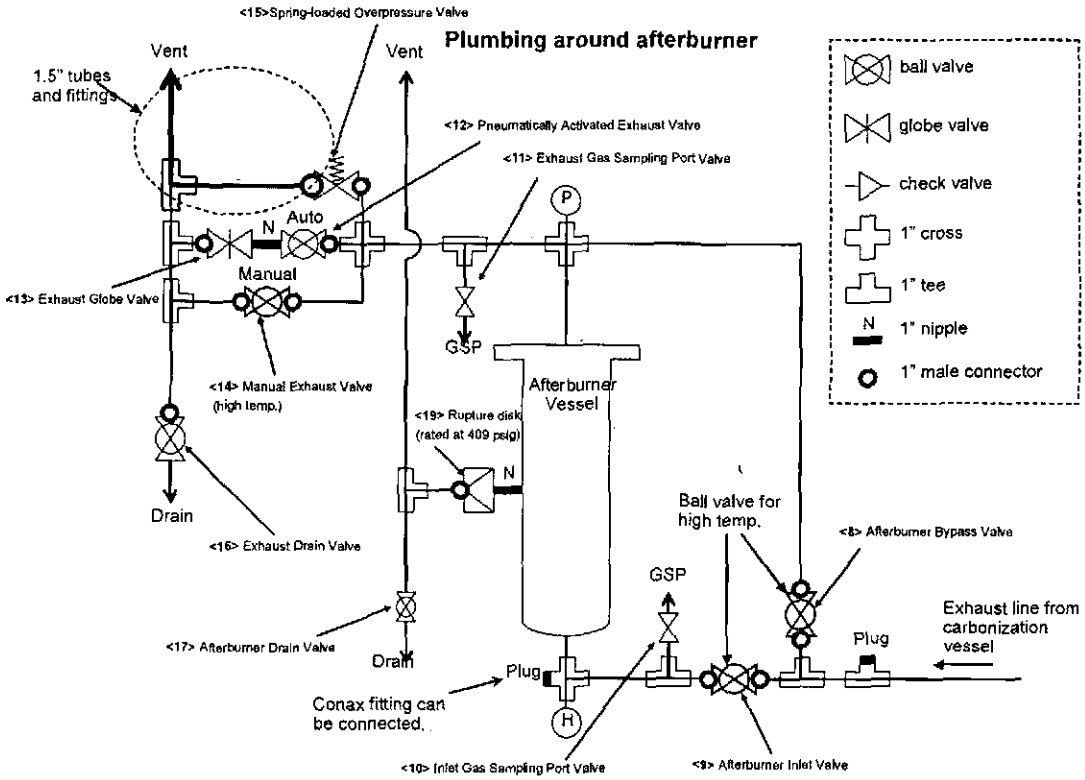

References

[1] USDOE and USDOA. *Biomass as a Feedstock for a Bioenergy and Bioproducts Industry: The Technical Feasibility of a Billion-Ton Annual Supply.* U.S. Department of Energy and U.S. Department of Agriculture, 2005.

[2] R.E.H. Sims. *Bioenergy Options for a Cleaner Environment in Developed and Developing Countries.* Elsevier, 2003.

[3] American Society of Testing and Materials. Standard test method for determination of total solids in biomass. *ASTM E 1756-95.*

[4] American Society of Testing and Materials. Standard method for chemical analysis of wood charcoal. *ASTM D 1762-84.*

[5] M.J. Antal and M. Gronli. The art, science, and technology of charcoal production. *Industrial and Engineering Chemistry Research*, 42:1619–1640, 2003.

[6] M.J. Antal, S.G. Allen, X. Dai, B. Shimizu, M.S. Tam, and M. Gronli. Attainment of the theoretical yield of carbon from biomass. *Industrial and Engineering Chemistry Research*, 39:4024–4031, 2000.

[7] T. Nunoura, S.R. Wade, J.P. Bourke, and M.J. Antal. Flash carbonization of biomass-propagation of flaming pyrolysis reaction and performance of catalytic afterburner. *Submitted to Industrial and Engineering Chemistry Research*, 2005.

[8] American Society of Testing and Materials. Standard test method for ash in biomass. *ASTM E 1755-95.*

[9] A. Demirbas. Combustion characteristics of different biomass fuels. *Progress in Energy and Combustion Science*, 30:219–230, 2004.

[10] D.A. Tillman, A.J. Rossi, and W.D. Kitto. *Wood Combustion.* Academic Press, 1981.

[11] R. H. Perry and D.W. Green. *Perry's Chemical Engineers' Handbook.* McGraw-Hill, 1997.

[12] R.J. Lewis. *Condensed Chemical Dictionary.* Van Norstrand Reinhold, 1993.

[13] M.J. Antal, K. Mochidzuki, and L. Parades. Flash carbonization of biomass. *Industrial and Engineering Chemistry Research*, 42:3690–3699, 2003.

[14] T. Nussbaumer. Combustion and co-combustion of biomass: Fundamentals, technologies, and primary measures for emission reduction. *Energy and Fuels*, 17:1510–1521, 2003.

[15] T. Nunoura and M.J. Antal. The black gold from green waste project at the university of hawaii. 2004.

[16] USEPA. *Emission Factor Documentation AP-42 Section 10.7: Charcoal.* U.S. Environmental Protection Agency, 1995.

[17] E. Bard. Extending the calibrated radiocarbon record. *Science*, 292:2443–2444, 2001.

[18] W. Emrich. *Handbook of Charcoal Making: The Traditional and Industrial Methods.* D. Reidel Publishing, 1985.

[19] M.J. Antal, E. Croiset, X. Dai, C. DeAlmeida, W. Mok, and N. Norberg. High-yield biomass charcoal. *Energy and Fuels*, 10:652–658, 1996.

[20] M.S. Tam, M.J. Antal, E. Jakab, and G. Varhegyi. Activated carbon from macadamia nut shell by air oxidation in boiling water. *Industrial and Engineering Chemistry Research*, 40:578–588, 2001.

[21] B. Glaser, J. Lehmann, and W.Zech. Ameliorating physical and chemical properties of highly weathered soils in the tropics with charcoal-a review. *Biology and Fertility of Soils*, 35:219–230, 2002.

[22] R. Balis, M. Ezzati, and D.M. Kammen. Greenhouse gas implications of household energy technology in kenya. *Environmental Science and Technology*, 37:2051–2059, 2003.

[23] M. Ezzati and D.M. Kammen. Indoor air pollution from biomass combustion and acute respiratory infections in kenya: an exposure-response study. *The Lancet*, 358:619–624, 2001.

[24] J.S. Lighty, J.M. Veranth, and A.F. Sarofim. Combustion aerosols: Factors governing their size and composition and implications to human health. *Journal of the Air and Waste Management Association*, 50:1565–1618, 2000.

[25] W.J. Gauderman, E. Avol, F. Gilliland, H. Vora, D. Thomas, K. Berhane, R. McConnell, N. Kuenzli, F. Lurmann, E. Rappaport, H. Margolis, D. Bates, and J. Peters. The effect of air pollution on lung development from 10 to 18 years of age. *The New England Journal of Medicine*, 351:1057–1067, 2004.

[26] R. Bailis, M. Ezzati, and D. Kammen. Mortality and greenhouse gas impacts of biomass and petroleum energy futures in africa. *Science*, 308:98–103, 2005.

[27] M. Gronli, M.J. Antal, Y.Schenkel, and R. Crehay. *The Science and Technology of Charcoal Production.* PyNe Subject Group Report.

[28] J.P. Lacaux, D. Brocard, C. Lacaux, R. Delmas, A. Brou, V. Yoboue, and M. Koffi. Traditional charcoal making: An important source of atmospheric pollution in the african tropics. *Atmospheric Research*, 35:71–76, 1994.

[29] K. Mochidzuki, F. Soutric, K Tadokoro, and M.J. Antal. Electrical and physical properties of carbonized charcoals. *Industrial and Engineering Chemistry Research*, 42:5140–5151, 2003.

[30] S.A. Watson and P.E. Ramstad. *Corn: Chemistry and Technology.* American Association of Cereal Chemists, 1987.

[31] J.B. Jones and G.A. Hawkins. *Engineering Thermodynamics.* John Wiley and Sons, Inc., 1986.

[32] Wikipedia. *Standard Conditions for Temperature and Pressure.* http://en.wikipedia.org/wiki/Standard_temperature_and_pressure.

[33] E. Ower and R. C. Pankhurst. *The Measurement of Air Flow.* Pergamon Press, 1977.

[34] R.E. Sonntag, C. Borgnakke, and G.J. Van Wylen. *Fundamentals of Thermodynamics.* John Wiley and Sons, 1998.

[35] V. Molkov, R. Dobashi, M. Suzuki, and T. Hirano. Modeling of vented hydrogen-air deflagrations and correlations for vent sizing. *Journal of Loss Prevention in the Process Industries*, 13:397–409, 2000.

[36] V. Molkov. Modeling of vented hydrogen-air deflagrations and correlations for vent sizing. *Journal of Loss Prevention in the Process Industries*, 12:147–156, 1999.

[37] G. Ciccarelli, V.M. Gthenakis, and J.L. Boccio. A method of analysis for gas explosions: h_2se case study. *Journal of Loss Prevention in the Process Industries*, 12:157–165, 1999.

[38] D. Bradely and A. Mitcheson. The venting of gaseous explosions in spherical vessles. i-theory. *Combustion and Flame*, 32:221–236, 1978.

[39] D. Bradely and A. Mitcheson. The venting of gaseous explosions in spherical vessles. ii-theory and experiment. *Combustion and Flame*, 32:237–255, 1978.

[40] J.F. Louvar and D.A. Crowl. *Chemical Process Safety: Fundamentals with Applications.* Prentice Hall, 1990.

[41] D.A. Crowl. *Understanding Explosions.* American Institute of Chemical Engineers, 2003.

[42] NFPA. *NFPA 68: Venting of Deflagrations.* National Fire Protection Agency, 1998.

[43] NFPA. *NFPA 69: Standard on Explosion Prevention Systems.* National Fire Protection Agency, 2002.

[44] C.V. Mashuga and D.A. Crowl. Problems with identifying a standard procedure for determining k_g values for flammable vapors. *Journal of Loss Prevention in the Process Industries*, 13:369–376, 2000.

[45] W. Bartknecht. *Explosions: Course, Prevention, Protection.* Springer-Verlag, 1981.

[46] G.E.P. Box, W.G. Hunter, and J.S. Hunter. *Statistics for Experimenters.* John Wiley and Sons, 1978.

[47] NMAB. *NMAB 367-2: Prevention of Grain Elevator and Mill Explosions.* National Material Advisory Board, 1982.

[48] R.L. Mason, R.F. Gunst, and J.L. Hess. *Statistical Design and Analysis of Experiments.* John Wiley and Sons, 1989.

[49] E.A. Avallone and T. Baumeister. *Marks' Standard Handbook for Mechanical Engineers.* McGraw-Hill, 1996.

[50] W.M. Rohsenow, J.P. Hartnett, and Y.I. Cho. *Handbook of Heat Transfer.* McGraw-Hill, 1998.

[51] W.Z. Black and J.G. Hartley. *Thermodynamics.* Harper and Row, 1985.

[52] R.T. Morrison and R.N. Boyd. *Organic Chemistry.* Allyn and Bacon, 1973.

[53] R.C. Dorf and J.A. Svoboda. *Introduction to Electric Circuits.* John Wiley and Sons, Inc., 2001.

[54] T. Cordero, F. Marquez, J. Rodrigurez-Mirasol, and J.J. Rodriguez. Predicting heating values of lignocellulosics and carbonaceous materials from proximate analysis. *Fuel*, 80:1567–1571, 2001.

[55] J. Parikh, S.A. Channiwala, and G.K. Ghosal. A correlation for calculating hhv from proximate analysis of solid fuels. *Fuel*, 84:487–494, 2005.

[56] MatlabHelp. *www.mathworks.com*. The Mathworks, 2005.

Index